ON THE VALIDITY OF THE WAGNER HYPOTHESIS IN THIN-WALLED OPEN-PROFILE MEMBERS

by

Monica Kaeline Falgoust

BS in Civil Engineering, University of Pittsburgh, 2002

Submitted to the Graduate Faculty of

School of Engineering in partial fulfillment

of the requirements for the degree of

Master of Science in Civil Engineering

University of Pittsburgh

2004

UNIVERSITY OF PITTSBURGH

SCHOOL OF ENGINEERING

This thesis was presented

by

Monica Kaeline Falgoust

It was defended on

December 3, 2004

and approved by

Dr. Kent A. Harries, Assistant Professor, Department of
Civil and Environmental Engineering

Dr. Jeen-Shang Lin, Associate Professor, Department of
Civil and Environmental Engineering

Dr. John F. Oyler, Adjunct Professor, Department of
Civil and Environmental Engineering

Dr. Christopher J. Earls, Chairman and Associate Professor, Department of
Civil and Environmental Engineering
Thesis Director

ON THE VALIDITY OF THE WAGNER HYPOTHESIS FOR THIN-WALLED OPEN-PROFILE MEMBERS

Monica K. Falgoust, MS

University of Pittsburgh, 2004

The Wagner Hypothesis states that when a thin-walled open-profile member is subjected to an axial loading leading to global instability, the longitudinal stresses developing within the fibers composing the cross-section become inclined to the normal plane; thus taking on a helical shape with respect to the longitudinal axis of the member. It is assumed that the longitudinal fiber stresses act as "follower-forces" and thus assume the same inclination as the cross-sectional fibers and thus produce a torsional moment about the longitudinal axis of the member. Classical second-order theories for calculating critical buckling loads based on the line of shear centers for thin-walled open-profile members have been developed by Timoshenko and Vlasov, which include the use of the Wagner effect. However, a competing theory has been developed by Ojalvo that utilizes the line of cross-sectional centroids (rather than cross-sectional shear centers) as a reference axis while at the same time rejecting the use of the Wagner Hypothesis. Ojalvo proposes that the Wagner Hypothesis violates common statical principles as well as is deficient for not identifying the free body with which torsional equilibrium is expressed.

The current study explored the validity of the second-order theories using nonlinear finite element techniques to produce critical buckling loads for various thin-walled open-profile members. Critical buckling loads obtained from this analysis were compared with numerical results provided by each theory as well as experimental results. Not only did the present research evaluate the behavior of various torsional members at their critical buckling loads, but it

also explored the notion that the principal stresses take on a helical shape once torsion has occurred (i.e. the stresses do indeed behave as “follower-forces”) using graphical representations of the members created within the finite element software. Conclusions were made based on the comparison of finite element results compared with theoretical results and experimental tests. The current study found that the Wagner Hypothesis is valid due to positive agreement between finite element results, numerical solutions, and experimental tests. Recommendations were made concerning the possibility of further research regarding this topic.

TABLE OF CONTENTS

LIST OF TABLES

LIST OF FIGURES

NOTATION

a	Distance between a point on the cross section and the shear center
B_x, B_y	Bending Stiffness about the x and y axis
C_T	St. Venant Torsional Stiffness
C_W	Warping Stiffness
E	Modulus of Elasticity
e(Ojalvo)	$e_y - y_o$
e_y	Eccentricity
G	Shear Modulus
I_x, I_y	Moment of Inertia about x and y axis
I_ω	Warping Moment of Inertia
K_T	St. Venant Torsion Constant
k(Ojalvo)	π/L
L	Length of Member
m(Ojalvo)	Couples
n	Energy State
r_o	Radius of Gyration
T(Ojalvo)	Internal Moment
V	Shear Force
u, v	Displacements
x, y	Coordinates of any point on a cross section
x_o, y_o	Coordinates of the Shear Center

β_x	Cross Sectional Constant Defined by Eqn. 1-3
ϕ	Angle of Twist

ACKNOWLEDGEMENTS

I would like to thank my thesis advisor, Dr. Christopher Earls, for providing me with guidance, insight, and his vast wisdom throughout my academic pursuits.

I would like to thank my family for their unending love and support; without their faith in me, none of my dreams would be possible.

I would like to thank all of my friends, and especially those who resided on the 11th floor of Benedum hall; sharing fun experiences with you allowed me to stay balanced throughout my academic career.

I would like to thank Muharrem Aktas, Brandon Chavel, and Brian Kozy; their engineering understanding has been an enormous aid in the completion of this project.

Last but certainly not least, I would like to thank my best friend, Jason O'Neil, for reminding me to laugh, since that is one of the most important things in life.

1.0 INTRODUCTION

The Wagner Hypothesis provides that when a thin-walled open-profile member is subjected to an axial loading leading to global instability, the longitudinal stresses developing within the fibers composing the cross-section become inclined to the normal plane and thus produce a torsional moment about the longitudinal axis of the member. This theory relies on the assumption that a bar is comprised of a bundle of filaments that act somewhat independently of one another; a useful analog is a cross-section composed of bundle of straws. Before the bar becomes unstable and begins to twist, the filaments have a compressive stress in them due to the axial loading. Once the member begins to twist due to the activation of some global instability mode, the filaments are no longer parallel to the longitudinal axis of the member. It is assumed that the longitudinal fiber stresses act as "follower forces" and thus assume the same inclination as the cross-sectional fibers. These inclined stresses then create a torsional moment about the longitudinal axis as well as an axial force resultant (Goodier 1950). It is assumed that as the section twists the stresses will begin to form a helical shape around a longitudinal axis formed by the line of shear centers of all cross-sections occurring along the member length; this helix, therefore, will follow the geometry of the deformed shape. The timeline under which the hypothesis evolved began with the classical theory for lateral-torsional buckling of thin-walled open-profile bars developed by Michell (1899) and Prandtl (1899). It was then extended further by Timoshenko (1905) to I-shaped bars with two axes of symmetry in the same plane. Wagner (1929) then applied these principles to the case of the shear center of thin-walled open-profile bars of arbitrary cross-section. The classical theories based on the assumptions that Wagner made have endured.

Second-order theories have been further developed based on the work of Timoshenko and Wagner, more recently by Galambos (1968). These theories apply to various thin-walled open-profile sections that are subjected to various loadings which cause some form of torsional failure. Also recently, a competing theory has been developed by Ojalvo (1990), which is not based on the shear center as the torsional axis and does not accept the Wagner Hypothesis. Ojalvo proposes that the Wagner Hypothesis violates common statical principles as well as is deficient for not identifying the free body with which torsional equilibrium is expressed (Ojalvo 1987). Ojalvo develops his version of the second-order theories for thin-walled open-profile bars based on the line of centroids in order to create a free body for use in formulating higher order governing equations. Ojalvo states that using the line of shear centers to develop the critical buckling load without employing the Wagner effect will lead to various problems, largely the fact that a mono-symmetric I-beam loaded with a constant moment will buckle at the same critical value regardless of whether the smaller or larger flange is in compression. While Ojalvo seems to recognize that the current theories based on application of the lines of shear centers in conjunction with a consideration of Wagner's Hypothesis work, his contention is that the Wagner hypothesis is an objectionable contrivance with no physical basis. In fact, Ojalvo criticizes the Wagner hypothesis on the fundamental grounds that it is notionally inconsistent with the hypothesis of Navier (i.e. the "plane section law") which is also applied at the very same cross-sections where filament distortion is considered to be occurring in the hypothesis of Wagner.

Various experts have attempted to contradict Ojalvo's new theory regarding buckling loads, while supporting the classical theory which makes use of the Wagner Hypothesis. In an attempt to further explore the validity of the second-order theory that Ojalvo has proposed, the

behavior of thin-walled open-profile members under axial loading is evaluated under the scope of this project utilizing the second-order theories provided by Ojalvo and Galambos, finite element analysis, and the results of past experimental tests. The finite element analysis software ABAQUS 6.4 is used for each of the finite element projects. Thin-walled open-profile members are used to first verify that ABAQUS is an appropriate tool for this project. Once the finite element analysis software has been tested to confidence, models are built and tested, and the results of those analyses are compared with the theories presented by both Galambos and Ojalvo.

It is known that one of the distinguishing features of a non-circular member subjected to torsion is that sections that were originally plane prior to torsional loading will warp under torsional loading. It is also known that thin-walled open-profile members are not very efficient at resisting torsion, and thus, as a result of a lack of torsional rigidity, typically will fail in a torsion mode. For singly symmetric sections, lateral-torsional buckling will commonly occur. It is crucial to study the stability of each member while performing the finite element analysis portion of the current research to ensure that the models are behaving as "real-life" members. A load-displacement curve is developed for each model to do just that.

An in-depth review of the literature published by both Galambos and Ojalvo is presented in the next section of this text. These works outline the derivations for the second-order theories including the Wagner effect, as well as those neglecting its validity. In addition to these texts, a short paper presented by Shao-Fan Chen is discussed within the context of identifying experimental test results to be used as a basis for comparison with the theoretical results and finite element analysis results. To provide conclusive results, it is important to find agreement between the theoretical results, finite element analysis results, and the experimental testing results. This is the main objective of the current study. Not only will the present research

evaluate the behavior of various thin-walled open-profile sections at their critical buckling load, but it will also explore the notion that the principal stresses take on a helical shape once torsion is induced (i.e. the stresses do indeed behave as “follower-forces”).

1.1 LITERATURE REVIEW

To verify the validity of Wagner’s Hypothesis, it is necessary to prove (or conversely discount) that its validity. Theories of various experts are presented. Within the scope of this project, a variety of thin-walled open-profile sections are loaded and tested to analyze the torsional behavior of the member. There have been several experts within the field that have dealt with the concept of Wagner’s Hypothesis. The subject has been worked on by V. Z. Vlasov, S. P. Timoshenko, and T. V. Galambos (1968), who are each in agreement on the validity of the theory; although Vlasov’s consideration of the Wagner hypothesis might be characterized as somewhat intricate. There is also a competing theory presented by M. Ojalvo (1990) wherein the Wagner Hypothesis is dismissed as erroneous.

In general, the analysis of a given structure for a specified loading is performed in two steps: first the force distribution within the structural member is determined based on either elastic or plastic theory; then the member is studied to determine whether it is able to support the imposed loading. The second part of the analysis will also involve an examination of the overall stability of the member (Galambos 1968). The present work deals strictly with the study of metal structures, and more specifically steel structures.

Many times the behavior of structures can be represented by assuming elastic behavior; meaning that when the loading is removed, the member will return to its original, pre-loaded configuration. For the current study, members will be considered in their elastic state only. The assumptions for the members under consideration are: the material is elastic; the members are prismatic and inititally straight; the column or beam has an open-profile thin-walled cross-section; plane sections will remain plane; the deformations of the member are relatively small; shear deformations are neglected; and the shape of the cross-section will remain unchanged. These assumptions are used to develop first-order theories associated with elastic members, and as such are germane to the current work as the assumptions at the very heart of the fundamental mechanical theories at issue herein. Due to the nature of the project, torsion will be the next focus of the discussion. Torsional response considered extends beyond the elementary uniform, or St. Venant's torsion, as covered in elementary undergraduate curricula.

One of the principle distinguishing features of the response of members to non-uniform torsion is that sections that were originally plane are no longer so after a twisting moment is applied: the section will warp. Exceptions to this statement are solid or tubular circular sections and thin-walled sections for which all elements intersect at a point, such as the cruciform, angle, and tee-shaped cross-sections (Galambos 1968). While these cross-sections will not warp under torsion, they are somewhat inefficient under torsional loading and are subject to lateral-torsional buckling even when only an incidental torsional load is applied. It is also known that when the section is free to warp, uniform or St.Venant torsion will occur in these non-circular sections, and when the member is restrained against warping, non-uniform torsion will occur (except in the case of a non-circular cross-section wherein the middle surfaces of all constituent plate components intersect at the shear center). The shear center, *S*, of any section is defined as the

point in the plane of the cross-section where a shear force must act if no twisting of the section is to take place. When a warping restraint is imposed anywhere along the member length, longitudinal stresses and shear stresses will develop in addition to the St.Venant shear stresses commonly associated with uniform torsion.

In direct opposition to the governing differential equations employed in a linear analysis, the nonlinear differential equations developed for an elastic member formulated to consider various global instabilities are developed using the deformed shape of the structural element as the basis for formulating equilibrium requirements. Because the deformations and internal forces are not independent of one another, they must be considered simultaneously. Thus, when an initially straight and prismatic member is subject to a compressive axial force in addition to bending moments applied at the ends of the section, the member will experience additional lateral deflections due to so-called “P-Delta” effects. The section may also twist about the shear center, *S*, through an angle of twist, ϕ. Within the span of the member the cross-sections will no longer be in the original x-y-z coordinate system after the deformations have taken place (Galambos 1968). The cross-section will rotate and translate as shown in the following:

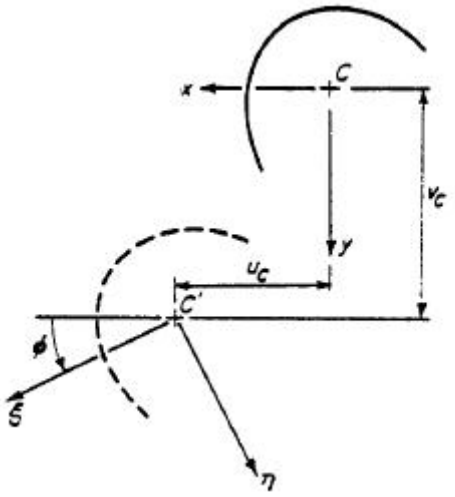

Figure 1: Translation and Rotation of Elastic Cross-Sectional Slice. (Galambos 1968)

The principal centroidal axes will have potentially translated and rotated with respect to a stationary global rectangular coordinate system and the original moments will be transformed as projections onto these axes. In addition to the twist caused by the moments placed on the section, there are other stresses that contribute to the torque once the section has deformed; one is due to the fact that the axial load will retain its original direction and will cause a twisting moment about the shear center. Another contribution to the moment is the fact that the two resulting cross-sections will warp with respect to one another as in the following image (intimately related to the Wagner Hypothesis):

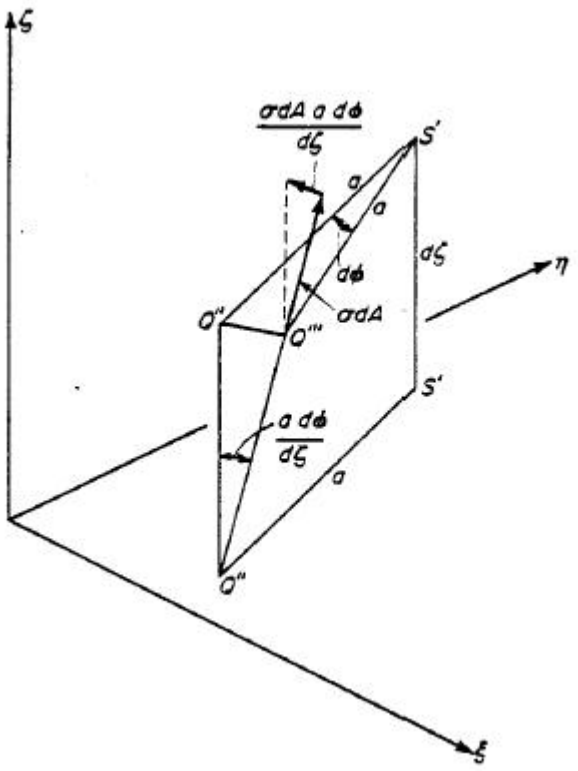

Figure 2: Twist Due to Differential Warping of Two Adjacent Cross-sections. (Galambos 1968)

The final contribution to the twisting moment is due to the end shears on the member. Figure 2 shows the twist due to differential warping of two adjacent cross-sections. The value *a* on the figure is the distance from the shear center out to the extreme fiber of the point in question. At the top of the figure there are two forces applied to the section. The force shown in the horizontal direction is the "Wagner Force".

Beams are typically designed to resist loads that cause bending about the major principal axis of the section. It has already been stated that open-sections do not possess significant resistance to torsional deformations, and although in-plane bending does not produce torsion directly, it does result from the initial imperfections in the beam geometry and the unintentional small eccentricity of the loads. Another more important consideration would be how elastic

strain energy is stored in the beam. When in-plane bending occurs, the internal moments act through the rotations of each plane section along the beam longitudinal axis to store significant amounts of energy. At some critical value, it becomes slightly easier for the beam to deform torsionally rather then in bending, and as a result, the slightest amount of perturbation of the beam due to loading imperfections or geometry imperfections activates the torsional deformation mode; a mode in which the beam is less efficient to resist external actions and thus a large torsional displacement occurs. Lateral-torsional buckling occurs when out-of-plane deformations in the transverse direction become magnified to the extent that they terminate the usefulness of the beam (Galambos 1968). In each of the models studied within this project, the member is not subject to a torsional load, but will exhibit a torsional failure mode. Galambos developed two differential equations for lateral-torsional buckling for any elastic beam subjected to in-plane concentrated end moments:

$$EI_y u^{iv} + M_x \phi'' + 2M'_x \phi' = 0$$

Eqn. 1-1

$$EI_\omega \phi^{iv} - (GK_T + M_x \beta_x)\phi'' - M'_x \beta_x \phi' + M_x u'' = 0$$

Eqn. 1-2

where,

$$\beta_x = \frac{\int_A y(x^2 + y^2)dA}{I_x} - 2y_0$$

Eqn. 1-3

β_x is a property of the cross-section. To apply these equations to a doubly symmetric, simply supported cross-section, a few manipulations must be made. For a section with double symmetry it can be shown that,

$$\beta_x = \frac{1}{I_x}\int_{-y_t}^{+y_t}\int_{-x_t}^{+x_t} y(x^2 + y^2)dxdy = 0$$

Eqn. 1-4

and

$$M_x = M_0$$

Eqn. 1-5

$$M'_x = 0$$

Eqn. 1-6

The differential equations now become,

$$EI_y u^{iv} + M_0 \phi'' = 0$$

Eqn. 1-7

$$EI_{\omega}\phi^{iv} - GK_T\phi'' + M_0 u'' = 0$$

Eqn. 1-8

Once these equations have been integrated, solved and manipulated, the critical moment for a simply supported, doubly symmetric section is found to be equal to the following:

$$(M_0)_{cr} = \frac{\pi n}{L}\sqrt{EI_y GK_T\left(1 + \frac{n^2\pi^2 EI_{\omega}}{GK_T L^2}\right)}$$

Eqn. 1-9

The lowest energy state corresponds to n = 1. The use of this equation will allow for a comparison with a moment arrived at using a finite element analysis for a simply supported I-beam. Both the differential equations as well as the equation for critical moment developed in the theory provided by Galambos employ the Wagner Hypothesis for thin-walled open-profile sections, and more specifically beams.

The next section of the project deals with columns and their behavior relative to Wagner's Hypothesis. Within this study there were two columns modeled in a finite element analysis and there are theoretical equations presented by both Galambos and Ojalvo. A column is defined as a member subject to an axial compressive load applied through the centroid, or at some very small eccentricity; for practical purposes columns typically stand on end. When evaluating any column member, one of the main concerns is stability. A member loaded by an axial force may tend to buckle. Within the scope of this study, only long, slender columns will be considered, and typically this type of column will buckle while the material is still elastic. The

practical maximum load that can be carried by an elastic column is the load where the column buckles (Galambos 1968).

Each of the sections chosen for the finite element analysis is found to be subject to a buckling failure mode, and in each case the stability of the structure is to be scrutinized. Instability is a condition wherein a compression member loses the ability to resist increasing loads and exhibits instead a decrease in load-carrying capacity as deflections increase; therefore instability occurs at the maximum point on a load-deflection curve (Galambos 1998). To ensure that each of the finite element models analyzed are achieving accurate results, the stability of each will be considered. It is known that the critical load of a member subject to compression does not necessarily equal the load at which a real imperfect member will collapse. To evaluate the point at which a real member will fail, it is necessary to consider the members' imperfections. In determining the load carrying capacity of a structural member it is possible that when subjected to increasing load, a member will initially deform in one mode, then reach a critical loading, and then continue to deform in a different pattern. This is referred to as the bifurcation of equilibrium. There are two types of bifurcation buckling for initially perfect systems depicted in the following diagram:

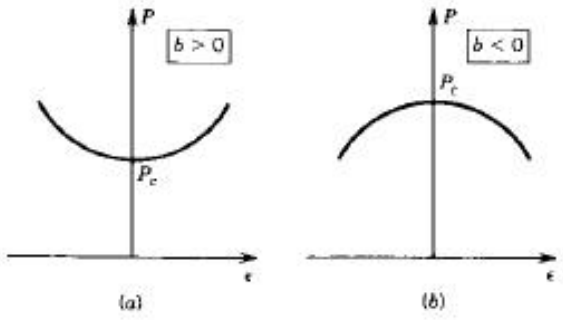

Figure 3: Postbuckling of Perfect Column. (a) Stable (b) Unstable Curve. (Galambos 1998)

In each of the plots, the member initially deforms in one mode, the prebuckling deformation, and then at the critical load, due to a branch in the load-deflection curve, the deformation suddenly changes into a different pattern, the buckling mode. An example of this phenomenon is when an axially loaded column initially shortens and then bends once it reaches the critical load. The plots above represent the fact that a structure's stiffness may increase or decrease at the onset of buckling. The structure is said to have a stable postbuckling curve if it can support an increasing load following the onset of buckling. On the other hand if the load decreases, the structure has an unstable postbuckling curve (Galambos 1998).

The postbuckling curve of an initially perfect system does not by itself give sufficient information to allow one to determine when failure takes place (Galambos 1998). There are initial imperfections that exist in all members, and these characteristics of the real structure must be considered. The load deflection curves for both stable and unstable systems with initial imperfections are as follows:

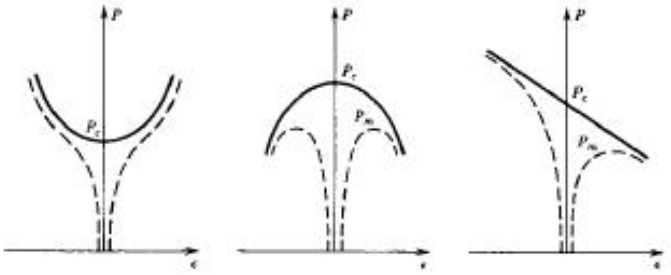

Figure 4: Postbuckling Curves for Initially Imperfect Systems. (Galambos 1998)

It is obvious from the plots that for a system with a stable postbuckling curve, very small imperfections have little effect on the behavior of the system. This type of structure is able to resist increasing loads after the critical load is reached, and a failure will occur only once the member has yielded. In contrast, for the system that has an unstable postbuckling curve the initial imperfections have a greater effect on the system, and the member will typically fail at a load less than the critical buckling load. It is evident that the behavior of real imperfect systems can be predicted from the shape of the postbuckling curve for perfect systems (Galambos 1998). Due to this fact, it is reasonable to evaluate the behavior of the columns analyzed using the finite element method by considering the load deflection plots produced from the output. If the output generates a plot similar to either stability curve, the user can be confident that the analysis is giving accurate results. All models included in the present research are analyzed assuming elastic behavior. When the member is elastic, it will return to its original undeflected position after loading is removed.

In order to develop the critical moment equations for the final set of finite element analysis runs, the behavior of elastic beam-columns must also be discussed. A beam-column is defined as a member that can support both axial compressive loads as well as moment at either end of the section. There are many practical applications for this type of member. A member is also considered a beam-column when it is subject to an axial compressive load with some amount of eccentricity, which produces a moment. The relationship between load and deformations for beam-columns differs from the behavior seen individually in either beams or columns. The axial load that is applied to a beam-column may be smaller than the maximum load that an equivalent column could carry, and therefore there is some reserve of capacity for moment that can be resisted (Galambos 1968). At the same time the moment that can be carried

is less than the full plastic moment that could be resisted by the beam if the axial load were equal to zero. The system of coupled differential equations governing the elastic behavior of beam-columns of arbitrary cross-section is (Galambos 1968):

$$B_x v'' + Pv - \phi[M_{B_y} - \frac{z}{L}(M_{T_y} + M_{B_y}) + Px_0] = M_{B_x} - \frac{z}{L}(M_{T_x} + M_{B_x})$$

Eqn. 1-10

$$B_y u'' + Pu - \phi[M_{B_x} - \frac{z}{L}(M_{T_x} + M_{B_x}) - Py_0] = -M_{B_y} + \frac{z}{L}(M_{T_y} + M_{B_y})$$

Eqn. 1-11

$$C_w \phi''' - (C_T + \tilde{K})\phi' + u'[-M_{B_x} + \frac{z}{L}(M_{B_x} + M_{T_x}) + Py_0] - v'[M_{B_y} - \frac{z}{L}(M_{T_y} + M_{B_y}) + Px_0] - \frac{v}{L}(M_{T_y} + M_{B_y}) - \frac{u}{L}(M_{T_x} + M_{B_x}) = 0$$

Eqn. 1-12

where the bending stiffness about each principal axis is:

$$B_x = EI_x$$

Eqn. 1-13

and

$$B_y = EI_y$$

Eqn. 1-14

the St.Venant torsional stiffness is

$$C_T = GK_T$$

Eqn. 1-15

the warping stiffness is equal to

$$C_W = EI_\omega$$

Eqn. 1-16

and

$$\tilde{K} = \int_A \sigma a^2 dA$$

Eqn. 1-17

These equations can be rewritten with the conditions that $M_{By} = M_{Ty} = 0$, $M_{Bx} = -M_0$, and $M_{Tx} = kM_0$ as:

$$B_x v'' + Pv - Px_0\phi = M_0[-1 + \frac{z}{L}(1-k)]$$

Eqn. 1-18

$$B_y u'' + Pu + M_0\phi[1 - \frac{z}{L}(1-k)] + Py_0\phi = 0$$

Eqn. 1-19

$$C_w\phi''' - (C_T + \tilde{K})\phi' + M_0 u'[1 - \frac{z}{L}(1-k)] + Py_0 u' - Px_0 v' + \frac{M_0}{L}(1-k)u = 0$$

Eqn. 1-20

It should be noted that these three equations are not independent of one another and that the first equation is not homogeneous. Lateral-torsional buckling is governed by the second and third differential equations presented above. After some manipulation and substitution into these equations, the buckling condition for a beam-column becomes:

$$(P_y - P)(\overrightarrow{r_0^-}P_z - P\overrightarrow{r_0^-} + M_0\beta_x) = (M_0 + Py_0)^2$$

Eqn. 1-21

where P_y and P_z are equal to:

$$P_y = \frac{\pi^2 EI_y}{L^2}$$

Eqn. 1-22

and

$$P_z = \frac{\pi^2 EI_\omega / L^2 + GK_T}{\overrightarrow{r_0^-}^2}$$

Eqn. 1-23

This equilibrium equation can be used to find the critical combination of P and M_0 for any beam-column section (Galambos 1968). Within the scope of this study, this development is used to compute the critical load for a column subjected to an axial load with a degree of eccentricity. For beams, columns, and beam-columns, Galambos has developed theoretical equations set forth by Vlasov and Timoshenko applying principles from the Wagner Hypothesis.

The competing theory presented by Ojalvo to discount the use of the Wagner Hypothesis includes the development of a new second-order theory for structures subjected to torsional failure. When developing the second-order theory, Ojalvo states that the line with which a deformed bar is modeled is the line of centroids. He states that the centroid line is

important because the transverse displacement of the centroid of a profile is the average transverse displacement of a profile and its longitudinal displacement corresponds to the average longitudinal displacement of the points of a profile (Ojalvo 1990). This differs from the theories developed by Galambos, which models deformations about the shear center of the section. Galambos affirms that when the line of shear centers is utilized the Wagner effect must be employed. The Wagner effect is redefined as the induced torsional moment in a normal plane arising from longitudinal stresses and twist deformations, and Ojalvo states that he does not support the use of this pheonmenon (Ojalvo 1990). The second-order theory that he develops is in complete agreement with classical buckling theory, in that the critical load associated with a member corresponds to the point where the member initially buckles. He derives equations associated with the critical moment of a simply supported beam subject to a constant moment, and the resulting equations presented are identical to the theory that Galambos puts forward.

Ojalvo begins his development of the equations that describe the nature of the buckling load for the second-order theory with the following differential equations:

$$EI_y u''''+Pu''-T_c x_0 \theta'''+[M_x + Py_0 - 2T_c' x_0]\theta''+[2V_y - T_c'' x_0]\theta'-q_y\theta + T_c v'''+2T_c' v''+T_c'' v'-q_x = 0$$

Eqn. 1-24

$$EI_{\tilde{\omega}}\theta''''+[M_x y_0 - M_y x_0 + P * r_0^{\,2} - GJ]\theta''+[V_y y_0 + V_x x_0]\theta'+[M_x + Py_0]u''+[M_y - Px_0]v''-m_z = 0$$

Eqn. 1-25

After some manipulation and substitution, Ojalvo develops an equation from which buckling loads can be calculated:

$$F(P) = P^2(1 - \frac{e}{y_0}) - P(P_y + \tilde{P}) + P_y \tilde{P} = 0$$

Eqn. 1-26

where,

$$\tilde{P} = \frac{(k^2 EI_{\tilde{\omega}} + GJ)}{ey_0}$$

Eqn. 1-27

These differential equations are used as the basis of other numerical solutions specific to the columns that were used to model the finite element analysis portion of the current study.

Ojalvo plainly states that the notion of longitudinal stresses inducing torsional moment on normal sections of a deformed bar is not valid (Ojalvo 1990). He therefore denies the possibility of torsional buckling as an admissible global instability (he instead explains experimental observations of such response as a by-product of local instabilities). He states that in general, the equilibrium method derivations in which the Wagner effect terms appear are deficient for not identifying the free body with which torsional equilibrium is expressed and for violating statical principles (Ojalvo 1987) (e.g. Navier's plane-section hypothesis). Ojalvo does not limit his criticism to only strong form statements of the problem at hand, and he contends that derivations based on variational methods (Bleich 1952) are just as incorrect, in that the theorem of stationary potential energy is misused. In other words, the components of a finite strain tensor are used in the strain energy expression when infinitesimal strain expressions are required (Ojalvo 1982, 1987). He also believes that adopting the line of shear centers without using the Wagner effect

leads to at least one major problem, which is that a mono-symmetric I-beam under uniform moment buckles at the same value of moment regardless of whether the smaller or larger flange is in compression (Ojalvo 1987). Another mono-symmetric column model will be studied within the current study to examine this claim.

In the case of the cruciform-shaped column, Ojalvo defines several equations for the torsional buckling load of the section. The buckling load presented by Ojalvo using the Wagner effect is:

$$EI_{\omega}\theta''''+[P\frac{I_o}{A}-GJ]\theta''=0$$

Eqn. 1-28

where I_o is the shear center polar moment of inertia of the profile area (Bleich 1952). When $\theta =$ $\theta'' = 0$ at either end of the section the critical buckling load is equal to the following:

$$P_{\theta}=\frac{A}{I_o}(GJ+EI_{\omega}\frac{\pi^2}{L^2})=\frac{16}{9}G\frac{t^3}{d}+\frac{16}{27}E\frac{\pi^2}{L^2}td^3$$

Eqn. 1-29

The analogous solution that does not employ the Wagner effect is equal to:

$$P_{\theta}=\frac{4}{a^2}[GJ+(EI_{\omega}+EI_y\{2d\}^2)\frac{\pi^2}{L^2}]=\frac{9}{4}G\frac{t^3}{d}+\frac{3}{4}\frac{\pi^2}{L^2}Etd^3$$

Eqn. 1-30

which is developed by using four identical tee-shaped columns whose web tips would all be connected to form the cruciform shape (See Figure 5) (Ojalvo 1990).

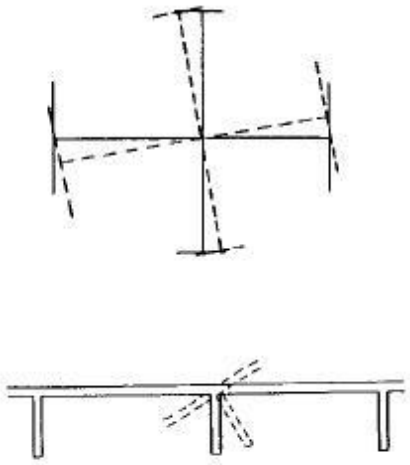

Figure 5: Cruciform Behaving as Tee Under Torsional Loading. (Ojalvo 1990)

To verify the use of the Wagner effect, it is necessary to not only compare finite element results with theoretical results, but to also compare these findings with experiments performed on so-called “real-life” members. In an attempt to make comparisons between failure loads and flexural-torsional buckling loads, Ojalvo presents the results of experimental tests performed by Shao-Fan Chen (1980) on various tee-shaped columns. The details of the experimental tests and the results will be discussed later in this presentation, but it is important to cover the numerical solutions that Ojalvo develops, which are to be applied to these tests. He derives a set of equations based on the line of shear centers for the normal planes which leads to a quadratic function of *P* where the buckling load may be calculated as:

$$\left[\frac{P}{P_y}\right]^2 (r_p{}^2 + 2\beta_x e_y - \{y_0 - e_y\}^2) - \left[\frac{P}{P_y}\right](r_p{}^2 + 2\beta_x e_y + \frac{GJ}{P_y}) = 0$$

Eqn. 1-31

in which,

$$2\beta_x = \frac{1}{I_x}\int_A (x^2 + y^2) y dA - 2y_0$$

Eqn. 1-32

He also develops a quadratic function from which the buckling load can be calculated based on the theory of the line of centroids defining the normal plane. It is developed from eqn. 1-25 presented previously in this discussion.

$$\left[\frac{P}{P_y}\right]^2 (e_y\{y_0 - e_y\}) - \left[\frac{P}{P_y}\right]\left(y_0\{y_0 - e_y\} + \frac{GJ}{P_y}\right) + \frac{GJ}{P_y} = 0$$

Eqn. 1-33

In an effort to verify the development of this new theory, the steps that Ojalvo lists for derivation of this equation were worked through, and it was not possible to achieve this final buckling equation. Therefore, when calculating the critical load for the tee-shaped column, eqn. 1-25 from this discussion was utilized (i.e. an error was found in Ojalvo's book indicating that eqn. 1-32 does not emanate from eqn. 1-25).

In an attempt to prove conclusively that the Wagner effect does exist, it is necessary to examine, firsthand, the paper of Shao-Fan Chen (1980) concerning the experimental tests performed on various tee-shaped columns at the Xian Institute of Metallurgy and Construction

Engineering, which is located in Xian, Shaanxi, China. A tee is a mono-symmetric section, and when acted on by an eccentric load, either a positive or negative eccentricity will exist. Chen states that based on an analytic study, most cases where this type of member fails under a lateral-torsional buckling mode, the resistance of the section will be smaller when there is the case of negative eccentricity (Chen 1980). Chen tested 24 columns with 18 sections experiencing a negative eccentrically placed axial compressive load. This current research makes use of what was designated a "PD" section (by Chen), therefore only that section will be covered in this discussion. This member is built-up using two plates welded together to form tee shapes with width to thickness ratios of 15. Each classification was given three column lengths. The members were also assigned an eccentricity ratio defined as:

$$\varepsilon = eA/w$$

Eqn. 1-34

where e is defined as the eccentricity, A is equal to the cross-sectional area, and w is the section modulus. This ratio differs with the various specimens, and each "PD" section was given a negative eccentricity ratio. The specimens are reported to be made of low carbon steel number 3, and each "PD" member had a mark of AD3. The members were hinged at each end and were supported by knife edges, where the center of the hinge was located at the load application point. The knife-edge at the top of the column was fixed to the testing frame with bolts, while the knife-edge at the bottom rested on the hydraulic jack. The loading during the test was stepped according to an estimated ultimate load and was tested until failure.

Overall, the 24 specimens saw three different failure modes including local buckling, in-plane stability, and lateral-torsional buckling. The PD3-1 was chosen for the finite element model in the current study due to a lateral-torsional buckling failure mode reported in the results from Chen's tests. Chen concludes from the results of the experiments that the width to thickness ratio for a tee-section should be limited by a slenderness ratio much like an I-section (Chen 1980). He also discusses equations related to the critical buckling load of the tee-section, but his formulation was not studied within the scope of this project; only his raw experimental results were of interest.

Within the literature presented by each of the authors including Galambos (1968), Ojalvo (1990), and Chen (1980), there are separate formulations for the critical buckling loads associated with different types of structural members. Galambos further develops a second-order theory based on the works of Vlasov and Timoshenko, which use the line of shear centers by which to model their numerical solutions. These solutions include the use of the Wagner Hypothesis. Ojalvo presents a competing theory where the Wagner effect is disregarded and the line of centroids is used to develop a substitution for the classical second-order theory by which to calculate the critical buckling loads for various members. Experimental tests performed by Chen are used to verify both theories.

1.2 OVERVIEW OF THESIS ORGANIZATION

Chapter 2 discusses the finite element method as it applies to the current study. Section 2.1 covers the procedure for modeling a structure using the finite element method, analyzing the

structure, and interpreting the results. It outlines the importance of the element mesh as well as mathematical models used to solve the models. Chapter 3 covers the finite element model used to verify that ABAQUS 6.4 would be an adequate tool for analyzing the models related to the problem at hand. Within the contents of Chapter 4, various models are analyzed in order to compare the finite element results for beam and column behavior to theoretical results provided by both Galambos and Ojalvo. Chapter 5 encompasses the results of the current study as well as conclusions that can be drawn from those results.

2.0 FINITE ELEMENT METHOD

The objective of the current study is to determine the validity of the Wagner Hypothesis as it relates to classical theories regarding lateral-torsional buckling of thin-walled open-profile members. The Finite Element Method (FEM) is employed in this research to create analytical models of thin-walled open-profile sections. In general, the finite element method is a numerical method for solving engineering problems which have complicated geometries, loadings, and material properties. It allows the user to solve complex problems without the requirement of the direct solution of ordinary or partial differential equations. The FEM analysis will result in a system of simultaneous algebraic equations for the solution, as opposed to a very complicated and almost impossible solution of differential equations. The method assembles a finite number of structural elements interconnected by a finite number of nodes. The analysis will provide an approximate solution to the actual structure since the original continuum is divided into an equivalent system of finite elements using one-, two- and three- dimensional structural elements. The material properties for the system will be retained by the elements chosen as part of the analysis. The commercial multipurpose finite element software package, ABAQUS 6.4, is employed in this research to execute nonlinear finite element analysis studies. Only geometric nonlinearity is considered herein.

2.1 FINITE ELEMENT ANALYSIS PROCEDURE

The process of modeling a body and analyzing that body under a particular loading begins with the discretization of the body into an equivalent system of smaller units (finite elements) interconnected at points common to two or more elements (nodes). An appropriate element type is chosen to closely simulate the behavior of the original continuum. In general, smaller elements are used to create a denser mesh which will produce better results from the model. In theory, when the mesh size of correctly formulated elements is reduced, the solution of the analysis will converge to the exact solution for the actual structure. The compatibility of elements with adjacent elements is very important for the proper convergence of the analysis. If the compatibility of the elements is not satisfied, gaps or overlaps within the model will occur, and may result in a less predictable convergence characteristic.

The evaluation of the element properties for the model involves developing the stiffness matrix for the given system which forms the relationship between the forces and displacements in the model. The individual element equations will be superimposed using the direct stiffness method to produce the global stiffness matrix, [*K*]. The following equation relates the forces, *F*, to the displacements, *d*, for the system using the global stiffness matrix, [*K*]:

$$\{F\} = [K]\{d\}$$

Eqn. 2-1

Boundary conditions must be imposed in order for numerical singularity to be avoided, so that the structure remains stationary during the analysis instead of moving as a rigid body.

Following the evaluation of the element properties, the actual analysis of the structural model must be completed. In order for the analysis to run correctly, the equilibrium, compatibility, and force-displacement relationships must be satisfied. The equations that result from the force-displacement relationships may be solved using the force method approach or the displacement method approach, both of which are appropriate for structural systems that are elastic. The mathematical system may be solved using any number of solution algorithms including elimination methods such as Gaussian elimination or iterative methods including the Gauss-Seidel method. For a nonlinear analysis, these methods are not sufficient to directly arrive at an equivalent approximate solution, and therefore the equilibrium path must be traced using iterative and incremental methods.

2.2 NONLINEAR FINITE ELEMENT ANALYSIS

To evaluate a problem of linearly elastic nature a linear analysis of the structure is performed, because it is assumed that the displacements of the members are infinitesimally small. Nonlinearity in structures can be classified as either material or geometric nonlinearity. Material nonlinearity results from changes in the material properties, such as plasticity, and geometric nonlinearity can result from changes in the configuration of the model, such as large deflections. A change in the geometry in the model may cause both the load distribution and magnitude to be altered.

During a nonlinear analysis the solution cannot be calculated by solving a system of linear algebraic equations directly. The solution is found by specifying the loading as a function

of time and incrementing the time intervals to obtain the nonlinear response (the term “time” is used in a generic sense since all analysis considered herein are static and thus time is a “dummy” variable used to connote incrementation of load). ABAQUS breaks the given analysis into a predetermined set of time increments and calculates the approximate equilibrium configurations at the end of each time period. ABAQUS assumes the response to be linear within each interval. After each increment, the structure is reconfigured and a new ideal linearized structural response, or tangent stiffness matrix, is calculated. For each increment, the linearized structural problem is solved for displacements, and these displacements are added to those determined at the end of the previous increment. ABAQUS uses the load proportionality factor as the load increment, and the load proportionality factors will vary in size as a function of the effort required to achieve convergence in the prior increment. After each converged increment is computed, the program will compute a new tangent stiffness matrix using the internal loading and the deformation of the structure at the beginning of the load increment. The tangent stiffness matrix, $[k_T]$, may be denoted as:

$$[k_T] = [k_o] + \lfloor k_p \rfloor$$

Eqn. 2-2

where $[k_O]$ is the common linear stiffness matrix for the uncoupled bending and force behavior, and the matrix $[k_P]$ is the initial stress matrix that is based on the force at the beginning of each load increment.

2.2.1 Nonlinear Equilibrium Solution Methods

For the current research, incremental solution procedures are necessary to trace the nonlinear equilibrium path of the model. ABAQUS utilizes either the Newton-Raphson Algorithm or the modified Riks-Wempner Method (arc length method) (ABAQUS 2003); both methods are powerful tools for determining the nonlinear response of a system. ABAQUS uses the Newton-Raphson method as its default solution algorithm. This method is useful for cases where there is mild nonlinear response. The Newton-Raphson method is advantageous because of its quadratic convergence rate when the approximation at a given iteration is within the radius of convergence (ABAQUS 2003). One drawback of this technique is its inability to traverse limit points in the equilibrium path being traced as part of the nonlinear solution process. The Riks-Wempner method does not suffer from this limitation and as such represents the solution strategy of choice when tackling problems with large degrees of nonlinearity.

2.3 ELEMENT TYPE

Shell elements found in the ABAQUS element library are chosen for this study due to their ability to economically model structures where one dimension, the thickness is much smaller than the other dimensions of the structure. A three-dimensional shell element is able to model either “thick” or “thin” shell problems. The nonlinear shell element chosen for various modeling applications throughout this project is the S4R shell element (ABAQUS 2003). The S4R element is defined by ABAQUS (2003) as a 4-node doubly curved general-purpose shell, with reduced integration, hourglass control, and finite membrane strains.

There are five aspects of an element that characterize its behavior. They include:

1. Family
2. Degrees of Freedom
3. Number of Nodes
4. Formulation
5. Integration

The S4R belongs to the shell family, and it possesses 4 nodes. There are two types of shell elements, thick and thin shells. Thick conventional shell elements are utilized in cases where transverse shear flexibility is important and second-order interpolation is desired (ABAQUS 2003). Thin conventional shell elements are used for modeling cases where transverse shear flexibility is negligible and the shell normal remains orthogonal to the shell reference surface. The general purpose conventional shell elements used in this research allow transverse shear deformation, and they use thick shell theory as the shell thickness increases and become discrete Kirchoff thin shell elements as the thickness decreases (ABAQUS 2003). This is important for this project because the shell thicknesses are changed for varying sized columns and beams. For each of the four nodes on the element there are six active degrees of freedom, which include displacements and rotations in each principal direction. The S4R element degrees of freedom are defined as:

$$1, 2, 3, 4, 5, 6\ (u_x, u_y, u_z, \phi_x, \phi_y, \phi_z,)$$

The S4R element uses reduced integration to form the element stiffness matrix, while the mass matrix and distributed loadings are integrated exactly. Reduced integration usually

provides more accurate results (e.g. relieves shear locking, etc.), provided that the elements are not distorted or loaded in in-plane bending, and it significantly reduces the running time for the model resulting in a more economical choice for the user (ABAQUS 2003). The S4R is said to be computationally inexpensive since the integration is performed at one Gauss point per element.

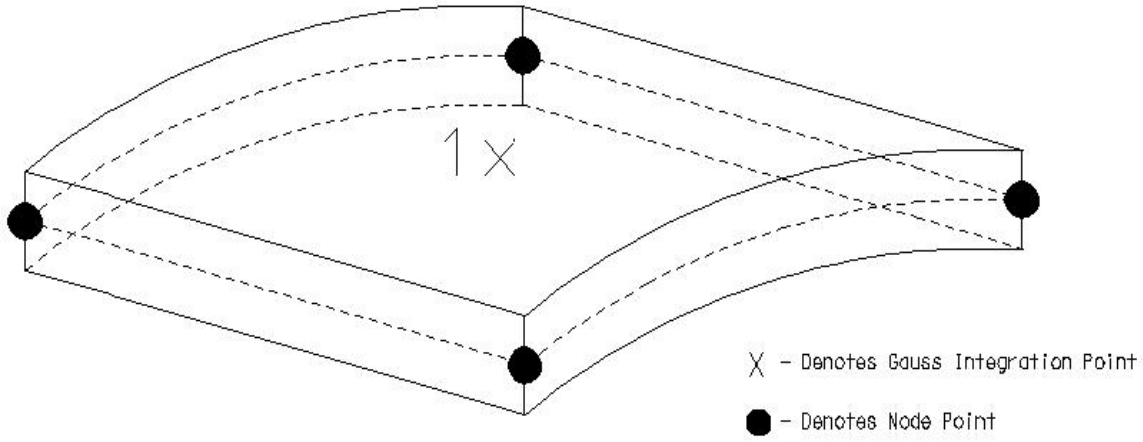

Figure 6: S4R Element

2.4 FINITE ELEMENT MESH

The analytical models created for this study are built from a dense finite element mesh of the ABAQUS S4R element described in the previous section. The mesh density is directly related to the computational time and the modeling accuracy. These two factors must be balanced in such a way that the model produces relatively accurate results while being analyzed

in an appropriate amount of time. The finer the mesh density is, the more accurate the results will become, but the computational time will also increase.

The elements used in each of the models including the verification study have an aspect ratio of one-to-one. In other words, all elements in each of the models have a square shape. The mesh density employed herein was proven to provide accurate results at both the local and global level, in the verification work provided by Earls and Shah (2001). The equally sized elements in the flanges and webs of each model allow the components to be compatible. This means that the mesh along the web segment can be integrated with the longitudinal mesh of the flange sets. This allows the user to accurately tie the meshes of separate elements together to make a single piece that performs as one.

2.5 IMPERFECTION SEED

In modeling studies where buckling is investigated, it is important that the evolution of the modeling solution be carefully monitored so that any indication of bifurcation in the equilibrium path is carefully assessed so as to guarantee that the equilibrium branch being followed corresponds to the lowest energy state of the system (Earls and Shah 2001). To ensure that the lowest energy path is followed, the current study uses an imperfection seed in the finite element analysis with some initial displacement or rotation. This initial displacement is obtained from a linearized-eigenvalue buckling analysis where an approximation of the buckling mode is found. This analysis will indicate which mode should be used as well as the initial displacement. This is then superimposed onto the finite element mesh in order to perform a postbuckling

analysis. The imperfection seed is scaled so that the maximum initial displacement is small enough so as to not affect gross cross-sectional properties of the model (Earls and Shah 2001). In order to find an accurate account of the critical loads achieved by the model, various scale factors are used. Although the technique of seeding a finite element mesh with an initial imperfection to ensure that the correct equilibrium path is followed is recognized to have shortcomings, the technique is employed in this project due to the fact that the results obtained from this method have agreed with experimental tests (Earls and Shah 2001). The imperfection seed is superimposed on to the mesh by using the *IMPERFECTION command in the ABAQUS finite element software.

2.6 MATERIAL PROPERTY DEFINITIONS

Steel is the material used for each of the models presented in this study, due to its widespread practical use. The input file for the finite element analysis requires that the material properties for each section of the model are defined appropriately. All analysis performed within the scope of this project is purely elastic. A material name is coded into the input file with a modulus of elasticity, E, and Poisson's Ratio, ν, for the analysis. In each of the models used in the current study, the modulus of the elasticity used is 29,000 ksi, and Poisson's Ratio is 0.3; this is typical for all grades of structural steel.

3.0 VERIFICATION STUDY

In order to create models using the finite element method, and to ensure that the analysis produces reliable results, the modeling techniques must be verified using a reliable data set. For the current project, a numerical model was selected from Galambos' text (1968) to recreate the variation of curvature, Φ, along the length of the beam. The model prescribed a W12x50 steel shape, simply supported, with an eccentric load at the mid-span of the structure.

ABAQUS was used to model the beam using the geometry and material properties described in the text. The beam was constructed by defining nodes, and then creating node sets and elements between those nodes; the elements used for this model are shells designated S4R. Each element corresponded to regions with separate material properties and shell thicknesses. The accuracy of the finite element analysis is dependant on the density of the mesh for the model. A dense mesh is used for all of the models throughout the project to obtain more accurate results, and an aspect ratio of one-to-one is maintained for all elements in these models. The element size is one square inch. For the verification study, the model generated includes approximately 7,000 nodes and 6,800 elements.

3.1 VERIFICATION STUDY RESULTS

The objective of the verification study chosen is to replicate the rate of curvature versus length curve presented by Galambos. Young's Modulus is set to 29,500 ksi and Poisson's Ratio is 0.3 in the finite element model. The example uses a W12x50 wide flange section where the

beam length is 240 inches. The depth of the beam used is 12.19 inches, and the flanges are 8.077 inches wide. The flange thickness used is 0.641 inches, and the web thickness is 0.371 inches (See Figure 7).

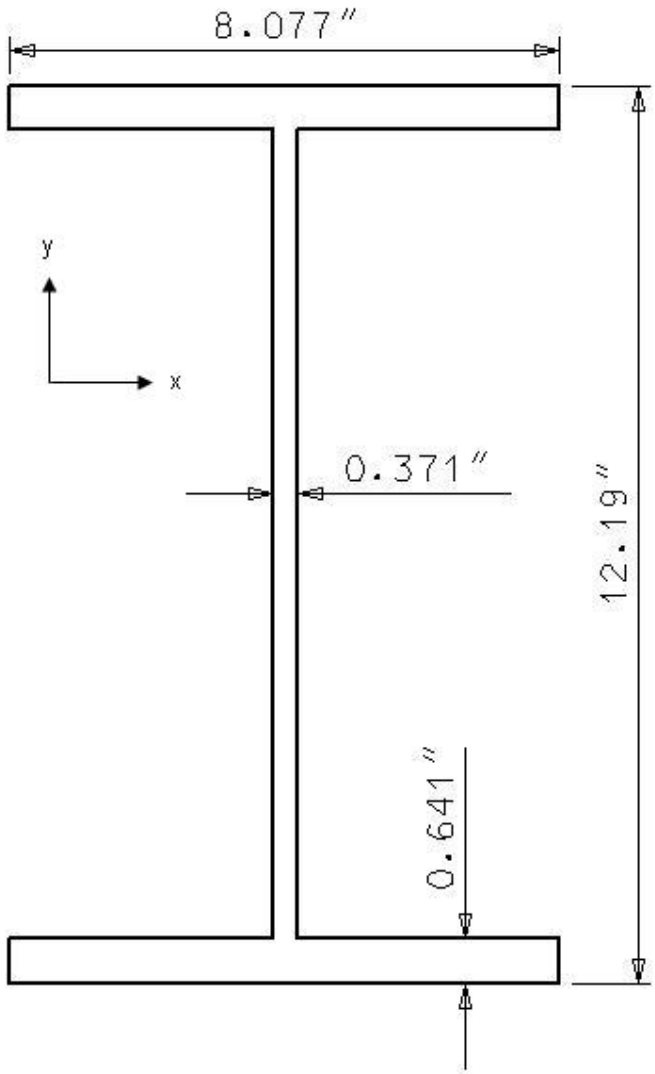

Figure 7: W12x50 Cross-section

The boundary conditions for the study include use of a roller and a pinned condition, where the pin was restrained against displacements in the x (strong axis), y (weak axis), and z (longitudinal axis) directions and rotation about the z-axis was also restricted. The roller was

restrained against displacements in the x and y directions, and rotation about the z-axis was again prohibited. The rotations were restrained so that the beam would not completely overturn while being loaded. So that the beam would be permitted to twist at the mid-span, rigid beam elements were employed at the support locations. These "rigid beam" elements were given an elastic modulus, E, ten times greater than the elastic modulus of the steel, as well as cross-section dimensions of five inches in length by five inches in width.

The load, *Q*, was applied with an eccentricity, *e*, to produce a twisting moment equivalent to,

$$M_z = Q * e$$

Eqn. 3-3-1

about the shear center of the cross-section. In order to model the eccentricity of the load, a small lever arm is attached to the beam at the mid-span of the beam at the center of the web. This arm is comprised of rigid beam elements so that the arm itself would not deform when loaded. It is not necessary that the arm see any portion of the load, and therefore the rigid beam elements allow the load to be transferred totally to the beam. The actual load for the example was not stated in the text; therefore, the end of the lever arm is loaded with a one kip load acting in the downward y direction.

When viewing the deformed shape through the ABAQUS 6.4 CAE viewer, it is obvious the beam is experiencing a lateral-torsional buckling mode of failure.

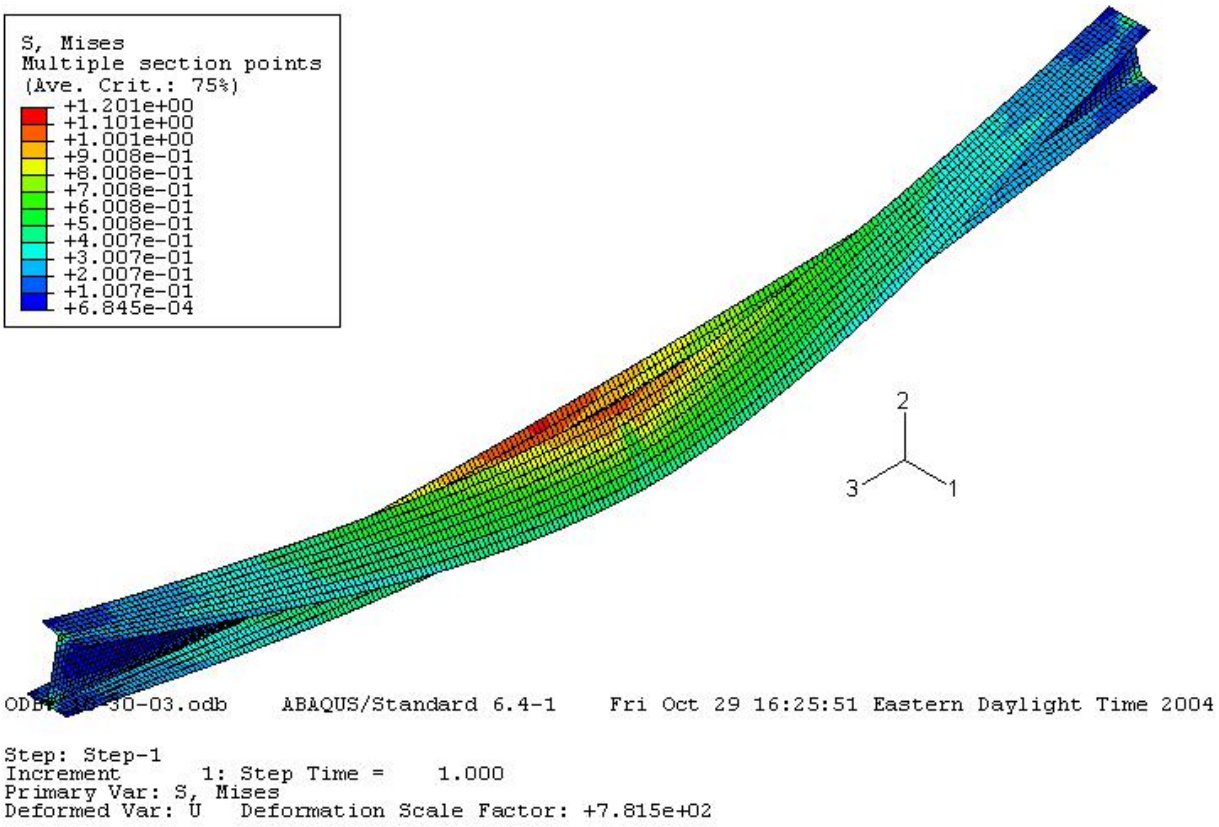

Figure 8: Deformed Shape of a Simply Supported Beam under Eccentric Loading

The plot developed by Galambos shows a curve of the location on the beam, z, divided by the total length of the beam versus a non-dimensionalized unit of the variation of the curvature.

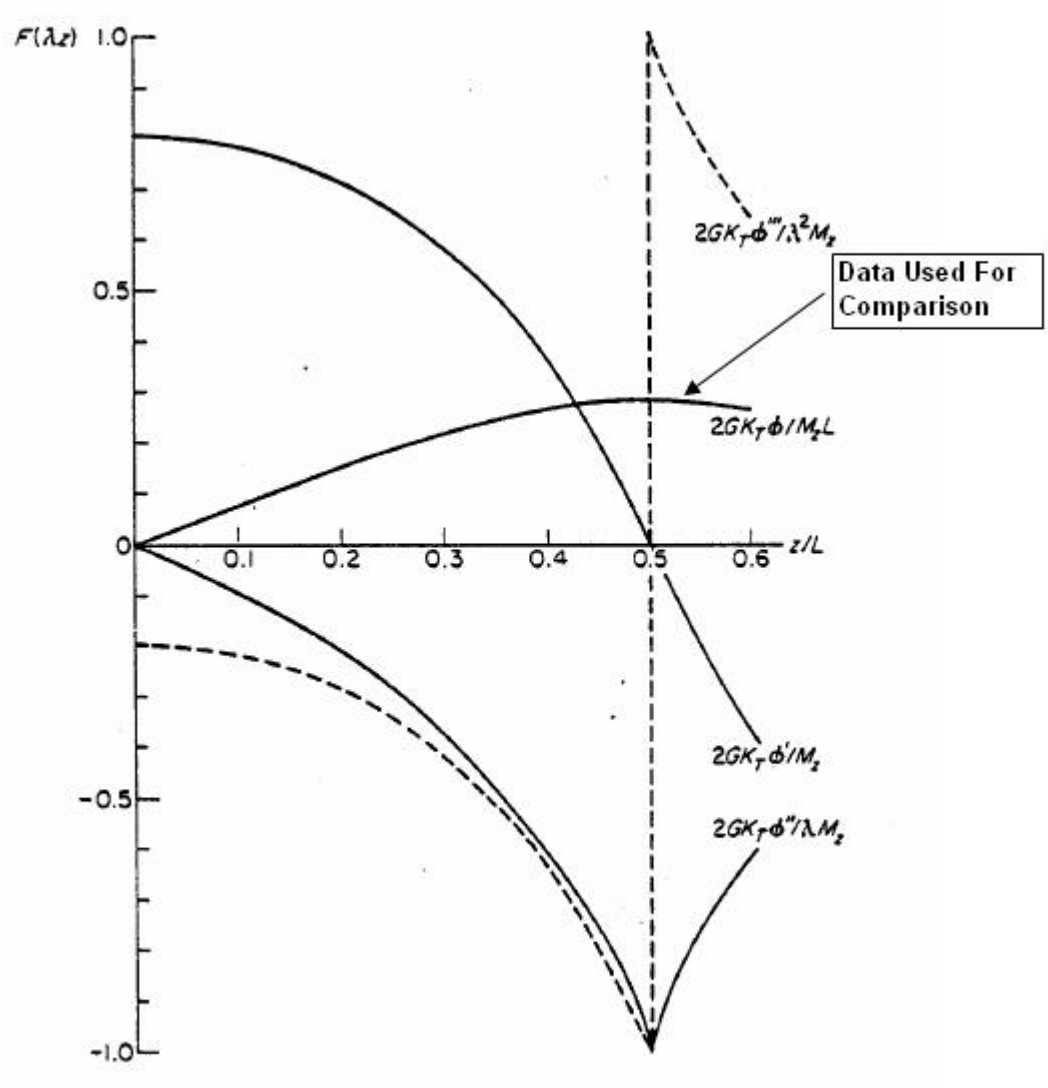

Figure 9: Variation of Angle of Twist and Derivatives Along Beam Length. (Galambos 1968)

Once the finite element model of the beam is built, it is important to duplicate this curve in order to verify that ABAQUS is providing accurate results. The rotation of the beam about the longitudinal, or z-axis, is exported from ABAQUS into Microsoft Excel. This rotation is reported at the intersection of top flange and web. The rotation, ϕ, is then non-dimensionalized in the same fashion as listed in the text. The rotation is multiplied by a unit-less factor of:

$$\frac{2GK_T}{M_z L}$$

Eqn. 3-3-2

which for this case yields a value of 174.4. The plot derived from the finite element analysis results is the following:

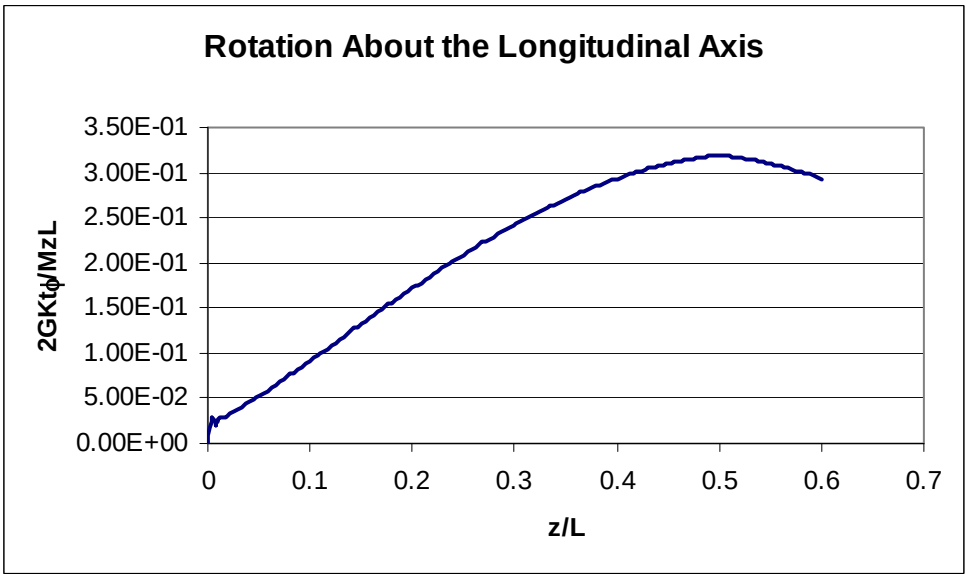

Figure 10: Rotation about Longitudinal Axis of W-Section Compared to Galambos' Plot

The maximum curvature achieved from the plot given in the text is approximately 0.30 radians. This value has been scaled off of the plot which was reproduced from the text. The finite element analysis results provide a maximum curvature of 0.319 radians. Therefore, the results of the verification study are satisfactorily showing that the ABAQUS finite element analysis software is a reasonable tool for producing models within an appropriate degree of accuracy for this study. The research will make use of the software to evaluate torsional deformations for

beams and columns in relation to their failure modes. Also, the models will be evaluated regarding the stresses relative to the theories presented.

4.0 FINITE ELEMENT MODELS

To support the existence of the Wagner Hypothesis, it is necessary to find compatibility between the results of finite element analyses, theoretical solutions, and experimental test results relative to the theory. A new second-order theory pertaining to thin-walled open-profile sections has been developed by Ojalvo in opposition to the classical theory that states when a bar is subject to an axial load and the section twists, the longitudinal stresses become inclined to the normal plane and produce a torsional moment in that plane. So that the classical theory may be verified, several different finite element models are created using the ABAQUS finite element analysis software so as to produce modeling results to compare with both second-order theories as well as experimental results. In making these comparisons, the validity of the competing theory presented by Ojalvo can be tested. The first model is similar to the verification study presented in the previous chapter. It is a doubly symmetric W-section that is loaded by a uniform moment across the length. A linearized-eigenvalue buckling analysis is performed on the model to find the critical buckling load; this value is then compared to the numerical solution applied to the W-section, which was provided by Galambos (1968).

Subsequent models are created to compare the new theories derived by Ojalvo to the classical theories further developed by Galambos. Along these lines, a second model is developed; a cruciform-shaped column that is axially loaded through the section's centroid. A linearized-eigenvalue buckling analysis is performed to capture the buckling mode of the column so that it can be utilized as an initial imperfection. This imperfection is then superimposed onto the column so that a postbuckling analysis can be performed to determine the critical buckling load of the structure. This value is compared to numerical solutions provided by both Galambos

and Ojalvo to determine whether the Wagner effect should be included in the second-order theories. The third and final finite element analysis is performed on a tee-shaped column that is loaded axially through a point of eccentricity. The consideration of these modeling results is essential since the cross-section is a mono-symmetric shape and thus offers the opportunity for important insights to be gained. The tee finite element analysis is performed in the same way that the cruciform is analyzed with an initial imperfection and a postbuckling analysis to determine the value of the critical buckling load. Not only are these results used for comparison with numerical solutions derived by Galambos and Ojalvo, but since the model is an analog to an actual experimental test specimen (Chen 1980); the results can be verified against the critical loads provided by the test results. The comparisons made in this chapter will give a solid indication as to whether the Wagner effect should be included in the second-order theories developed relative to the torsional behavior of open-profile thin-walled sections.

4.1 DOUBLY SYMMETRIC W-SECTION LOADED BY UNIFORM MOMENT

The finite element model that is used to verify that ABAQUS could achieve accurate results for this research is now modified to compare with theoretical equations provided by Galambos (1968). The model consists of a simply supported W12x50 section, which is specified as 240 inches in length. The cross-sectional shape has a flange width of 8.077 inches with a 0.641 inch thickness. The web depth is 11.5 inches with 0.371 inch thickness. The modulus of elasticity is given as 30,000 ksi, and the shear modulus is 11,500 ksi. The moment of inertia about the y-axis is 56.4 in^4, while about the x-axis the moment of inertia for the section is 394.5

in^4. The warping moment of inertia, I_w, is equal to 1,881 in^6 and the St.Venant torsion constant, K_T, is 1.82 in^4. The finite element model is built by defining node locations according to the shape of the beam and then filling in those nodes with elements to create a mesh with an aspect ratio of one-to-one. The element chosen for this model is an S4R shell element, and the element size is one square inch. This particular element gives accurate results while keeping the computational time of the models to a reasonable level. Along the outside middle lines of the cross-sections occurring at the member ends, rigid beam elements are placed between all nodes along the web to facilitate the imposition of idealized boundary conditions without producing unwanted warping restraint. With the use of the rigid beam elements, a single boundary condition can be placed at the mid-height of the section at either end of the beam. At one end the model is restrained against displacement in the x (stong axis), y (weak axis), and z (longitudinal axis) directions as well as rotation about the z-axis is prohibited. At the other end of the section, displacements in the x and y directions are restrained as well as the rotation about the z-axis. The rotation about the z-axis is restrained so that the model is able to twist at locations within the span length, while no twist is permitted to occur at the ends. The model is loaded at the boundary with a constant moment of 6000 kip-inches which grows according to the magnitude of a load proportionality factor that is determined as part of the nonlinear solution process in ABAQUS.

Owing to the fact that geometric or material nonlinearities may occur during the analysis of the section, a command line is included in the ABAQUS input deck to indicate whether these nonlinearities should be considered. For this analysis, the model uses 30 time increment steps and the results will include geometric nonlinearities that may arise during the model's execution; material nonlinearity is not considered. A static analysis is the contextual basis for the modeling

(i.e. the loads are applied slowly), and the Modified Riks method (ABAQUS 2003) solution technique is employed as part of the postbuckling analysis. The Modified Riks method is typically used to predict unstable, geometrically nonlinear collapse of a structure (ABAQUS 2003). There is an indication that the beam has reached the critical buckling load once a negative eigenvalue emerges in the numerical analysis (i.e. a negative eigenvalue is detected in the global stiffness matrix of the entire model). The occurrence of this first negative eigenvalue needs to also occur in the time step following the increment where it first appeared to ensure that the buckling mode is persisting (i.e. not subsequently eliminated by a reduction of the load proportionality factor). These eigenvalues are easily obtained from the message file produced by the analysis. The message file will give information regarding the progress of the solution as ABAQUS executes the file. It lists details including increment numbers, step times, equilibrium iterations, the load proportionality factor associated with the Riks analysis, etc. The load proportionality factor can be described as the fraction of the load that the model is seeing at a particular point in time, with the point in time being a specific increment. For this model, the first negative eigenvalue occurs at time increment nine, which corresponds to a load proportionality factor of 0.5025, or about fifty percent of the total load. This results in a critical buckling moment of 3015 kip-inches.

Galambos (1968) develops a theoretical result for this model. He states that the lateral-torsional buckling mode of a simple beam will develop a critical moment of:

$$(M_o)_{cr} = \frac{\pi n}{L}\sqrt{EI_y GK_T (1+\frac{n^2\pi^2 EI_w}{GK_T L^2})}$$

Eqn. 4-4-1

Setting “n” equal to one, the critical moment is calculated as 2978.52 kip-inches. The difference in the theoretical value and the result of the finite element analysis equals 1.2%, which proves that the finite element analysis results for this case are in definite agreement with the use of the Wagner Hypothesis.

4.2 FLANGED CRUCIFORM COLUMN LOADED BY AXIAL FORCE

A second finite element analysis is executed to further prove the validity of the Wagner Hypothesis. A flanged cruciform model presented by Ojalvo is utilized as the subject of this analysis. The column is a shape with length, L, and thickness, t; where t is very small when compared with its other dimensions. The area of the section is defined as $12td$, where d is the length of a flange piece. The depth and width of the cross-section are defined as $4d$. The polar moment of inertia, J, is defined as $4t^3d$, and both I_x and I_y are equal to $13.5td^3$. The warping torsion constant, I_ω, is $4/3\ td^3$. For the initial model, a trial thickness of $t = 0.1$ inches, a depth of $d = 6$ inches, and a length of $L = 240$ inches is used because actual dimensions were not provided by Ojalvo. Using these dimensions, the area of the section is 7.2 in^2, the polar moment of inertia is 0.024 in^4, both moments of inertia are 291.6 in^4, and the warping torsion constant is equal to 28.8 in^4. A graphical depiction of the cross-section is shown below:

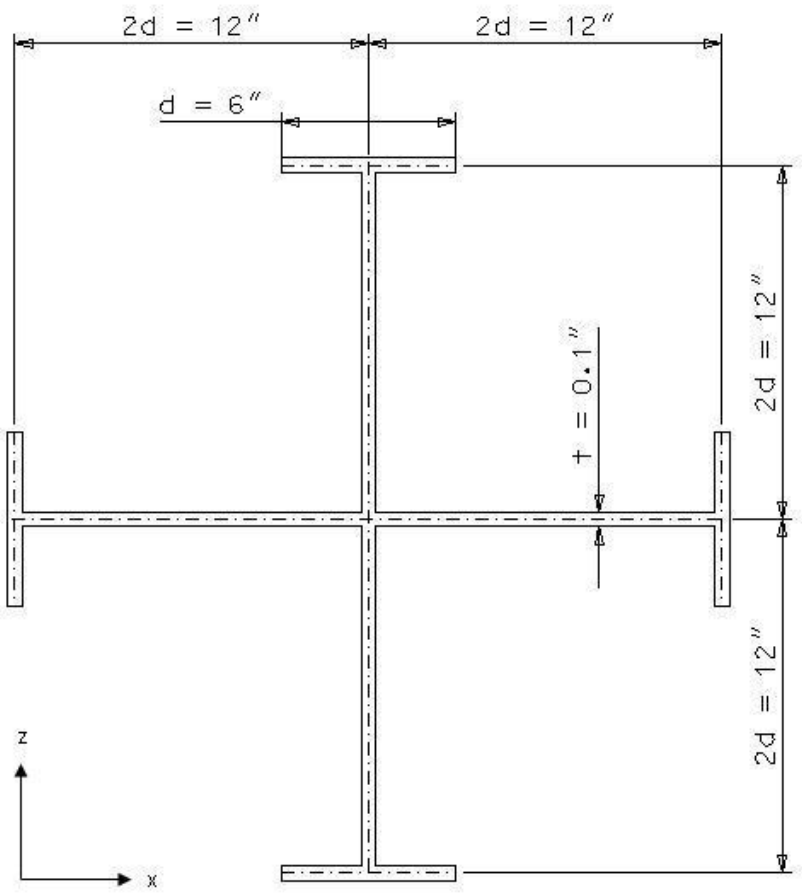

Figure 11: Cruciform Column Cross-sectional Dimensions

Because of the shape of the model, the two sections of the web and the four flanges are generated separately and then meshed together for the finite element analysis. The outline of the model is assigned nodes and then this outline is filled with nodes using the node generation command. The element generation is based on the specified nodes using an aspect ratio of one-to-one, with the element size being one square inch. The material properties for the cruciform model are assigned a modulus of elasticity of 29,000 ksi and Poisson's ratio of 0.3, which are typical properties of steel. Along the middle lines of the constituent plate surfaces at each end of the model, there are rigid beam elements placed between the nodes along the web members only

so that there is no warping restraint at the ends of the column. While it is that twisting of the members' ends is constrained, cross-sectional twisting within the span is unrestrained. These "rigid beam" elements are given a modulus of elasticity of 290,000 ksi and Poisson's ratio of 0.3. Since the outside surfaces are very rigid, the boundary conditions can be placed at the intersection of the two web sections at a single node location. At one end of the model, the column is restrained against displacements in the x, y, and z directions, and it is prohibited from twisting about the y-axis. At the other end of the column, the model is prevented from displacing in the x and z directions, as well as being restrained against rotation about the longitudinal y-axis. An axial compressive load of 100 kips was placed at the intersection of the two web sections at the top of the column; this is subsequently scaled according to the load proportionality factor. The model geometry required approximately 20,000 nodes and 18,000 elements. For comparison, this model is subject to a number of different analysis runs. The goal of this phase of the analysis is to compare the finite element results to the second-order theories provided by Ojalvo, as well as to provide plots of the load versus deflection so that the stability of the model may be evaluated.

The finite element analysis makes use of an imperfection file to account for initial imperfections in the model. Two analysis runs are performed: the first to arrive at the probable collapse mode, and the second to perform the postbuckling analysis. In the first analysis run a linearized-eigenvalue buckling analysis is executed on the perfect column to find the buckling mode and to ensure that the mesh discretizes those modes correctly. These results are written to a "node file" to subsequently be used as input into the postbuckling analysis as an initial displacement field. The imperfection is superimposed into the code using a single scale factor applied to the point of maximum displacement to define the maximum perturbation of the model,

and the amount of remaining imperfection inputted into the model is determined by relative scaling of the user input maximum at other locations. This scale factor is adjusted and evaluated to determine the structure's sensitivity to the imperfection seed. During the linearized-eigenvalue buckling analysis run, the model is set up to evaluate the first five buckling modes. For the first set of models, a series of scale factors was used ranging from L/100 to L/5000. As the scale factor becomes smaller, the imperfection also becomes smaller and the model parallels practical conditions. To utilize the imperfection command, the buckling mode retrieved from the linearized-eigenvalue buckling run must be inputted as well as the scale factor. The ABAQUS CAE pre- / post-processing software is used to look at each of the five buckling modes from the linearized-eigenvalue buckling analysis. Mode one corresponds to a twist about the longitudinal axis, and thus is used with the imperfection command as the seed displacement.

When the postbuckling analysis is complete, the ABAQUS CAE module is used to export the load proportionality factors as well as the rotation of the model about the y-axis (e.g. 2-axis in Figure 13). An Excel plot of the load versus deflection is then created for the model; this plot is used to study the torsional stability of the model. If the plot shows a smooth curve resembling the stability curves for an imperfect system, then the results are usable. The node located at the point of intersection of the two webs at the mid-height of the cruciform-shaped model is selected to provide the output of the load proportionality factors and rotations. The load versus deflection plot for this set of analysis runs shows various discontinuities in the rotation as the load approaches a critical value. As can be seen in the Excel plot below (See Figure 12), the curve does not resemble either of the stability plots that were discussed earlier in this text. Also note that while the shape of the plot is chaotic, there is no significant amount of deformation about the longitudinal axis. This discontinuity could be attributable to the fact the Modified Riks analysis

method is passing over the critical buckling load through its selection of load increments that are too large for the present investigation. This occurs when the model has an easy time converging during the solution process, and as a result permits the incremental load proportionality factors to grow large. By invoking the direct analysis parameter, the user may specify a constant load increment size and thus ensure that the critical load is not skipped. In addition, the ABAQUS CAE viewer is used to analyze the change in deformations as the model was stepped through the analysis.

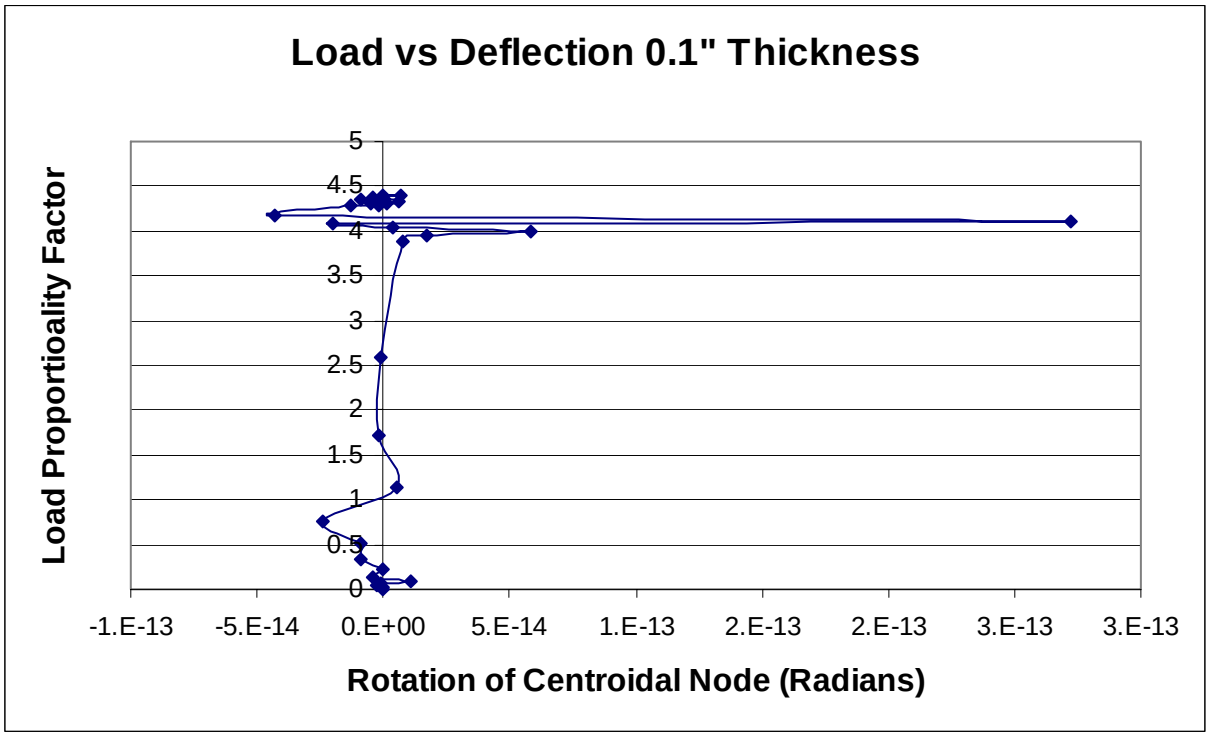

Figure 12: Load vs. Rotation for Section having t = 0.1

Through the use of ABAQUS CAE, it becomes obvious that the deformed shape exhibits the presence of local buckles along the length of the model (See Figure 13). This would cause

the local rotation of a node to be in the opposite direction in comparison to the global rotation of the model. At some locations along the length of the model, the local buckles caused the model to see a negative value for the rotation about the y-axis.

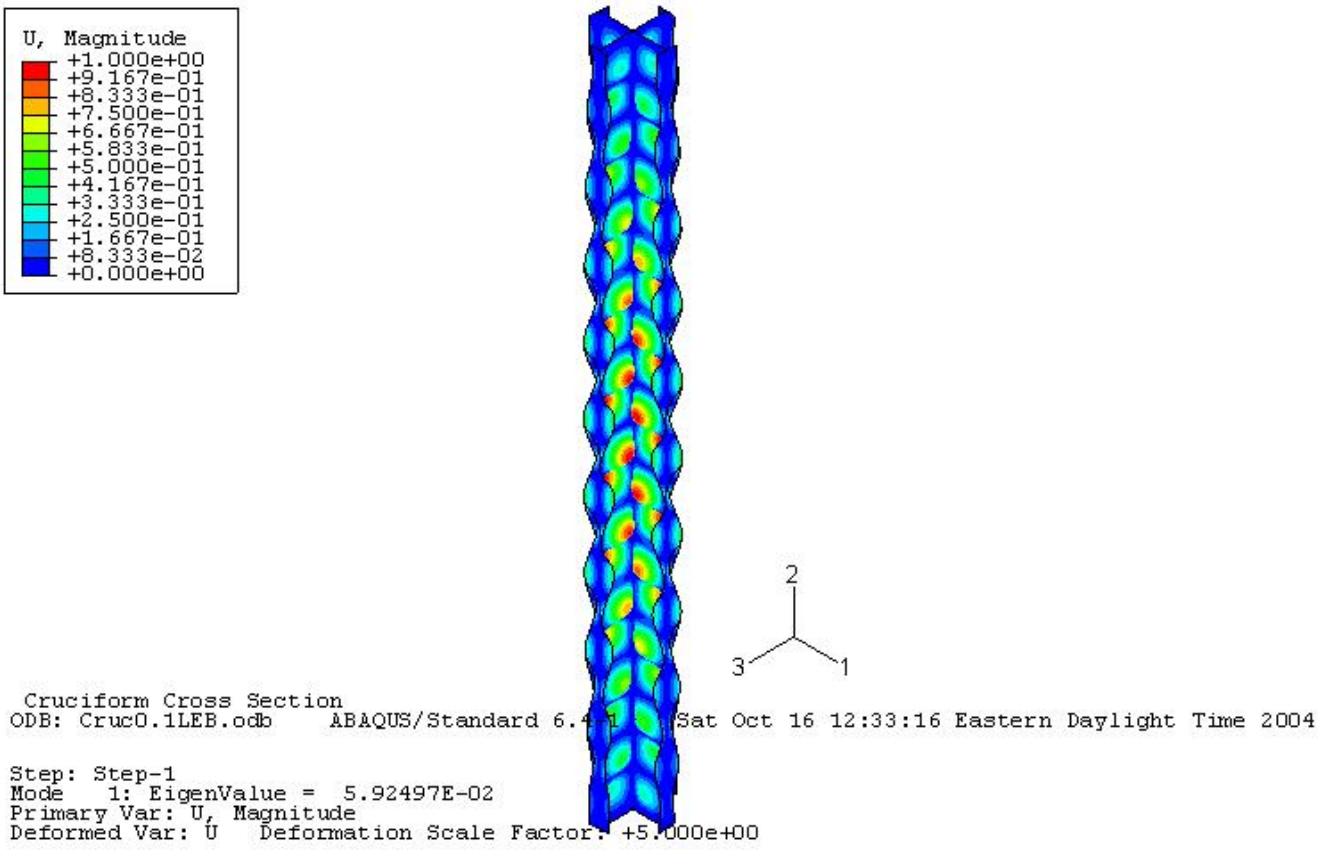

Figure 13: Mode 1 Deflected Shape of Cruciform Column Exhibiting Local Buckles

Once it is established that the occurrence of local buckles is causing the global critical load to be undetectable, it is necessary to re-evaluate the parameters of the model, and it is concluded that the thickness of 0.1 inches is not adequate for the column under consideration, and therefore the thickness of both the flange plates and web plates is increased to 0.25 inches. This increases the

area of the model to 18 in^2, the polar moment of inertia to 0.375 in^4, both moments of inertia to 729 in^4, and the warping torsion constant to 72 in^4.

When performing the finite element analysis on the cruciform-shaped column with the new thickness of 0.25", another linearized-eigenvalue buckling analysis is run to create the initial imperfection for the new model. After considering the five buckled shapes provided by the analysis, it is concluded that the mode 1 buckled shape should be used with a scale factor of L/1000 (the maximum out-straightness permitted by current steel design specifications) in the postbuckling analysis. The mode 1 buckled shape is shown below:

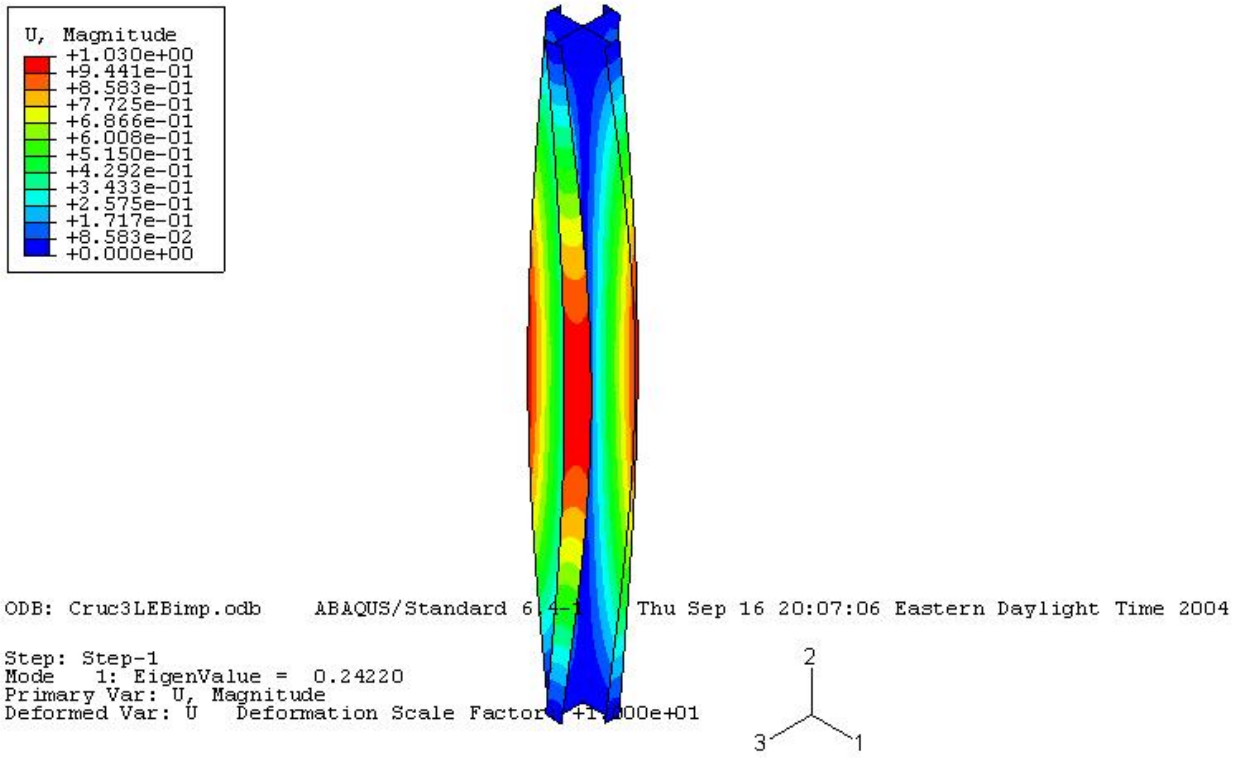

Figure 14: Mode 1 Buckled Shape of Cruciform Column with 0.25" Thickness

The image provided by the ABAQUS viewer shows the column experiencing a torsional deformation; with the section twisting once along the length of the column (i.e. torsional mode 1). This imperfection is superimposed into the postbuckling analysis; subsequently leading to the torsional buckling mode of failure seen in the following ABAQUS screen capture (from the postbuckling analysis):

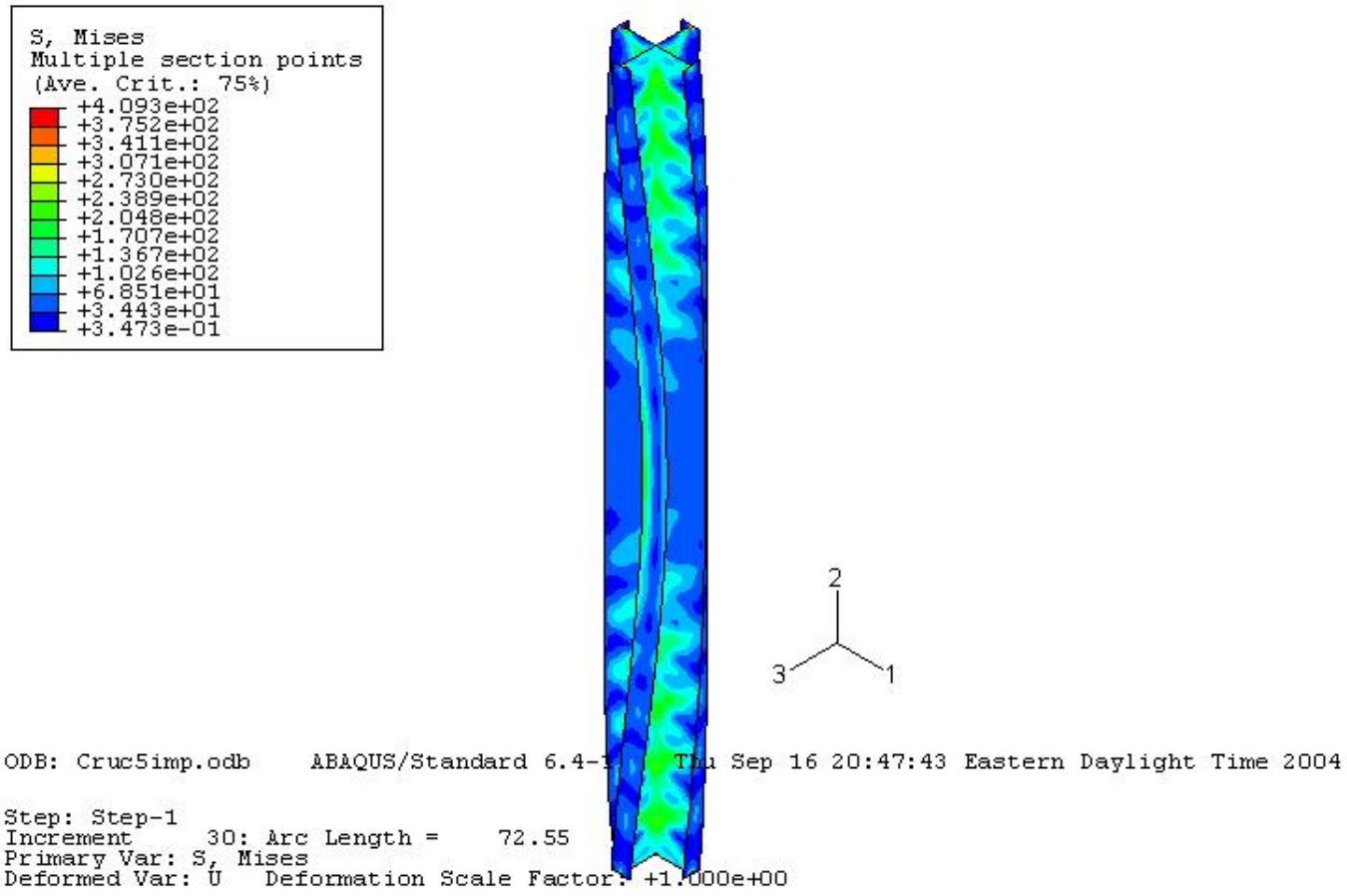

Figure 15: Postbuckled Shape of Cruciform Column with Scale Factor of L/1000

A plot of the load versus deflection verifies that the model is responding to the axial load as it should (See Figure 16). It can be seen that as the load increases so does the rotation of the model, which is consistent with intuition.

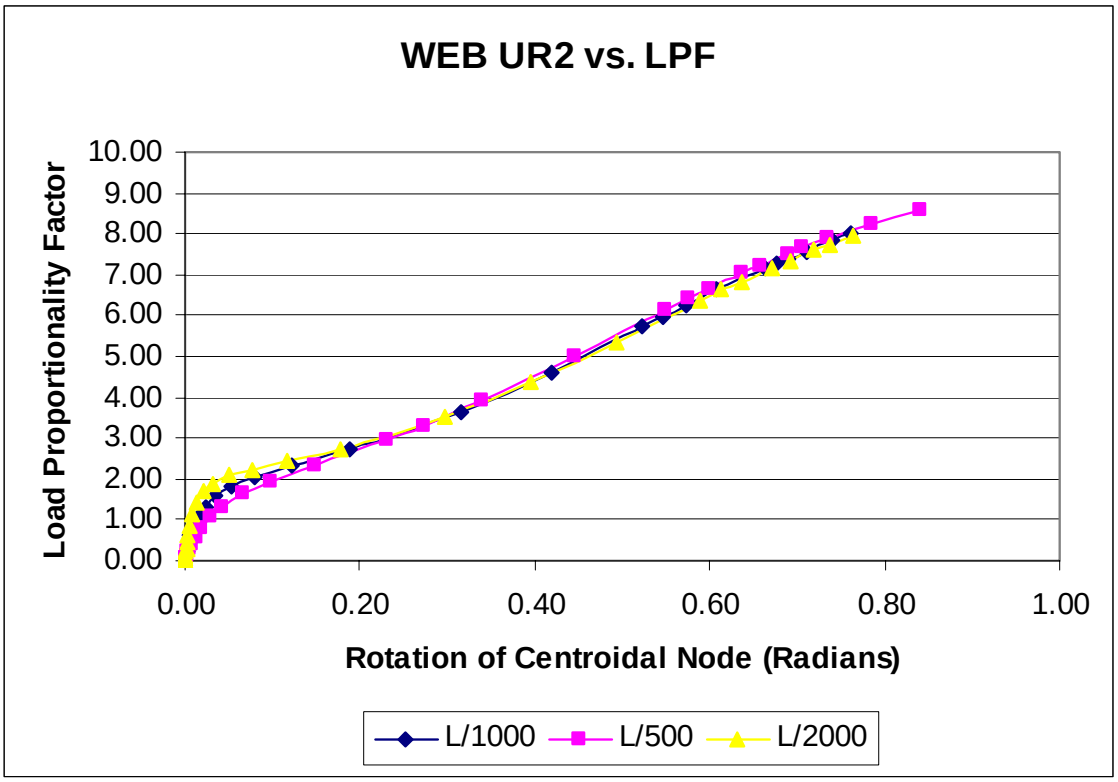

Figure 16: LPF vs. Rotation about Longitudinal Axis for Web Intersection at Mid-height

This plot also demonstrates the relative stability of the model; it can be stated that the model follows a curve such that after the member reaches a critical load, the member continues to be loaded and shows the capacity to resist additional load (i.e. stable postbuckling response). The modeling results indicate that the cruciform-shaped model possesses a critical load of 206.75 kips. This is extracted from the Excel plot at the point where the graph begins to turn and display a dramatic increase in the twisting deformation. These results are reasonable because the

deformed shape of the postbuckling analysis exhibits a purely torsional mode of failure (See Figure 15).

The form of the classical second-order theory pertaining to the cruciform case appears as:

$$P_\theta = \frac{A}{I_0}\left(GJ + EI_\omega \frac{\pi^2}{L^2}\right) = \frac{16}{9}G\frac{t^3}{d} + \frac{16}{27}E\frac{\pi^2}{L^2}td^3$$

Eqn. 4-4-2

Ojalvo, however, rejects the Wagner Hypothesis, as implied in the foregoing equation, and thus states that buckling of a cruciform, that is purely torsional, is fictitious and thus not covered by his new theory. He then assumes that the cruciform will behave in the same way that four tee-columns buckling simultaneously would respond to an axial compressive loading. The critical buckling load is then given as:

$$P_\theta = \frac{4}{a^2}\left[GJ + (EI_\omega + EI_y\{2d^2\})\frac{\pi^2}{L^2}\right] = \frac{9}{4}G\frac{t^3}{d} + \frac{3}{4}\frac{\pi^2}{L^2}Etd^3$$

Eqn. 4-4-3

When evaluating these two equations numerically, based on the dimensions of the model used for the finite element analysis, the critical buckling load calculated using the classical theory is equal to 210.65 kips; using the new second-order theory developed by Ojalvo the critical buckling load for the cruciform-shaped column is equal to 266.60 kips. The calculations that were performed to arrive at these results can be found in Appendix C2. It is obvious that when comparing the critical load resulting from the finite element analysis, to the critical loads

calculated from both second-order theories that the numerical solution that takes Wagner's effect into account is in closer agreement with the finite element analysis results.

In order to address the notion of whether or not the principal stresses within a structural member form a helix when the member is subject to a torsional failure mode, a graphical representation is made in ABAQUS to show the inclination of the principal stresses.

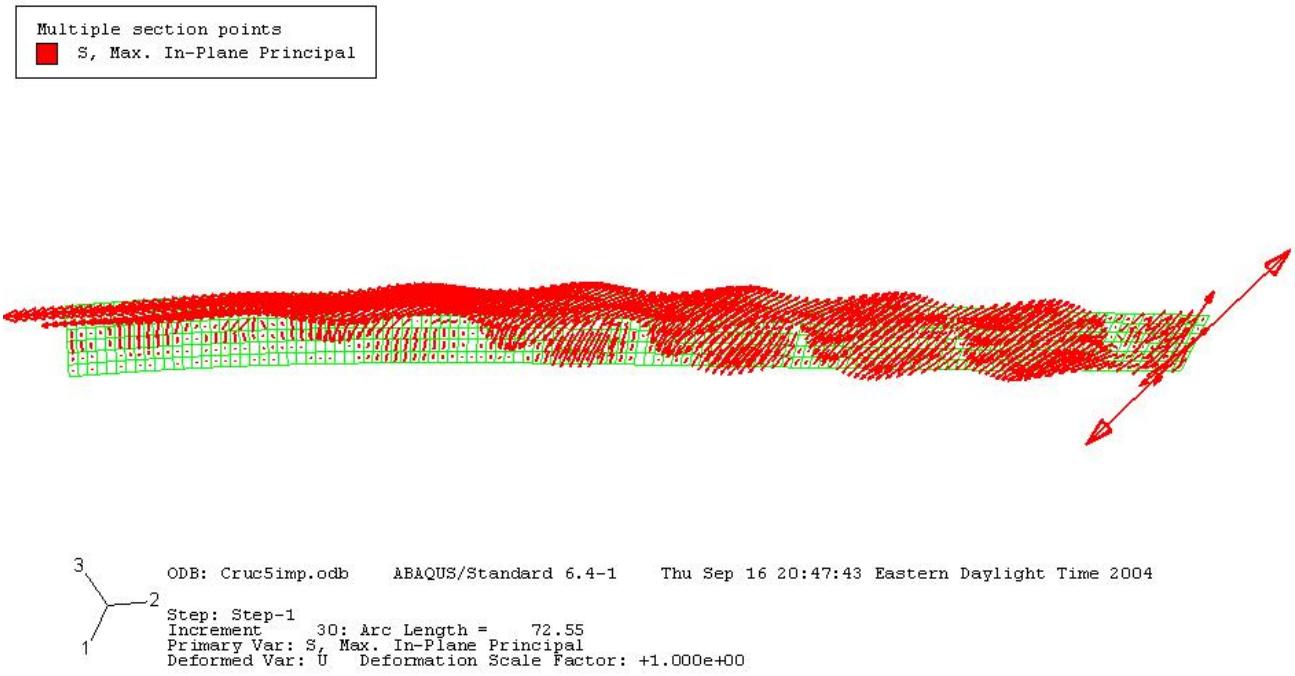

Figure 17: Maximum Principal Angle on Upper Half of Flange on Cruciform-Shaped Column

The screen capture shown above gives a plot of the maximum principal stresses on one of the flanges of the cruciform model. This plot shows elements from the top of the column to the mid-height only. The screen capture exhibits the column in the final step of the analysis under a maximum loading. It is obvious that the stresses are forming a helix type shape, yet it is necessary to verify the graphical representation numerically. The finite element analysis is used

to extract both the normal and shear stress for each element along a strip of elements in the flange to a data file. The flange used in this portion of the analysis lies in the 1-2 plane using the coordinates specified by ABAQUS; or in other words the x-y plane. In addition, the rotation about the 3 or z-axis for the same strip of elements is used. The normal and shear stresses are used to calculate the inclination of the principal plane, and then this value is plotted in addition to the rotation about the z-axis for the entire length of the column. The equation used to compute the angle of inclination of the principal stress, θ_p, is the following:

$$\tan 2\theta_p = \frac{\tau_{xy}}{(\sigma_x - \sigma_y)/2}$$

Eqn. 4-4-4

The calculations used for the following Excel plot are found in Appendix D1. The Excel plot depicts the inclination of the principal angle of each element along the length of the column in addition to the rotational deformation of each element in the same planar section.

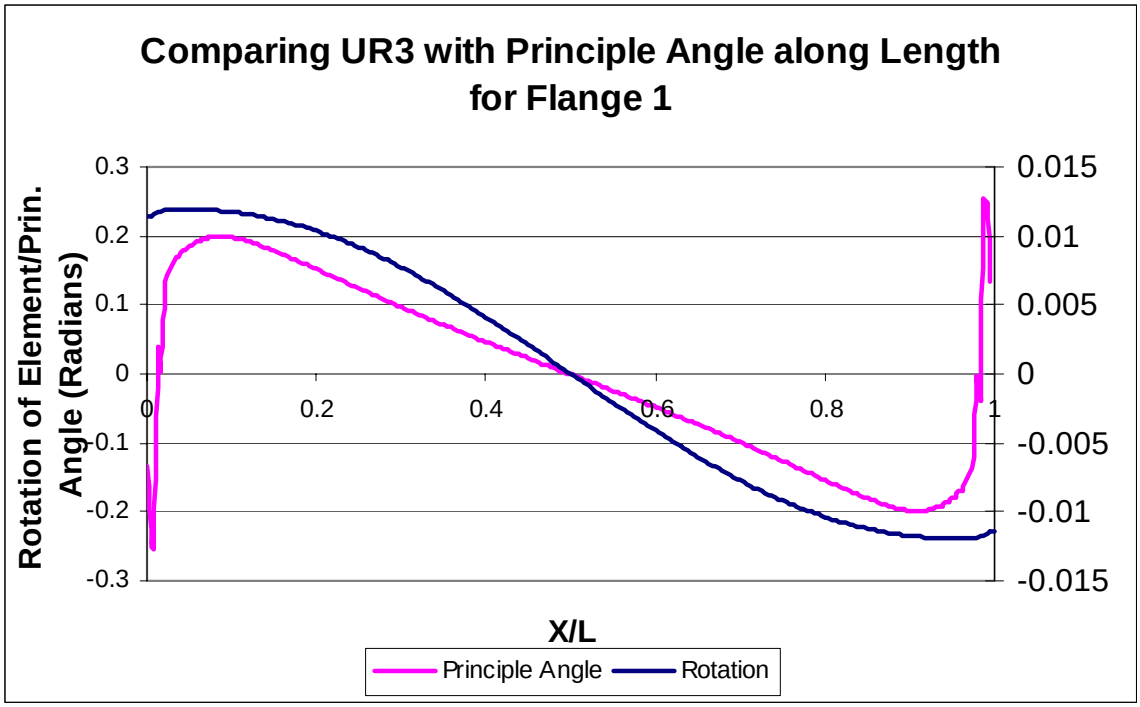

Figure 18: Principal Angle and Rotation about Z-Axis along Length of Cruciform

By examining the plots shown in Figure 18 it is concluded that the maximum principal angles are in fact forming a helix that follows the deformed shape of the column. This agrees with the graphical representation extracted from ABAQUS, and further verifies that the classical second-order theories including Wagner's effect are valid. Due to the fact that the plots do not match exactly, it is possible that the results are somewhat at odds with the Wagner Hypothesis. It is important to note that Wagner's Hypothesis was developed based on the idea of fiber orientation. Galambos' development of the theory does not rely heavily on the concept of fibers, and furthermore steel is a homogeneous material, which is not comprised of a bundle of fibers. This may account for the difference in the plot shown in Figure 18. Wagner's Hypothesis is valid based on the fact that the results follow the trend of the theory. For the cruciform model, the use of Wagner's effect is credible based on agreement between numerical solutions and finite

element analysis results relative to the critical buckling load as well as the existence of the helical pattern of the principal stresses shown in Figure 17.

4.3 TEE COLUMN LOADED BY ECCENTRIC AXIAL COMPRESSIVE FORCE

The final phase of modeling performed for this project involves a finite element analysis of a column with a tee-shaped cross-section. The tee is also considered an open-profile thin-walled shape, and was considered directly by Ojalvo in his alternate formulation. Ojalvo makes reference to Shao-Fan Chen's (1980) experimental testing (Ojalvo 1990) of 24 tee-shaped beam-columns in order to make comparisons between failure loads and flexural-torsional buckling loads. The tee section is a mono-symmetric shape and thus provides additional background for comparison beyond the doubly symmetric cases already considered. The experimental tee specimens were loaded eccentrically and thus the present discussion follows suit. This eccentric loading condition represents a departure from the other finite element analyses that are used for analysis within the scope of the current research in that they were loaded with a concentric load. Within the text of "Lateral-Torsional Buckling of T-Section Steel Beam-Columns", Chen (1980) notes that when a tee section is acted on by an eccentric compressive load, there are two locations where the section may be loaded: the section may be loaded with either a positive or negative eccentricity. The positive eccentricity case is characterized as when the load is placed on the flange-side of the centroid, and the negative eccentricity is when the load is placed axially on the web-side; as shown below:

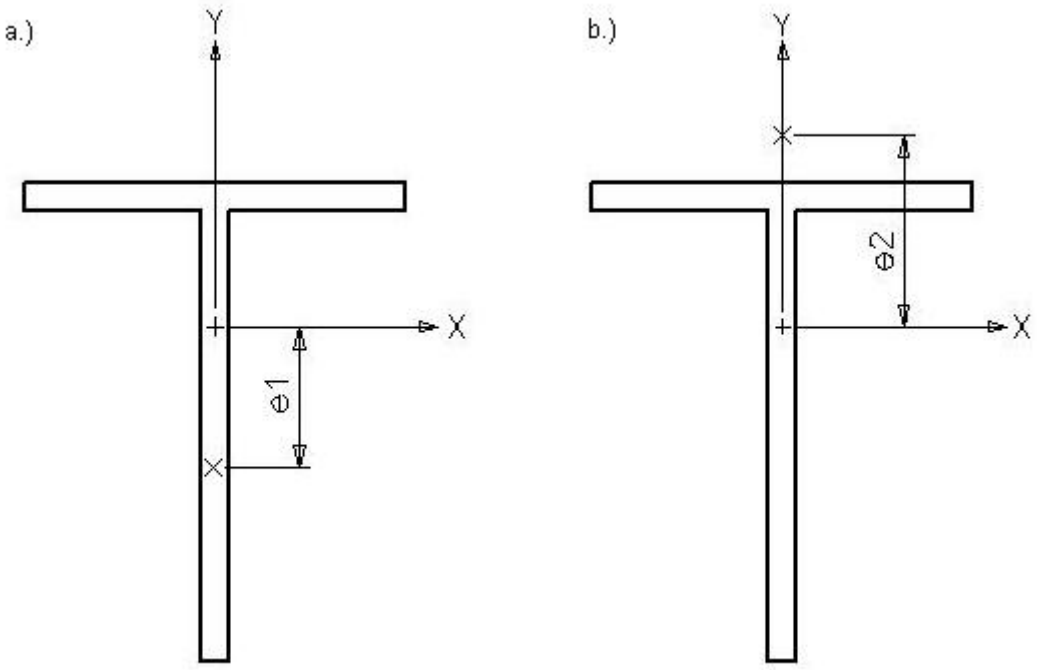

Figure 19: a) Negative Eccentricity b) Positive Eccentricity

The results presented for the 24 experimental specimens of different cross-sectional dimensions and lengths are presented in the paper by Chen (1980). There are some columns that fail due to local buckling, some that fail due to in-plane instability, and others that fail due to lateral-torsional buckling. The section that is used for the finite element analysis was chosen from the specimens that failed in a lateral-torsional mode: specimen PD3-1. The other cases were not within the scope of the current study. The column selected is comprised of two steel plates with flange dimensions of 102 millimeters in width by 7.7 millimeters thick. The web plate measures 121 millimeters in depth and 7.7 millimeters in thickness. The total column length is 2322 millimeters, and the area of the cross-section is listed as 1717 mm^2. Chen (1980) states that extreme care was taken to achieve the most accurate experimental results possible.

The specimen is made of low carbon steel, marked AD3 by the manufacturer, with a yield stress reported by Chen (1980) as 2910 kg/cm^2.

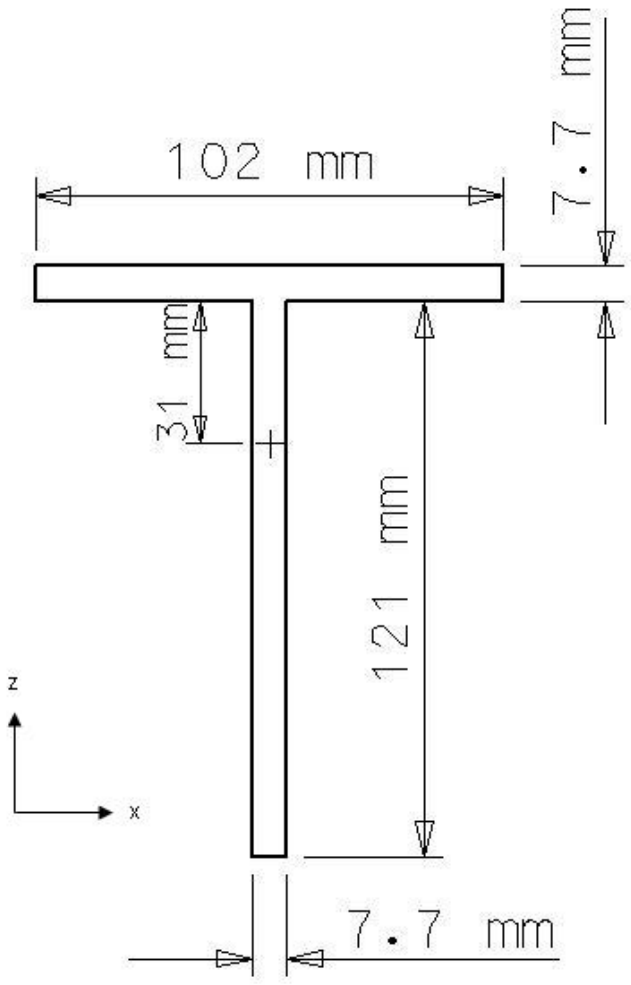

Figure 20: Metric Dimensions of Tee Cross-section

The experimental tests were performed in the Constructional Structure Laboratory of the Xian Institute of Metallurgy and Construction Engineering in Xian, Shaanxi, China. The loading installation consisted of a loading frame and hydraulic jack, and the test specimens were hinged at both ends with double knife-edge bearings. The center of the hinge coincided with the load

application point, and the knife-edge of the upper end bearing was fixed to the frame girder with bolts, while the lower bearing rested on the hydraulic jack (Chen 1980). The specimens were initially aligned by the marks on the end plate and then the column was loaded to approximately one-third of the failure load. At this stage, the column was further aligned so that two strain gauges placed symmetrically on the flange would provide equal readings; the ratio between the strain gauges placed on the flange and the web, in conformity with the eccentricity ratios provided for the section, were also monitored. The eccentricity ratio is defined by Chen to be:

$$\varepsilon = \frac{e * A}{S}$$

Eqn. 4-4-5

where ε is the non-dimensional eccentricity ratio, *e* is the position of the eccentricity, *A* is equal to the area of the section, and *S* is the elastic section modulus. Chen reports the eccentricity ratios for the experimental specimens instead of the actual location of the eccentricity. The test setup and experimental results provided by Chen (1980) were utilized in the construction of the finite element models. The theoretical equations provided by Ojalvo and Galambos are used to compare with the finite element analysis results in conjunction with the experimental results from the paper by Chen (1980). This part of the finite element analysis provides for very reliable conclusions due to the possibility of agreement between experimental results, finite element analysis results, as well as numerical results based on theories including (and excluding) Wagner's hypothesis.

The finite element model built using ABAQUS was formed using English units; therefore all of the dimensions were converted from metric to English. The flange plate measures 4.02"

wide by 0.303” thick, while the web plate measures 4.76” deep by 0.303” thick; the length of the column is 91.42”.

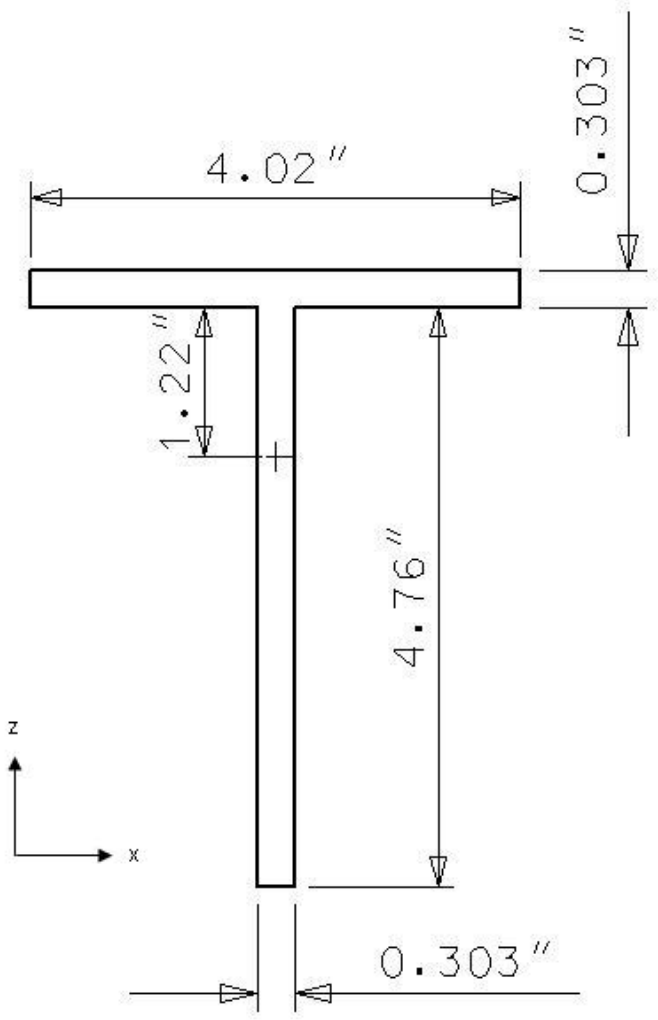

Figure 21: English Dimensions of Tee Cross-section

The model is developed in the same fashion that the other models are built. Nodes are specified to form the outline of the section, and the input file generates nodes and elements within that outline to create the mesh. The aspect ratio used for the elements is one-to-one as defined previously, and the element size is 0.9142 in. by 0.9142 in. The entire model uses approximately 1300 nodes and 1200 elements, with the element type being the S4R shell element from the

ABAQUS library. As with the other models analyzed for this project, rigid beam elements are superimposed at either end of the model, along the flange and web faces, to facilitate imposition of the boundary conditions without imposing warping restraint. The model is restrained against St. Venant's torsion at its ends.

The experimental tests were setup so that the load was placed at the point of eccentricity as well as the boundary conditions. However, according to the theoretical modeling approaches presented by Galambos and Ojalvo, the load must be placed at the point of eccentricity and the boundary conditions should be located at the centroid of the finite element model so as to facilitate a useful comparison. This applies to all open-profile shapes. In order to achieve results that would closely parallel the theory, the model is analyzed with the load at the specified eccentricity and the boundary conditions at the centroid of the section. Within the text of Chen's paper, the eccentricity was given in the form of the eccentricity ratio presented above (See Eqn. 4-5). The eccentricity ratio for the specimen of interest, PD3-1, was given as -1.55; this is a unitless value. Using the area, *A*, of the section and the elastic section modulus, *S*, the eccentricity of the model was found to be 2.52" from the shear center, which is located in the center of the flange plate. For the finite element analysis, an arbitrary axial compressive load of 10 kips is placed at this point (the reader will recall that a load proportionality factor will be applied to this reference load to suitably scale its magnitude during the nonlinear solution process). The boundary conditions are positioned at the centroid of the model, with the bottom of the model restrained against displacements in the x, y, and z-directions; with the rotation about the longitudinal axis prevented at that point. At the top of the column, the model was restrained against displacements in the x and z-directions in addition to the rotation about the y-axis.

The analysis is run using the Modified Riks method of analysis using an imperfection seed for the postbuckling analysis. An ABAQUS buckle file is run analyzing the first five buckling modes to locate the appropriate buckling shape for superposition onto the column as an initial imperfection. Using the CAE viewer, the buckling mode shapes could be evaluated and mode 1 was chosen as the appropriate shape (See Figure 22).

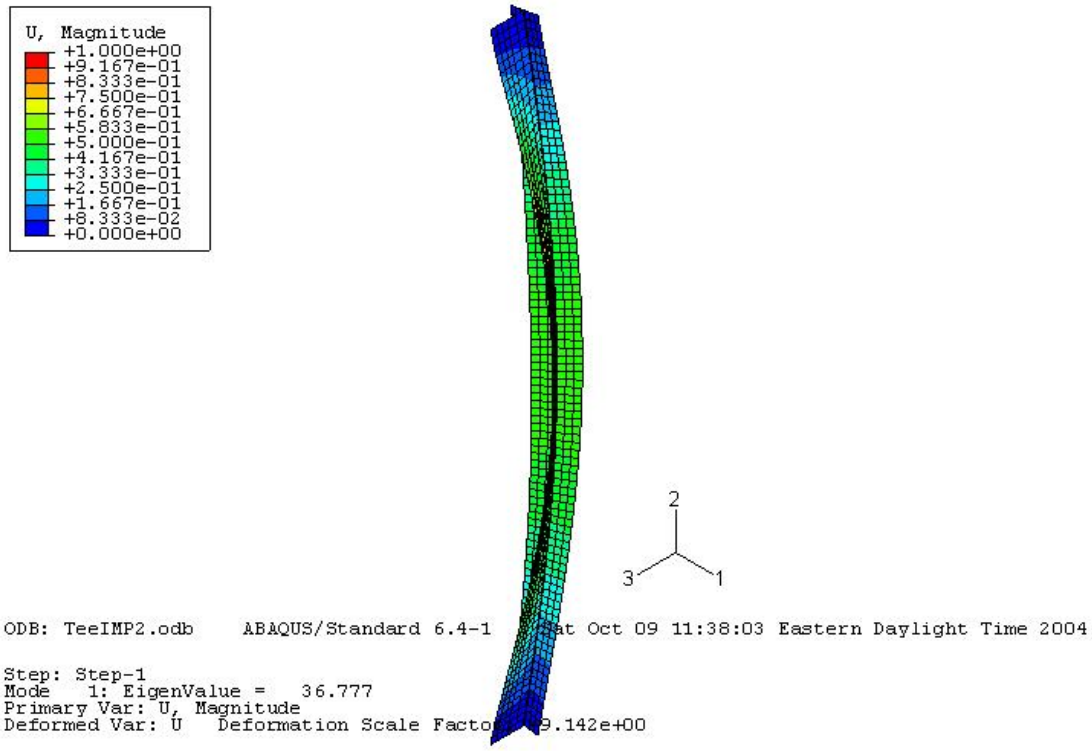

Figure 22: Mode 1 Buckled Shape of Tee Model at Scale Factor L/1000

The postbuckling analysis is run using this mode with multiple scale factors ranging between L/500 and L/5000. The message file produced by ABAQUS lists the eigenvalues for each increment of the analysis. The first occurrence of a negative eigenvalue indicates the increment where the critical load for the model is achieved. According to the message file, the critical load

occurs at increment 18, which corresponds to a load proportionality factor of 3.729, or a critical buckling load of 37.29 kips. This is the load at which the column begins to buckle. When looking at the shape in CAE, it is obvious that the tee shape is experiencing lateral-torsional buckling (See Figure 23); this is in agreement with the results of the experimental test column.

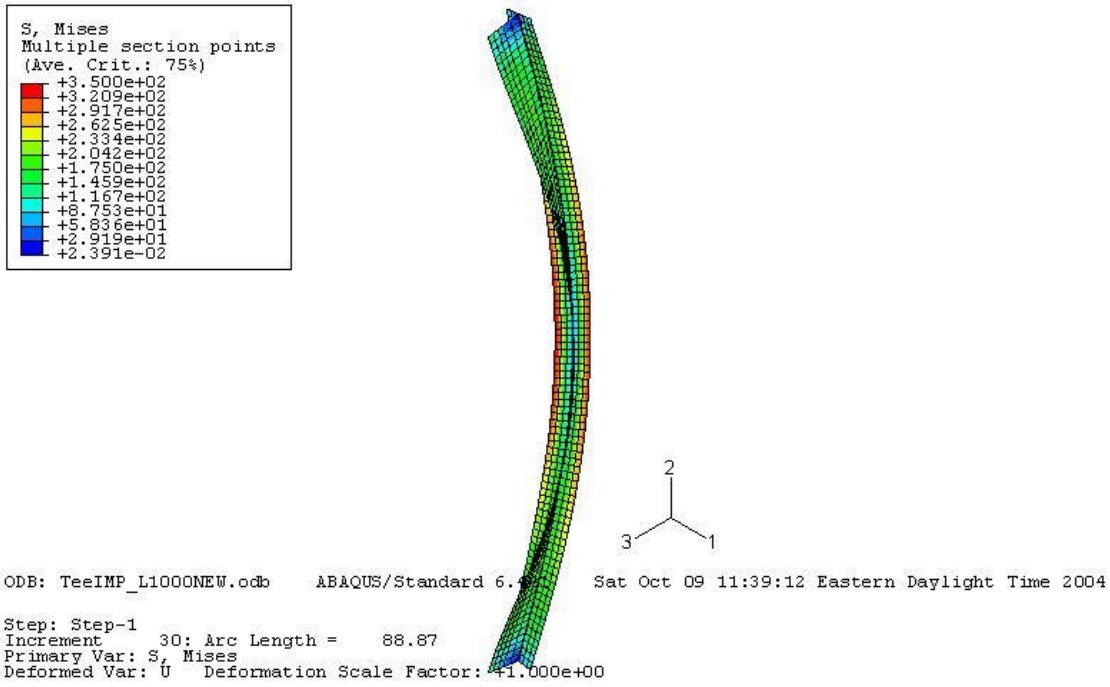

Figure 23: Postbuckled Shape of Tee Model at L/1000

To verify that the critical buckling load is captured, a plot of the load proportionality factors versus the rotation about the y-axis gives a critical load of approximately 37 kips shown below. It is important to utilize a number of scale factors to ensure that as the scale factor becomes smaller, the column parallels a perfect member. It is obvious from the plot that as the scale factor is decreased towards L/5000, the load versus deflection becomes more flat. This behavior

is representative of the effect of smaller initial imperfections and approaches the behavior of a "perfect" column.

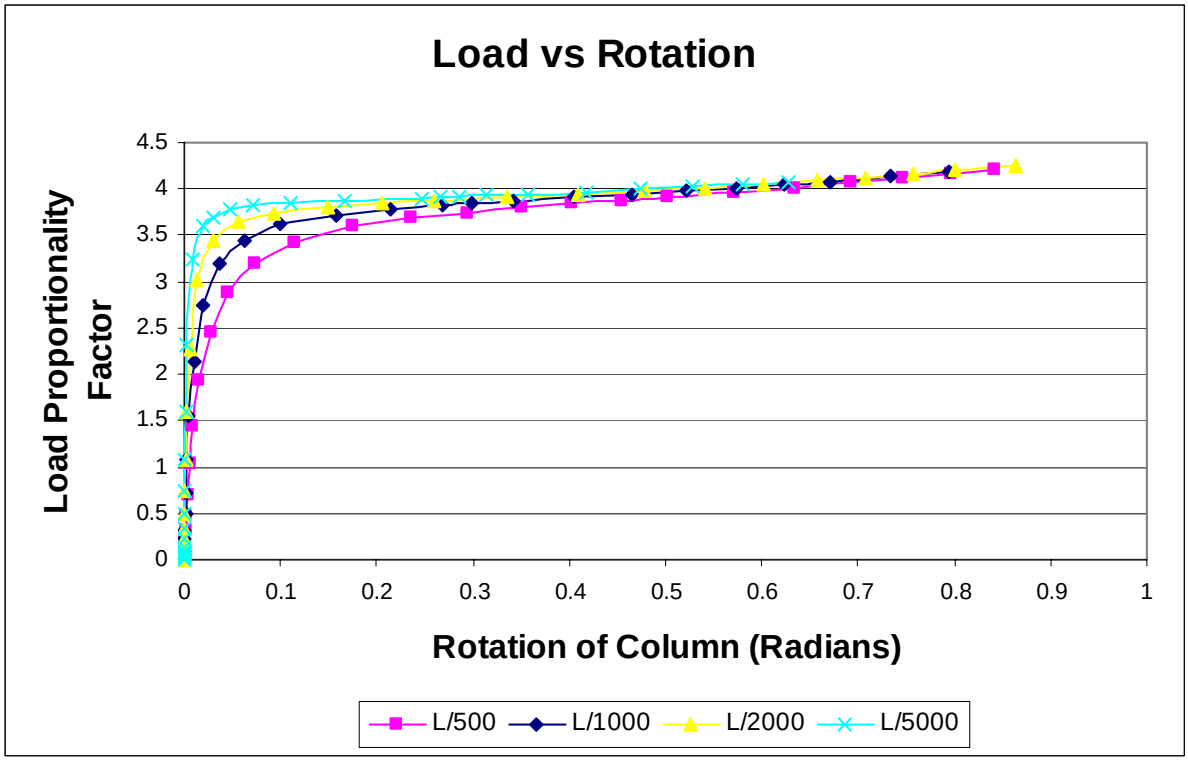

Figure 24: Load vs. Rotation for Tee Section for Various Scale Factors

Once it is established that the model is behaving as a column should according to stability theories, there is confidence established in the analysis.

In order to determine whether Wagner's Hypothesis is valid for the open-profile thin-walled section, the critical load must be calculated using both theories and then compared to the experimental results as well as the finite element analysis results. The equation provided by Ojalvo does not make use of Wagner's hypothesis and is equal to the following:

$$F(P) = P^2(1 - \frac{e}{y_0}) - P(P_y + \tilde{P}) + P_y \tilde{P} = 0$$

Eqn. 4-4-6

where,

$$\tilde{P} = \frac{(k^2 EI_{\tilde{\omega}} + GJ)}{ey_0}$$

Eqn. 4-4-7

The critical load found utilizing this equation is equal to 44 kips. The calculations performed to arrive at this result are included in Appendix C3. The equation provided by Galambos, which does make use of the Wagner Hypothesis, is presented as the following:

$$(P_y - P)(r_0^{\ 2} * P_z - P * r_0^{\ 2} + M_0 * \beta_x) = (M_0 + P * y_0)^2$$

Eqn. 4-4-8

where,

$$\beta_x = \frac{\int_A y(x^2 + y^2)dA}{I_x} - 2y_0$$

Eqn. 4-4-9

$$P_y = \frac{\pi^2 EI_y}{L^2}$$

Eqn. 4-4-10

and

$$P_z = \frac{P_y + GK_T}{r_0^{\,2}}$$

Eqn. 4-4-11

Calculating the critical load using these theoretical equations (Eqn 4-7), the buckling load is found to be equal to 39 kips (See Appendix C3). When converting the critical load stated in the results given in Chen's paper, the load is equal to 37 kips. The finite element analysis gives a result of 37.29 kips, and therefore it is shown that the finite element analysis is in good agreement with the experimental results, which are both in agreement with the theoretical results derived from Galambos' equation for the critical load. This series of finite element models also confirms that the Wagner effect should be included in the second-order theories used to compute critical buckling loads of thin-walled open-profile sections.

It is important to note that Ojalvo had analyzed the tee results provided by Chen (1980) (Ojalvo 1990). His results are not consistent with the results achieved from the finite element analysis or the experimental results presented by Chen (1980). In an attempt to duplicate Ojalvo's derivation of the critical buckling load, the equations presented were worked and an error in that derivation does exist. This possibly explains the inconsistent results that Ojalvo's second order theory provides when compared with the finite element results.

So as to further prove that the Wagner effect does exist for mono-symmetric cross-sections, the direction of the principal stresses for the model need to be evaluated. As in the case of the cruciform section, ABAQUS was used to look at a graphical representation of the inclination of the maximum principal stresses (See Figure 25).

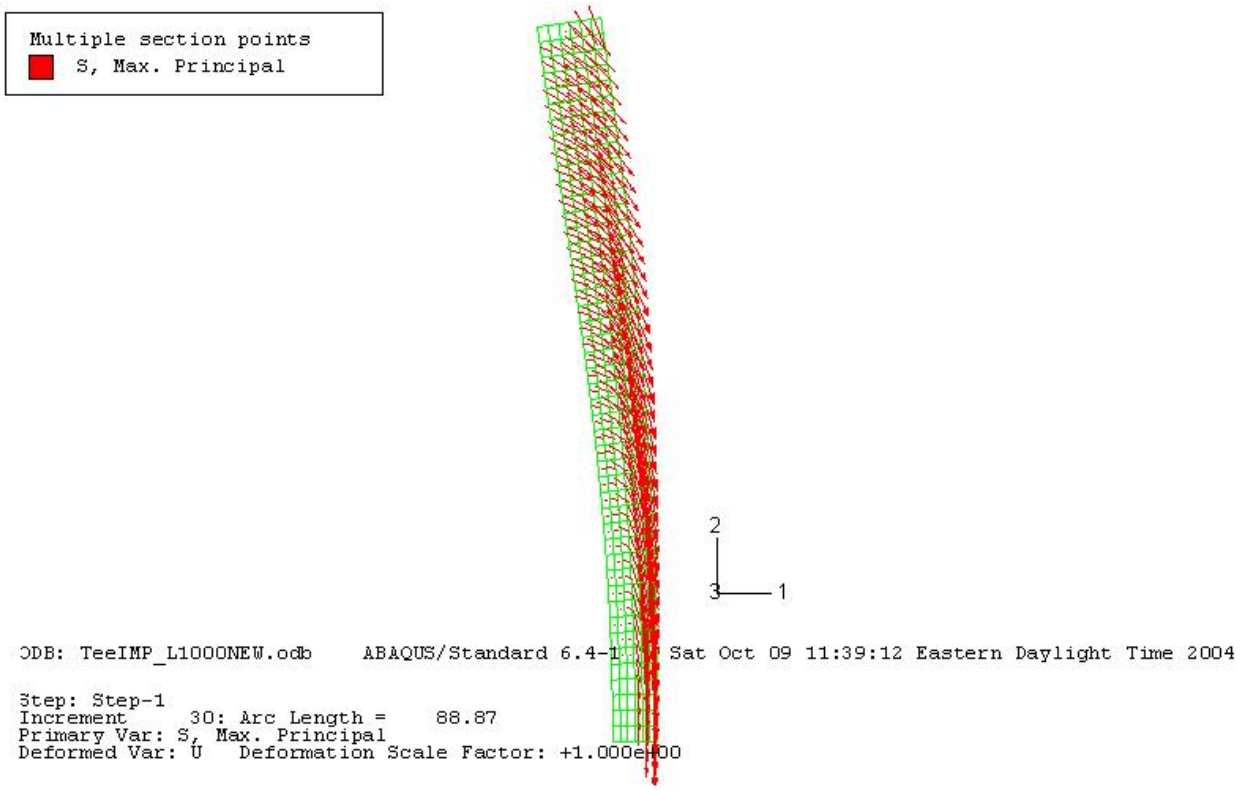

Figure 25: Maximum Principal Angles on Tee Flange Section

Note that the graphic shown in Figure 25 is the upper half of the flange section of the tee. By interpreting the graphical representation, it is obvious that the direction of the principal stresses follows the geometry of the deformation of the member. So that the reliability of the ABAQUS interface could be verified, it was essential to use the normal and shear stresses on each element to calculate the inclination of the principal plane in the same way that it was calculated for the cruciform section. This would prove numerically that the graphics are accurate. To calculate the inclination of the principal plane, it was coded into the input file that when the analysis was executed, a list of the normal stresses would be printed to the data file produced by the postbuckling analysis. Then using mechanics of materials principles, the angle is calculated

using the normal and shear stresses from each element (See Eqn. 4-4). These computations are included in Appendix D2. An Excel plot was then created including the principal angles along a strip of elements extracted from the flange of the tee, as well as the rotation about the z-axis for the same strip of elements along the length of the column at approximately 25% of the load, or increment 11 of the analysis (See Figure 26). This twist will correspond directly to the plane in which the inclination of the principal angles exists and therefore a direct relationship can be formed.

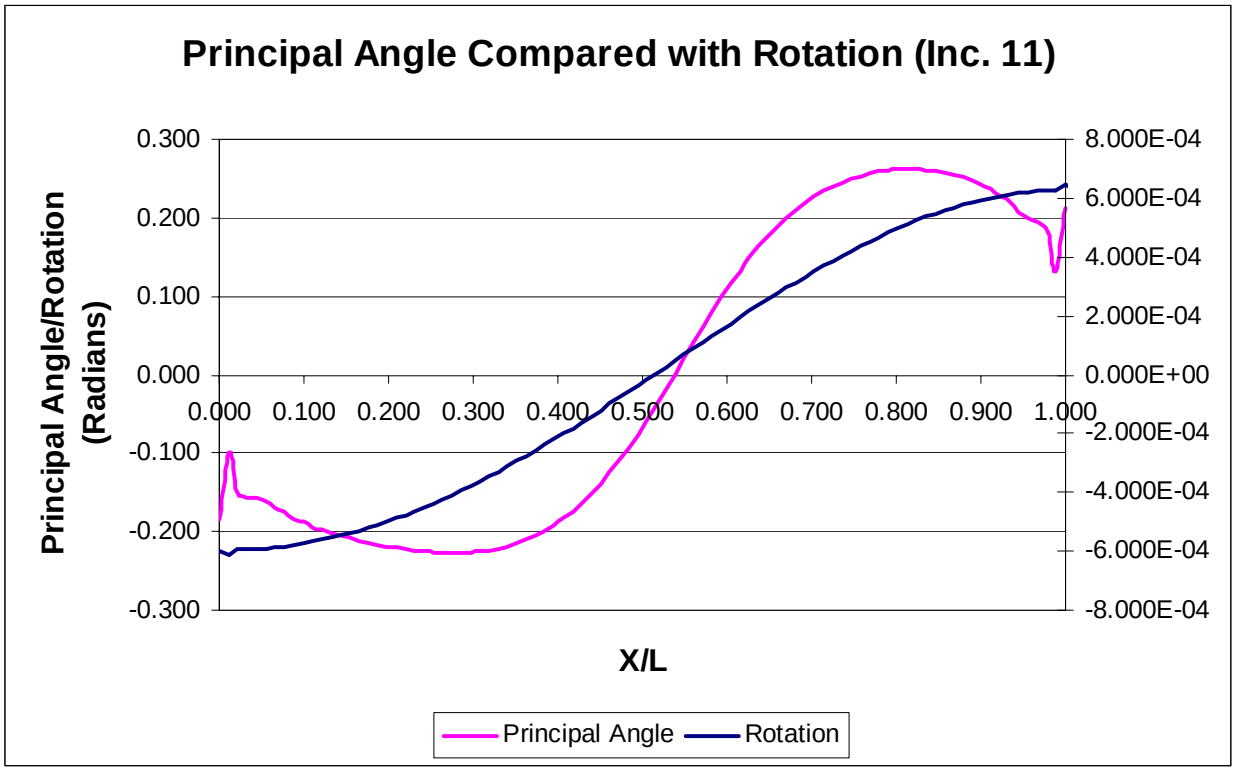

Figure 26: Principal Angles and Rotation about Z-Axis along Flange Length (1/4 of Pcr)

By interpreting the plot shown above, it can be concluded that the tee section is producing helical shaped principal angle inclinations as the model twists; these inclinations follow the geometric

deformation of the column. These plots do not match exactly, and therefore can be said to be in disagreement with the Wagner Hypothesis. Wagner's Hypothesis was developed based on the concept of a cross section being comprised of a bundle of fibers. Galambos' development of the theory does not rely heavily on the concept of fibers, and furthermore steel is a homogeneous material, which is not made of fibers. In fact, the plots do follow the same shape, and thus conform to the theory. These results, in conjunction with the agreement of the experimental test results, finite element analysis results, and numerical solutions further developed by Galambos verify that for a mono-symmetric cross-section the Wagner Hypothesis is valid.

5.0 CONCLUSIONS AND RECOMMENDATIONS

The current study examines the Wagner Hypothesis as it applies to torsional problems of thin-walled open-profile sections. Second-order theories have been developed based on the line of shear centers to calculate critical buckling loads for beams, columns, and beam-columns. In addition to the classical theory, considering a longitudinal axes defined by the line of shear centers, that has been accepted and used for nearly a hundred years, a new opposing second-order theory has been derived based on the line of centroids (Ojalvo 1990). This new theory does not accept the use of the Wagner effect, while the classical theories do make use of the hypothesis. The Wagner Hypothesis states that when a thin-walled open-profile member is subjected to a loading that will cause a torsional failure mode, the longitudinal stresses become inclined to the normal plane and produce a torsional moment in that plane. The principal stresses along the length of the member will form a helical shape that follows the geometry of the deformed member. Ojalvo does not trust that this phenomenon is possible, and therefore felt it was necessary to develop a new theory excluding the Wagner effect.

Based on the results obtained from the current study, it can be concluded that the Wagner Hypothesis is valid for thin-walled open-profile sections. There is close agreement between the analytical solutions, developed by Timoshenko (1905) and reported by Galambos (1968) and the finite element analysis results for a doubly symmetric beam section. In addition, there is similar agreement for the case of a flanged cruciform section. It is necessary to perform a finite element analysis on a mono-symmetric cross-section due to the question of the capacity calculated when the Wagner effect is used. Ojalvo states that if the critical buckling load of a mono-symmetric I-beam is calculated using theories that employ the Wagner effect, the same value will be achieved

regardless of whether the larger or smaller flange is in compression. A tee-shaped column presented by Ojalvo was used to verify the behavior of a mono-symmetric section. This finite element analysis is based on experimental tests performed by Chen with the results of those tests presented by both Chen (1980) and Ojalvo (1990). Again, there is agreement of the critical buckling loads achieved from the finite element analysis, the experimental test results, and the numerical solutions developed by Timoshenko (i.e. the classical theory that includes Wagner's Hypothesis). The supporting calculations can be found in Appendix C. Due to the agreement between finite element analysis results and classical theories related to the models, it is reasonable to believe that the Wagner Hypothesis valid.

To further verify that the Wagner effect is valid, graphical representations of the maximum principal stresses for the cruciform and tee-shaped columns are created. In both cases, the stresses for each element follow the deformation of the model. These graphical representations were verified numerically to ensure the accuracy of the picture. The calculations found in Appendix D prove that the helical shape of principal stresses does exist, and there is good basis for use of the Wagner effect in second-order theories. However, the inclination of the principal plane for the elements does not match the deformations exactly, and the agreement of the plots is therefore somewhat at odds with the Wagner Hypothesis. Wagner's Hypothesis was developed based on the concept of the cross-section being comprised of a bundle of fibers. The helical plots are said to follow the deformation of those fibers. Galambos' further development of the classical second-order theories does not rely heavily on the idea of fiber orientations. Steel is a homogeneous material that is not made from a bundle of fibers, and this may account for the difference in the plot of the principal angles compared with the rotations of the elements. Based on the fact that the plots follow the trend that the Hypothesis prescribes in addition to the

agreement between the finite element results and the classical second-order theories, the Wagner Hypothesis is valid for thin-walled open-profile members.

Further research should be performed to confirm that Wagner's effect is valid for all thin-walled open-profile sections. The current study proves that the hypothesis is warranted based on finite element results. To further discredit the opposing theory it would be effective to perform experimental tests on mono-symmetric I-beams to determine the critical buckling load as well as record the stresses for the specimen along its length at multiple stages of the loading. This would ensure that ABAQUS is computing the principal stresses correctly. It is also important to further explore the agreement between the principal angles and the deformations of each section. The plots created during the current study exhibit the same helical shape; yet do not show exact agreement. In addition to performing the experimental tests, a finite element analysis could be executed on the mono-symmetric I-beam model to find agreement with the numerical solutions as well as with the new experimental results.

APPENDIX A

ELEVATION VIEWS OF COLUMN SECTIONS

Appendix A includes elevation views of the column sections used for the finite element analyses employed to verify the validity of the Wagner Hypothesis. Appendix A1 shows the elevation for the cruciform model with the boundary conditions placed at the intersection of the two web sections; the loading is also placed at this location. The length of the column is shown as L = 240". Appendix A2 includes the elevation views of the tee section. The first set of views shows the column with metric dimensions. It depicts the setup used by Chen for the experimental tests as well as the column used for the finite element analysis with both the boundary conditions and loadings shown. The second set of elevations is the same as the first with the exception that the dimensions are shown in English units. The length of the tee column is equal to 2322 millimeters or 91.42 inches.

APPENDIX A1

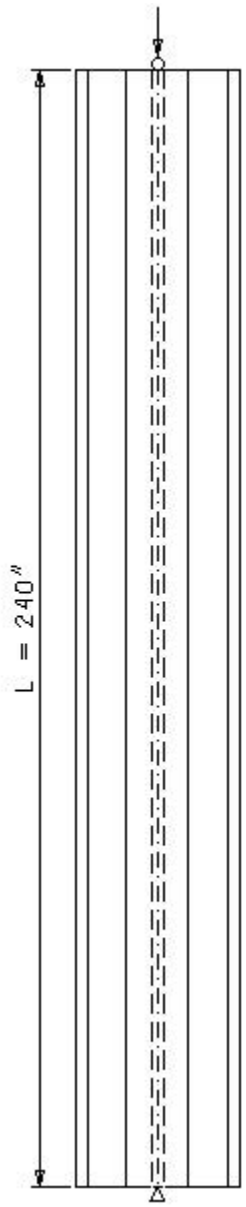

Figure 27: Elevation of Cruciform Model

APPENDIX A2

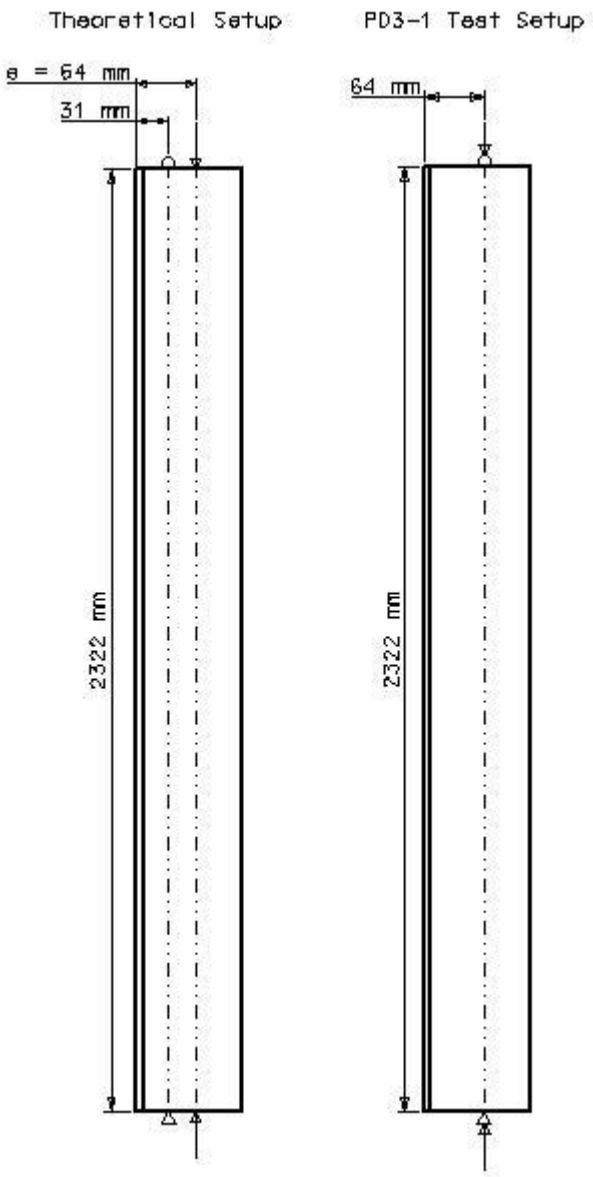

Figure 28: Elevation of Tee Model with Metric Dimensions

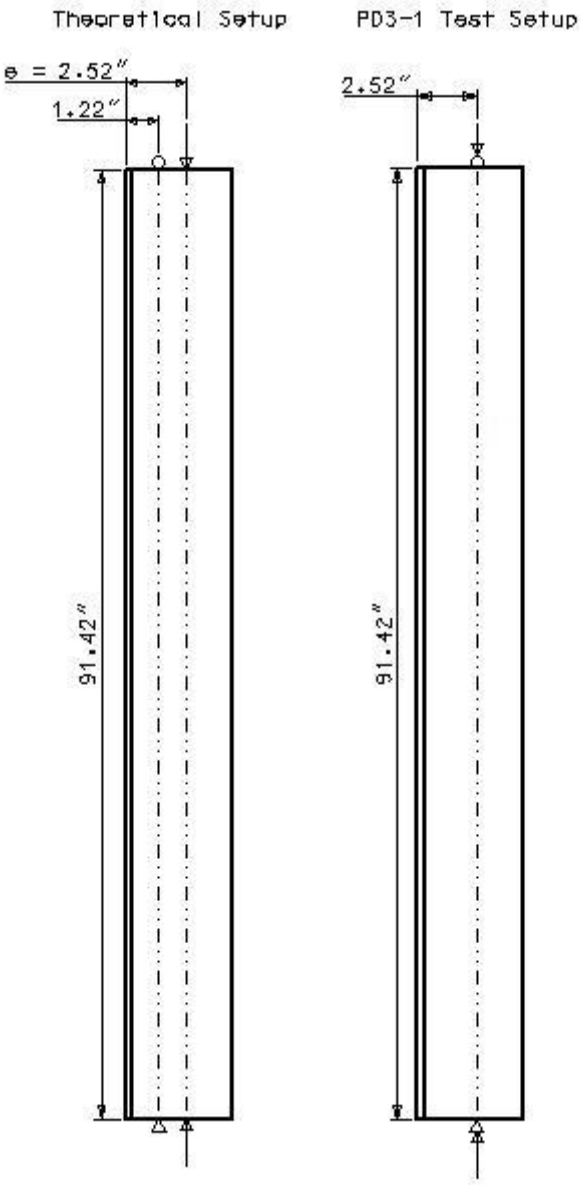

Figure 29: Elevation of Tee Model with English Dimensions

APPENDIX B

ABAQUS INPUT FILES

Typical input files created in ABAQUS that were used to perform the finite element analysis section of the study are presented in this appendix. There are files included for each segment of the project. The first section, B1, includes the file used to complete the verification study which analyzed a simply supported beam with an eccentric loading at the mid-span. The results from this analysis were used to duplicate a plot presented by Galambos to verify that ABAQUS would give accurate results for this project. Appendix B2 shows an input file used for a linearized-eigenvalue buckling analysis performed on a simply supported I-beam with a uniform moment loading. This model was used to aid in finding the critical moment. Appendix A3 is similar to the input file shown in Appendix B2 with the exception of how the analysis is performed. The model in B3 is analyzed using nonlinear geometry and Modified Riks computation. This model is used to detect the critical moment in the section and compare it to the closed form solution.

Appendix B4 includes a linearized-eigenvalue buckling analysis for a cruciform-shaped column with an axial compressive load applied. This analysis is used as an imperfection seed to input the buckling mode shape into the postbuckling analysis for the same column. Appendix B5 is identical to B4 with the exception that there is an imperfection file used to account for initial imperfections in the column. B5 is a postbuckling analysis of the cruciform column and is used to compare the critical load at the point of bifurcation to the theoretical equations provided by Ojalvo. The final input files for the study are included in Appendix B6 and Appendix B7. Appendix B6 shows an input file for the linearized-eigenvalue buckling analysis of a tee-shaped

column. It is used as an imperfection seed for the postbuckling analysis of the same member. The input files presented in Appendix B do not include all input files analyzed during this study, but are representative of each type of structure that was considered.

APPENDIX B1

```
*HEADING
      Verification of Galambos' Plot shown on
      page 64 of "Structural Members and Frames"
      Simply supported I-Beam 12WF50
      Eccentric Loading
*NODE
**Left side of the TOP Flange
1,0,12.19,0
965,4.0385,12.19,0
1929,8.077,12.19,0
**Right side of the TOP Flange
241,0,12.19,240
1205,4.0385,12.19,240
2169,8.077,12.19,240
**Left side of the BOTTOM Flange
2170,0,0,0
3134,4.0385,0,0
4098,8.077,0,0
**Right side of the BOTTOM Flange
2410,0,0,240
3374,4.0385,0,240
4338,8.077,0,240
**Web
4339,4.0385,11.174,0
5544,4.0385,6.095,0
6749,4.0385,1.016,0
4579,4.0385,11.174,240
5784,4.0385,6.095,240
6989,4.0385,1.016,240
**TOP FLANGE
*NGEN,NSET=TFB
1,241,1
*NGEN,NSET=TFM
965,1205,1
*NGEN,NSET=TFT
1929,2169,1
*NFILL,NSET=TF1
TFB,TFM,4,241
*NFILL,NSET=TF2
TFM,TFT,4,241
**BOTTOM FLANGE
*NGEN,NSET=BFB
2170,2410,1
*NGEN,NSET=BFM
3134,3374,1
*NGEN,NSET=BFT
4098,4338,1
*NFILL,NSET=BF1
BFB,BFM,4,241
*NFILL,NSET=BF2
BFM,BFT,4,241
**WEB NODES
```

```
**
*NGEN,NSET=WEBB
6749,6989,1
*NGEN,NSET=WEBM
5544,5784,1
*NGEN,NSET=WEBT
4339,4579,1
*NFILL,NSET=W1
WEBT,WEBM,5,241
*NFILL,NSET=W2
WEBM,WEBB,5,241
**NSET FOR BOUNDARY CONDITION
*NSET,NSET=PINNED
5544
*NSET,NSET=ROLLER
5784
*NODE
6990,5.0385,6.095,120
**
**ELEMENT DEFINITIONS

**
**
*ELEMENT,TYPE=S4R
1,1,2,243,242
*ELGEN,ELSET=TOPFLANGE
1,240,1,1,8,241,240
*ELEMENT,TYPE=S4R
1921,2170,2171,2412,2411
*ELGEN,ELSET=BOTTOMFLANGE
1921,240,1,1,8,241,240
*ELEMENT,TYPE=S4R
3841,965,966,4340,4339
*ELGEN,ELSET=WEBTOP
3841,240,1,1
*ELEMENT,TYPE=S4R
4081,4339,4340,4581,4580
*ELGEN,ELSET=WEBMIDDLE
4081,240,1,1,10,241,240
*ELEMENT,TYPE=S4R
6481,6749,6750,3135,3134
*ELGEN,ELSET=WEBBOTTOM
6481,240,1,1
**GROUPING ELEMENTS
*ELSET,ELSET=WEB
WEBTOP,WEBBOTTOM,WEBMIDDLE
*ELEMENT,TYPE=B31,ELSET=LEVERARM
6722,5664,6990
*BEAM SECTION, SECTION=RECT, ELSET=LEVERARM, MATERIALS=RIGID

5.,5.
*ELEMENT,TYPE=B31,ELSET=RIGIDBEAMTF
6723,121,362
6724,362,603
6725,603,844
6726,844,1085
6727,1085,1326
```

```
6728,1326,1567
6729,1567,1808
6730,1808,2049
*BEAM SECTION, SECTION=RECT,ELSET=RIGIDBEAMTF, MATERIALS=RIGID
5.,5.
*ELEMENT,TYPE=B31,ELSET=RIGIDBEAMBF
6731,2290,2531
6732,2531,2772
6733,2772,3013
6734,3013,3254
6735,3254,3495
6736,3495,3736
6737,3736,3977
6738,3977,4218
*BEAM SECTION, SECTION=RECT,ELSET=RIGIDBEAMBF, MATERIALS=RIGID
5.,5.
*ELEMENT,TYPE=B31,ELSET=RIGIDBEAMWEB
6739,1085,4459
6740,4459,4700
6741,4700,4941
6742,4941,5182
6743,5182,5423
6744,5423,5664
6745,5664,5905
6746,5905,6146
6747,6146,6387
6748,6387,6628
6749,6628,6869
6750,6869,3254
*ELEMENT, TYPE=B31,ELSET=RIGIDBEAMLEFT
6751,3374,6989
6752,6989,6748
6753,6748,6507
6754,6507,6266
6755,6266,6025
6756,6025,5784
6757,5784,5543
6758,5543,5302
6759,5302,5061
6760,5061,4820
6761,4820,4579

6762,4579,1205
*BEAM SECTION, SECTION=RECT,ELSET=RIGIDBEAMLEFT, MATERIALS=RIGID
5.,5.
*ELEMENT,TYPE=B31,ELSET=RIGIDBEAMRIGHT
6763,3134,6749
6764,6749,6508
6765,6508,6267
6766,6267,6026
6767,6026,5785
6768,5785,5544
6769,5544,5303
6770,5303,5062
6771,5062,4821
6772,4821,4580
6773,4580,4339
```

```
6774,4339,965
*BEAM SECTION, SECTION=RECT,ELSET=RIGIDBEAMRIGHT, MATERIALS=RIGID
5.,5.
*NSET, NSET=OUTPUT, GENERATE
965,1205,1
3134,3374,1
*BEAM SECTION, SECTION=RECT,ELSET=RIGIDBEAMWEB, MATERIALS=RIGID
5.,5.
**MATERIAL PROPERTIES
*SHELL SECTION,MATERIAL=STEEL,ELSET=TOPFLANGE
0.641
*SHELL SECTION,MATERIAL=STEEL,ELSET=BOTTOMFLANGE
0.641
*SHELL SECTION,MATERIAL=STEEL,ELSET=WEB
0.371
*MATERIAL,NAME=STEEL
*ELASTIC
29500,0.3
*MATERIAL, NAME=RIGID
*ELASTIC
295000,0.3
*BOUNDARY
PINNED,1
PINNED,2
PINNED,3
PINNED,6
ROLLER,1
ROLLER,2
ROLLER,6
*STEP
*STATIC
*CLOAD
6990,2,-1
*ELPRINT,FREQUENCY=0
*NODE PRINT,FREQUENCY=1,NSET=OUTPUT
U
*END STEP
```

APPENDIX B2

```
*HEADING
      Linearized-eigenvalue Buckling Analysis
      Simply supported 12WF50 with Uniform
      Moment Applied
*NODE
**Left side of the TOP Flange
1,0,12.19,0
965,4.0385,12.19,0
1929,8.077,12.19,0
**Right side of the TOP Flange
241,0,12.19,240
1205,4.0385,12.19,240
2169,8.077,12.19,240
**Left side of the BOTTOM Flange
2170,0,0,0
3134,4.0385,0,0
4098,8.077,0,0
**Right side of the BOTTOM Flange
2410,0,0,240
3374,4.0385,0,240
4338,8.077,0,240
**Web
4339,4.0385,11.174,0
5544,4.0385,6.095,0
6749,4.0385,1.016,0
4579,4.0385,11.174,240
5784,4.0385,6.095,240
6989,4.0385,1.016,240
**
**TOP FLANGE
**
*NGEN,NSET=TFB
1,241,1
*NGEN,NSET=TFM
965,1205,1
*NGEN,NSET=TFT
1929,2169,1
*NFILL,NSET=TF1
TFB,TFM,4,241
*NFILL,NSET=TF2
TFM,TFT,4,241
**BOTTOM FLANGE
*NGEN,NSET=BFB
2170,2410,1
*NGEN,NSET=BFM
3134,3374,1
*NGEN,NSET=BFT
4098,4338,1
*NFILL,NSET=BF1
BFB,BFM,4,241
*NFILL,NSET=BF2
BFM,BFT,4,241
```

```
**
**WEB NODES
**
*NGEN,NSET=WEBB
6749,6989,1
*NGEN,NSET=WEBM
5544,5784,1
*NGEN,NSET=WEBT
4339,4579,1
*NFILL,NSET=W1
WEBT,WEBM,5,241
*NFILL,NSET=W2
WEBM,WEBB,5,241
**NSET FOR BOUNDARY CONDITION
*NSET,NSET=PINNED
5544
*NSET,NSET=ROLLER
5784
**
**ELEMENT DEFINITIONS
**
**
*ELEMENT,TYPE=S4R
1,1,2,243,242
*ELGEN,ELSET=TOPFLANGE
1,240,1,1,8,241,240
*ELEMENT,TYPE=S4R
1921,2170,2171,2412,2411
*ELGEN,ELSET=BOTTOMFLANGE
1921,240,1,1,8,241,240
*ELEMENT,TYPE=S4R
3841,965,966,4340,4339
*ELGEN,ELSET=WEBTOP
3841,240,1,1
*ELEMENT,TYPE=S4R
4081,4339,4340,4581,4580
*ELGEN,ELSET=WEBMIDDLE
4081,240,1,1,10,241,240
*ELEMENT,TYPE=S4R
6481,6749,6750,3135,3134
*ELGEN,ELSET=WEBBOTTOM
6481,240,1,1
**GROUPING ELEMENTS
*ELSET,ELSET=WEB
WEBTOP,WEBBOTTOM,WEBMIDDLE
*ELEMENT, TYPE=B31,ELSET=RIGIDBEAMLEFT
6751,3374,6989
6752,6989,6748
6753,6748,6507
6754,6507,6266
6755,6266,6025
6756,6025,5784
6757,5784,5543
6758,5543,5302
6759,5302,5061
6760,5061,4820
6761,4820,4579
```

```
6762,4579,1205
*BEAM SECTION, SECTION=RECT,ELSET=RIGIDBEAMLEFT, MATERIALS=RIGID
5.,5.
*ELEMENT,TYPE=B31,ELSET=RIGIDBEAMRIGHT
6763,3134,6749
6764,6749,6508
6765,6508,6267
6766,6267,6026
6767,6026,5785
6768,5785,5544
6769,5544,5303
6770,5303,5062
6771,5062,4821
6772,4821,4580
6773,4580,4339
6774,4339,965
*BEAM SECTION, SECTION=RECT,ELSET=RIGIDBEAMRIGHT, MATERIALS=RIGID
5.,5.
*NSET, NSET=OUTPUT, GENERATE
965,1205,1
3134,3374,1
**MATERIAL PROPERTIES
*SHELL SECTION,MATERIAL=STEEL,ELSET=TOPFLANGE
0.641
*SHELL SECTION,MATERIAL=STEEL,ELSET=BOTTOMFLANGE
0.641
*SHELL SECTION,MATERIAL=STEEL,ELSET=WEB
0.371
*MATERIAL,NAME=STEEL
*ELASTIC
30000,0.3
*MATERIAL, NAME=RIGID
*ELASTIC
300000,0.3
*BOUNDARY
PINNED,1
PINNED,2
PINNED,3
PINNED,6
ROLLER,1
ROLLER,2
ROLLER,6
*STEP
*BUCKLE
2,2,50,100
*CLOAD
5544,4,6000
5784,4,-6000
*NODE FILE,LAST MODE=1,GLOBAL=YES
U
*ELPRINT,FREQUENCY=0
*NODE PRINT,FREQUENCY=1
CF
*END STEP
```

APPENDIX B3

```
*HEADING
      Simply supported 12WF50 with Uniform
      Moment applied to each end
      Compared to Eqn. 3.32 on Page 91
      of "Structural Members and Frames"
*NODE
**Left side of the TOP Flange
1,0,12.19,0
965,4.0385,12.19,0
1929,8.077,12.19,0
**Right side of the TOP Flange
241,0,12.19,240
1205,4.0385,12.19,240
2169,8.077,12.19,240
**Left side of the BOTTOM Flange
2170,0,0,0
3134,4.0385,0,0
4098,8.077,0,0
**Right side of the BOTTOM Flange
2410,0,0,240
3374,4.0385,0,240
4338,8.077,0,240
**Web
4339,4.0385,11.174,0
5544,4.0385,6.095,0
6749,4.0385,1.016,0
4579,4.0385,11.174,240
5784,4.0385,6.095,240
6989,4.0385,1.016,240
**
**TOP FLANGE
**
*NGEN,NSET=TFB
1,241,1
*NGEN,NSET=TFM
965,1205,1
*NGEN,NSET=TFT
1929,2169,1
*NFILL,NSET=TF1
TFB,TFM,4,241
*NFILL,NSET=TF2
TFM,TFT,4,241
**BOTTOM FLANGE
*NGEN,NSET=BFB
2170,2410,1
*NGEN,NSET=BFM
3134,3374,1
*NGEN,NSET=BFT
4098,4338,1
*NFILL,NSET=BF1
BFB,BFM,4,241
*NFILL,NSET=BF2
BFM,BFT,4,241
**
```

```
**WEB NODES
**
*NGEN,NSET=WEBB
6749,6989,1
*NGEN,NSET=WEBM
5544,5784,1
*NGEN,NSET=WEBT
4339,4579,1
*NFILL,NSET=W1
WEBT,WEBM,5,241
*NFILL,NSET=W2
WEBM,WEBB,5,241
**NSET FOR BOUNDARY CONDITION
*NSET,NSET=PINNED
5544
*NSET,NSET=ROLLER
5784
**
**ELEMENT DEFINITIONS
**
**
*ELEMENT,TYPE=S4R
1,1,2,243,242
*ELGEN,ELSET=TOPFLANGE
1,240,1,1,8,241,240
*ELEMENT,TYPE=S4R
1921,2170,2171,2412,2411
*ELGEN,ELSET=BOTTOMFLANGE
1921,240,1,1,8,241,240
*ELEMENT,TYPE=S4R
3841,965,966,4340,4339
*ELGEN,ELSET=WEBTOP
3841,240,1,1
*ELEMENT,TYPE=S4R
4081,4339,4340,4581,4580
*ELGEN,ELSET=WEBMIDDLE
4081,240,1,1,10,241,240
*ELEMENT,TYPE=S4R
6481,6749,6750,3135,3134
*ELGEN,ELSET=WEBBOTTOM
6481,240,1,1
**GROUPING ELEMENTS
*ELSET,ELSET=WEB
WEBTOP,WEBBOTTOM,WEBMIDDLE
*ELEMENT, TYPE=B31,ELSET=RIGIDBEAMLEFT
6751,3374,6989
6752,6989,6748
6753,6748,6507
6754,6507,6266
6755,6266,6025
6756,6025,5784
6757,5784,5543
6758,5543,5302
6759,5302,5061
6760,5061,4820
6761,4820,4579
6762,4579,1205
```

```
*BEAM SECTION, SECTION=RECT,ELSET=RIGIDBEAMLEFT, MATERIALS=RIGID
5.,5.
*ELEMENT,TYPE=B31,ELSET=RIGIDBEAMRIGHT
6763,3134,6749
6764,6749,6508
6765,6508,6267
6766,6267,6026
6767,6026,5785
6768,5785,5544
6769,5544,5303
6770,5303,5062
6771,5062,4821
6772,4821,4580
6773,4580,4339
6774,4339,965
*BEAM SECTION, SECTION=RECT,ELSET=RIGIDBEAMRIGHT, MATERIALS=RIGID
5.,5.
*NSET, NSET=OUTPUT, GENERATE
965,1205,1
3134,3374,1
**MATERIAL PROPERTIES
*SHELL SECTION,MATERIAL=STEEL,ELSET=TOPFLANGE
0.641
*SHELL SECTION,MATERIAL=STEEL,ELSET=BOTTOMFLANGE
0.641
*SHELL SECTION,MATERIAL=STEEL,ELSET=WEB
0.371
*MATERIAL,NAME=STEEL
*ELASTIC
30000,0.3
*MATERIAL, NAME=RIGID
*ELASTIC
300000,0.3
*BOUNDARY
PINNED,1
PINNED,2
PINNED,3
PINNED,6
ROLLER,1
ROLLER,2
ROLLER,6
*STEP,NLGEOM,INC=30
*STATIC,RIKS
0.01,1.,0.0000000001
*CLOAD
5544,4,6000
5784,4,-6000
*ELPRINT,FREQUENCY=0
*NODE PRINT,FREQUENCY=1,NSET=OUTPUT
U
*END STEP
```

APPENDIX B4

```
*Heading
      Cruciform Cross-section
      Linearized-eigenvalue Buckling Analysis
      Axial Compressive Loading
*NODE
**BOTTOM 1ST FLANGE
1,9,0,0
724,12,0,0
1447,15,0,0
**TOP 1ST FLANGE
241,9,240,0
964,12,240,0
1687,15,240,0
**BOTTOM 2ND FLANGE
1688,0,0,9
2411,0,0,12
3134,0,0,15
**TOP 2ND FLANGE
1928,0,240,9
2651,0,240,12
3374,0,240,15
**BOTTOM 3RD FLANGE
3375,9,0,24
4098,12,0,24
4821,15,0,24
**TOP 3RD FLANGE
3615,9,240,24
4338,12,240,24
5061,15,240,24
**BOTTOM 4TH FLANGE
5062,24,0,9
5785,24,0,12
6508,24,0,15
**TOP 4TH FLANGE
5302,24,240,9
6025,24,240,12
6748,24,240,15
**WEB 1
6749,12,0,1
6869,12,120,1
6989,12,240,1
9400,12,0,12
9520,12,120,12
9640,12,240,12
12051,12,0,23
12171,12,120,23
12291,12,240,23
**WEB 2
12300,1,0,12
12540,1,240,12
14710,11,0,12
14950,11,240,12
16000,13,0,12
```

```
16240,13,240,12
18410,23,0,12
18650,23,240,12
**
**1ST FLANGE
**
*NGEN,NSET=R1
1,241,1
*NGEN,NSET=M1
724,964,1
*NGEN,NSET=L1
1447,1687,1
*NFILL,NSET=O1
R1,M1,3,241
*NFILL,NSET=O2
M1,L1,3,241
**
**2ND FLANGE
**
*NGEN,NSET=R2
1688,1928,1
*NGEN,NSET=M2
2411,2651,1
*NGEN,NSET=L2
3134,3374,1
*NFILL,NSET=T1
R2,M2,3,241
*NFILL,NSET=T2
M2,L2,3,241
**
**3RD FLANGE
**
*NGEN,NSET=R3
3375,3615,1
*NGEN,NSET=M3
4098,4338,1
*NGEN,NSET=L3
4821,5061,1
*NFILL,NSET=TH1
R3,M3,3,241
*NFILL,NSET=TH2
M3,L3,3,241
**
**4TH FLANGE
**
*NGEN,NSET=R4
5062,5302,1
*NGEN,NSET=M4
5785,6025,1
*NGEN,NSET=L4
6508,6748,1
*NFILL,NSET=F1
R4,M4,3,241
*NFILL,NSET=F2
M4,L4,3,241

**
```

```
**WEB 1
**
*NGEN,NSET=WEB1L
6749,6989,1
*NGEN,NSET=WEB1M
9400,9640,1
*NGEN,NSET=WEB1R
12051,12291,1
*NFILL,NSET=WEB11
WEB1L,WEB1M,11,241
*NFILL,NSET=WEB12
WEB1M,WEB1R,11,241
**
**WEB 2
**
*NGEN,NSET=WEB2R
12300,12540,1
*NGEN,NSET=WEB2M1
14710,14950,1
*NGEN,NSET=WEB2M2
16000,16240,1
*NGEN,NSET=WEB2L
18410,18650,1
*NFILL,NSET=WEB21
WEB2R,WEB2M1,10,241
*NFILL,NSET=WEB22
WEB2M2,WEB2L,10,241
**
**BOUNDARY CONDITIONS
**
*NSET,NSET=PINNED
9400
*NSET,NSET=ROLLER
9640
**
**ELEMENT DEFINITIONS
**
*ELEMENT,TYPE=S4R
1,1,2,243,242
*ELGEN,ELSET=FLANGE1
1,240,1,1,6,241,240
**
*ELEMENT,TYPE=S4R
1441,1688,1689,1930,1929
*ELGEN,ELSET=FLANGE2
1441,240,1,1,6,241,240
**
*ELEMENT,TYPE=S4R
2881,3375,3376,3617,3616
*ELGEN,ELSET=FLANGE3
2881,240,1,1,6,241,240
**
*ELEMENT,TYPE=S4R
4321,5062,5063,5304,5303
*ELGEN,ELSET=FLANGE4
4321,240,1,1,6,241,240
**
```

```
*ELEMENT,TYPE=S4R
5761,724,725,6750,6749
*ELGEN,ELSET=WEB111
5761,240,1,1
**
*ELEMENT,TYPE=S4R
6001,6749,6750,6991,6990
*ELGEN,ELSET=WEB112
6001,240,1,1,22,241,240
**
*ELEMENT,TYPE=S4R
11281,12051,12052,4099,4098
*ELGEN,ELSET=WEB113
11281,240,1,1
**
*ELSET,ELSET=WEB1
WEB111,WEB112,WEB113
**
*ELEMENT,TYPE=S4R
11600,2411,2412,12301,12300
*ELGEN,ELSET=WEB2R1
11600,240,1,1
**
*ELEMENT,TYPE=S4R
11841,12300,12301,12542,12541
*ELGEN,ELSET=WEB2R2
11841,240,1,1,10,241,240
**
*ELEMENT,TYPE=S4R
14241,14710,14711,9401,9400
*ELGEN,ELSET=WEB2M1
14241,240,1,1
**
*ELEMENT,TYPE=S4R
14481,9400,9401,16001,16000
*ELGEN,ELSET=WEB2M2
14481,240,1,1
**
*ELEMENT,TYPE=S4R
14721,16000,16001,16242,16241
*ELGEN,ELSET=WEB2L1
14721,240,1,1,10,241,240
**
*ELEMENT,TYPE=S4R
17121,18410,18411,5786,5785
*ELGEN,ELSET=WEB2L2
17121,240,1,1
**
*ELSET,ELSET=WEB2
WEB2R1,WEB2R2,WEB2M1,WEB2M2,WEB2L1,WEB2L2
**
**
*ELEMENT, TYPE=B31,ELSET=RIGIDTOP1
18000,964,6989
18001,6989,7230
18003,7230,7471
18004,7471,7712
```

```
18005,7712,7953
18006,7953,8194
18007,8194,8435
18008,8435,8676
18009,8676,8917
18010,8917,9158
18011,9158,9399
18012,9399,9640
18013,9640,9881
18014,9881,10122
18015,10122,10363
18016,10363,10604
18017,10604,10845
18018,10845,11086
18019,11086,11327
18020,11327,11568
18021,11568,11809
18022,11809,12050
18023,12050,12291
18024,12291,4338
*BEAM SECTION, SECTION=RECT,ELSET=RIGIDTOP1, MATERIALS=RIGID
5.,5.
0,-1,0
*ELEMENT,TYPE=B31,ELSET=RIGIDBOTTOM1
18025,724,6749
18026,6749,6990
18027,6990,7231
18028,7231,7472
18029,7472,7713
18030,7713,7954
18031,7954,8195
18032,8195,8436
18033,8436,8677
18034,8677,8918
18035,8918,9159
18036,9159,9400
18037,9400,9641
18038,9641,9882
18039,9882,10123
18040,10123,10364
18041,10364,10605
18042,10605,10846
18043,10846,11087
18044,11087,11328
18045,11328,11569
18046,11569,11810
18047,11810,12051
18048,12051,4098
*BEAM SECTION, SECTION=RECT,ELSET=RIGIDBOTTOM1, MATERIALS=RIGID
5.,5.
0,-1,0
*ELEMENT, TYPE=B31,ELSET=RIGIDTOP2
18049,2651,12540
18050,12540,12781
18051,12781,13022
18052,13022,13263
18053,13263,13504
```

```
18054,13504,13745
18055,13745,13986
18056,13986,14227
18057,14227,14468
18058,14468,14709
18059,14709,14950
18060,14950,9640
18061,9640,16240
18062,16240,16481
18063,16481,16722
18064,16722,16963
18065,16963,17204
18066,17204,17445
18067,17445,17686
18068,17686,17927
18069,17927,18168
18070,18168,18409
18071,18409,18650
18072,18650,6025
*BEAM SECTION, SECTION=RECT,ELSET=RIGIDTOP2, MATERIALS=RIGID
5.,5.
0,-1,0
*ELEMENT,TYPE=B31,ELSET=RIGIDBOTTOM2
18073,2411,12300
18074,12300,12541
18075,12541,12782
18076,12782,13023
18077,13023,13264
18078,13264,13505
18079,13505,13746
18080,13746,13987
18081,13987,14228
18082,14228,14469
18083,14469,14710
18084,14710,9400
18085,9400,16000
18086,16000,16241
18087,16241,16482
18088,16482,16723
18089,16723,16964
18090,16964,17205
18091,17205,17446
18092,17446,17687
18093,17687,17928
18094,17928,18169
18095,18169,18410
18096,18410,5785
*BEAM SECTION, SECTION=RECT,ELSET=RIGIDBOTTOM2, MATERIALS=RIGID
5.,5.
0,-1,0
**
**
**MATERIAL PROPERTIES
**
*SHELL SECTION,MATERIAL=STEEL,ELSET=FLANGE1
0.25
*SHELL SECTION,MATERIAL=STEEL,ELSET=FLANGE2
```

```
0.25
*SHELL SECTION,MATERIAL=STEEL,ELSET=FLANGE3
0.25
*SHELL SECTION,MATERIAL=STEEL,ELSET=FLANGE4
0.25
*SHELL SECTION,MATERIAL=STEEL,ELSET=WEB1
0.25
*SHELL SECTION,MATERIAL=STEEL,ELSET=WEB2
0.25
*MATERIAL,NAME=STEEL
*ELASTIC
29000,0.3
*MATERIAL, NAME=RIGID
*ELASTIC
290000,0.3
*BOUNDARY
PINNED,1
PINNED,2
PINNED,3
PINNED,5
ROLLER,1
ROLLER,3
ROLLER,5
*STEP
*BUCKLE
5,5,50,100
*CLOAD
9640,2,-1000
*ELPRINT,FREQUENCY=0
*NODE FILE,LAST MODE=1,GLOBAL=YES
U
*END STEP
```

APPENDIX B5

```
*Heading
      Postbuckling Analysis of Cruciform Column
      Axial Compressive Load
      Scale Factor=L/1000
*NODE
**BOTTOM 1ST FLANGE
1,9,0,0
724,12,0,0
1447,15,0,0
**TOP 1ST FLANGE
241,9,240,0
964,12,240,0
1687,15,240,0
**BOTTOM 2ND FLANGE
1688,0,0,9
2411,0,0,12
3134,0,0,15
**TOP 2ND FLANGE
1928,0,240,9
2651,0,240,12
3374,0,240,15
**BOTTOM 3RD FLANGE
3375,9,0,24
4098,12,0,24
4821,15,0,24
**TOP 3RD FLANGE
3615,9,240,24
4338,12,240,24
5061,15,240,24
**BOTTOM 4TH FLANGE
5062,24,0,9
5785,24,0,12
6508,24,0,15
**TOP 4TH FLANGE
5302,24,240,9
6025,24,240,12
6748,24,240,15
**WEB 1
6749,12,0,1
6869,12,120,1
6989,12,240,1
9400,12,0,12
9520,12,120,12
9640,12,240,12
12051,12,0,23
12171,12,120,23
12291,12,240,23
**WEB 2
12300,1,0,12
12540,1,240,12
14710,11,0,12
14950,11,240,12
16000,13,0,12
```

```
16240,13,240,12
18410,23,0,12
18650,23,240,12
**
**1ST FLANGE
**
*NGEN,NSET=R1
1,241,1
*NGEN,NSET=M1
724,964,1
*NGEN,NSET=L1
1447,1687,1
*NFILL,NSET=O1
R1,M1,3,241
*NFILL,NSET=O2

M1,L1,3,241
**
**2ND FLANGE
**
*NGEN,NSET=R2
1688,1928,1
*NGEN,NSET=M2
2411,2651,1
*NGEN,NSET=L2
3134,3374,1
*NFILL,NSET=T1
R2,M2,3,241
*NFILL,NSET=T2
M2,L2,3,241
**
**3RD FLANGE
**
*NGEN,NSET=R3
3375,3615,1
*NGEN,NSET=M3
4098,4338,1
*NGEN,NSET=L3
4821,5061,1
*NFILL,NSET=TH1
R3,M3,3,241
*NFILL,NSET=TH2
M3,L3,3,241
**
**4TH FLANGE
**
*NGEN,NSET=R4
5062,5302,1
*NGEN,NSET=M4
5785,6025,1
*NGEN,NSET=L4
6508,6748,1
*NFILL,NSET=F1
R4,M4,3,241
*NFILL,NSET=F2
M4,L4,3,241
**
```

```
**WEB 1
**
*NGEN,NSET=WEB1L
6749,6989,1
*NGEN,NSET=WEB1M
9400,9640,1
*NGEN,NSET=WEB1R
12051,12291,1
*NFILL,NSET=WEB11
WEB1L,WEB1M,11,241
*NFILL,NSET=WEB12
WEB1M,WEB1R,11,241
**
**WEB 2
**
*NGEN,NSET=WEB2R
12300,12540,1
*NGEN,NSET=WEB2M1
14710,14950,1
*NGEN,NSET=WEB2M2
16000,16240,1
*NGEN,NSET=WEB2L
18410,18650,1
*NFILL,NSET=WEB21
WEB2R,WEB2M1,10,241
*NFILL,NSET=WEB22
WEB2M2,WEB2L,10,241
**
**BOUNDARY CONDITIONS
**
*NSET,NSET=PINNED
9400
*NSET,NSET=ROLLER
9640
**
**ELEMENT DEFINITIONS
**
*ELEMENT,TYPE=S4R
1,1,2,243,242
*ELGEN,ELSET=FLANGE1
1,240,1,1,6,241,240
**
*ELEMENT,TYPE=S4R
1441,1688,1689,1930,1929
*ELGEN,ELSET=FLANGE2
1441,240,1,1,6,241,240
**
*ELEMENT,TYPE=S4R
2881,3375,3376,3617,3616
*ELGEN,ELSET=FLANGE3
2881,240,1,1,6,241,240
**
*ELEMENT,TYPE=S4R
4321,5062,5063,5304,5303
*ELGEN,ELSET=FLANGE4
4321,240,1,1,6,241,240
**
```

```
*ELEMENT,TYPE=S4R
5761,724,725,6750,6749
*ELGEN,ELSET=WEB111
5761,240,1,1
**
*ELEMENT,TYPE=S4R
6001,6749,6750,6991,6990
*ELGEN,ELSET=WEB112
6001,240,1,1,22,241,240
**
*ELEMENT,TYPE=S4R
11281,12051,12052,4099,4098
*ELGEN,ELSET=WEB113
11281,240,1,1
**
*ELSET,ELSET=WEB1
WEB111,WEB112,WEB113
**
*ELEMENT,TYPE=S4R
11600,2411,2412,12301,12300
*ELGEN,ELSET=WEB2R1
11600,240,1,1
**
*ELEMENT,TYPE=S4R
11841,12300,12301,12542,12541
*ELGEN,ELSET=WEB2R2
11841,240,1,1,10,241,240
**
*ELEMENT,TYPE=S4R
14241,14710,14711,9401,9400
*ELGEN,ELSET=WEB2M1
14241,240,1,1
**
*ELEMENT,TYPE=S4R
14481,9400,9401,16001,16000
*ELGEN,ELSET=WEB2M2
14481,240,1,1
**
*ELEMENT,TYPE=S4R
14721,16000,16001,16242,16241
*ELGEN,ELSET=WEB2L1
14721,240,1,1,10,241,240
**
*ELEMENT,TYPE=S4R
17121,18410,18411,5786,5785
*ELGEN,ELSET=WEB2L2
17121,240,1,1
**
*ELSET,ELSET=WEB2
WEB2R1,WEB2R2,WEB2M1,WEB2M2,WEB2L1,WEB2L2
**
**
*ELEMENT, TYPE=B31,ELSET=RIGIDTOP1
18000,964,6989
18001,6989,7230
18003,7230,7471
18004,7471,7712
```

```
18005,7712,7953
18006,7953,8194
18007,8194,8435
18008,8435,8676
18009,8676,8917
18010,8917,9158
18011,9158,9399
18012,9399,9640
18013,9640,9881
18014,9881,10122
18015,10122,10363
18016,10363,10604
18017,10604,10845
18018,10845,11086
18019,11086,11327
18020,11327,11568
18021,11568,11809
18022,11809,12050
18023,12050,12291
18024,12291,4338
*BEAM SECTION, SECTION=RECT,ELSET=RIGIDTOP1, MATERIALS=RIGID
5.,5.
0,-1,0
*ELEMENT,TYPE=B31,ELSET=RIGIDBOTTOM1
18025,724,6749
18026,6749,6990
18027,6990,7231
18028,7231,7472
18029,7472,7713
18030,7713,7954
18031,7954,8195
18032,8195,8436
18033,8436,8677
18034,8677,8918
18035,8918,9159
18036,9159,9400
18037,9400,9641
18038,9641,9882
18039,9882,10123
18040,10123,10364
18041,10364,10605
18042,10605,10846
18043,10846,11087
18044,11087,11328
18045,11328,11569
18046,11569,11810
18047,11810,12051
18048,12051,4098
*BEAM SECTION, SECTION=RECT,ELSET=RIGIDBOTTOM1, MATERIALS=RIGID
5.,5.
0,-1,0
*ELEMENT, TYPE=B31,ELSET=RIGIDTOP2
18049,2651,12540
18050,12540,12781
18051,12781,13022
18052,13022,13263
18053,13263,13504
```

```
18054,13504,13745
18055,13745,13986
18056,13986,14227
18057,14227,14468
18058,14468,14709
18059,14709,14950
18060,14950,9640
18061,9640,16240
18062,16240,16481
18063,16481,16722
18064,16722,16963
18065,16963,17204
18066,17204,17445
18067,17445,17686
18068,17686,17927
18069,17927,18168
18070,18168,18409
18071,18409,18650
18072,18650,6025
*BEAM SECTION, SECTION=RECT,ELSET=RIGIDTOP2, MATERIALS=RIGID
5.,5.
0,-1,0
*ELEMENT,TYPE=B31,ELSET=RIGIDBOTTOM2
18073,2411,12300
18074,12300,12541
18075,12541,12782
18076,12782,13023
18077,13023,13264
18078,13264,13505
18079,13505,13746
18080,13746,13987
18081,13987,14228
18082,14228,14469
18083,14469,14710
18084,14710,9400
18085,9400,16000
18086,16000,16241
18087,16241,16482
18088,16482,16723
18089,16723,16964
18090,16964,17205
18091,17205,17446
18092,17446,17687
18093,17687,17928
18094,17928,18169
18095,18169,18410
18096,18410,5785
*BEAM SECTION, SECTION=RECT,ELSET=RIGIDBOTTOM2, MATERIALS=RIGID
5.,5.
0,-1,0
**
**
**MATERIAL PROPERTIES
**
*SHELL SECTION,MATERIAL=STEEL,ELSET=FLANGE1
0.25
*SHELL SECTION,MATERIAL=STEEL,ELSET=FLANGE2
```

```
0.25
*SHELL SECTION,MATERIAL=STEEL,ELSET=FLANGE3
0.25
*SHELL SECTION,MATERIAL=STEEL,ELSET=FLANGE4
0.25
*SHELL SECTION,MATERIAL=STEEL,ELSET=WEB1
0.25
*SHELL SECTION,MATERIAL=STEEL,ELSET=WEB2
0.25
*MATERIAL,NAME=STEEL
*ELASTIC
29000,0.3
*MATERIAL, NAME=RIGID
*ELASTIC
290000,0.3
*IMPERFECTION, FILE=Cruc3LEBimp, STEP=1
1,0.24
*BOUNDARY
PINNED,1
PINNED,2
PINNED,3
PINNED,5
ROLLER,1
ROLLER,3
ROLLER,5
*STEP,NLGEOM,INC=30
*STATIC,RIKS
0.01,1.,0.0000000001
*CLOAD
9640,2,-100
*EL PRINT,FREQUENCY=16,ELSET=FLANGE1
S
*NODE PRINT,FREQUENCY=16
UR3
*END STEP
```

APPENDIX B6

```
*Heading
      Tee-shaped Column with Eccentric Loading
      Linearized-eigenvalue Buckling Analysis

*NODE
**BOTTOM OF FLANGE
1,0,0,0
280,2.01,0,0
559,4.02,0,0
**TOP OF FLANGE
93,0,91.42,0
372,2.01,91.42,0
651,4.02,91.42,0
**BOTTOM OF WEB
700,2.01,0,0.152
793,2.01,0,1.3705
886,2.01,0,2.52
1165,2.01,0,4.912
**TOP OF WEB
792,2.01,91.42,0.152
885,2.01,91.42,1.3705
978,2.01,91.42,2.52
1257,2.01,91.42,4.912
**
**NODE SETS
**
**FLANGE
**
*NGEN,NSET=FLL
1,93,1
*NGEN,NSET=FLM
280,372,1
*NGEN,NSET=FLR
559,651,1
*NFILL,NSET=FLANGE1
FLL,FLM,3,93
*NFILL,NSET=FLANGE2
FLM,FLR,3,93
**
**WEB
**
*NGEN,NSET=WEB1
700,792,1
*NGEN,NSET=WEB2
886,978,1
*NFILL,NSET=WEB4
WEB1,WEB2,2,93
*NGEN,NSET=WEB3
1165,1257,1
*NFILL,NSET=WEB5
WEB2,WEB3,3,93
**
**BC'S
```

```
**
*NSET,NSET=PINNED
793
*NSET,NSET=ROLLER
885
**
**ELEMENT DEFINITIONS
**
*ELEMENT,TYPE=S4R
1,1,2,95,94
*ELGEN,ELSET=FLANGE1
1,92,1,1,3,93,92
*ELEMENT,TYPE=S4R
277,280,281,374,373
*ELGEN,ELSET=FLANGE2
277,92,1,1,3,93,92
**
*ELEMENT,TYPE=S4R
553,280,281,701,700
*ELGEN,ELSET=WEB1
553,92,1,1
**
*ELEMENT,TYPE=S4R
645,700,701,794,793
*ELGEN,ELSET=WEB2
645,92,1,1,2,93,92
**
*ELEMENT,TYPE=S4R
829,886,887,980,979
*ELGEN,ELSET=WEB3
829,92,1,1,3,93,92
**
*ELSET,ELSET=WEB
WEB1,WEB2,WEB3
**
*ELEMENT, TYPE=B31,ELSET=RIGIDTOPFLANGE
1106,93,186
1107,186,279
1108,279,372
1109,372,465
1110,465,558
1111,558,651
*BEAM SECTION, SECTION=RECT,ELSET=RIGIDTOPFLANGE, MATERIALS=RIGID
5.,5.
0,-1,0
*ELEMENT, TYPE=B31,ELSET=RIGIDBOTTOMFLANGE
1112,1,94
1113,94,187
1114,187,280
1115,280,373
1116,373,466
1117,466,559
*BEAM SECTION, SECTION=RECT,ELSET=RIGIDBOTTOMFLANGE, MATERIALS=RIGID
5.,5.
*ELEMENT, TYPE=B31,ELSET=RIGIDTOPWEB
1118,372,792
1119,792,885
```

```
1120,885,978

1121,978,1071
1122,1071,1164
1123,1164,1257
*BEAM SECTION, SECTION=RECT,ELSET=RIGIDTOPWEB, MATERIALS=RIGID
5.,5.
0,-1,0
**
*ELEMENT, TYPE=B31,ELSET=RIGIDBOTTOMWEB
1124,280,700
1125,700,793
1126,793,886
1127,886,979
1128,979,1072
1129,1072,1165
*BEAM SECTION, SECTION=RECT,ELSET=RIGIDBOTTOMWEB, MATERIALS=RIGID
5.,5.
0,-1,0
**
**
**MATERIAL PROPERTIES
**
*SHELL SECTION,MATERIAL=STEEL,ELSET=FLANGE1
0.303
*SHELL SECTION,MATERIAL=STEEL,ELSET=FLANGE2
0.303
*SHELL SECTION,MATERIAL=STEEL,ELSET=WEB
0.303
*MATERIAL,NAME=STEEL
*ELASTIC
29000,0.3
*MATERIAL, NAME=RIGID
*ELASTIC
290000,0.3
*BOUNDARY
PINNED,1
PINNED,2
PINNED,3
PINNED,5
ROLLER,1
ROLLER,3
ROLLER,5
*STEP
*BUCKLE
5,5,50,100
*CLOAD
1164,2,-1
*NODE FILE,LAST MODE=1,GLOBAL=YES
U
*END STEP
```

APPENDIX B7

```
*Heading
      Tee-shaped Column with Eccentric Loading
      Postbuckling Analysis
      Scale Factor =L/1000
*NODE
**BOTTOM OF FLANGE
1,0,0,0
280,2.01,0,0
559,4.02,0,0
**TOP OF FLANGE
93,0,91.42,0
372,2.01,91.42,0
651,4.02,91.42,0
**BOTTOM OF WEB
700,2.01,0,0.152
793,2.01,0,1.3705
886,2.01,0,2.52
1165,2.01,0,4.912
**TOP OF WEB
792,2.01,91.42,0.152
885,2.01,91.42,1.3705
978,2.01,91.42,2.52
1257,2.01,91.42,4.912
**
**NODE SETS
**
**FLANGE
**
*NGEN,NSET=FLL
1,93,1
*NGEN,NSET=FLM
280,372,1
*NGEN,NSET=FLR
559,651,1
*NFILL,NSET=FLANGE1
FLL,FLM,3,93
*NFILL,NSET=FLANGE2
FLM,FLR,3,93
**
**WEB
**
*NGEN,NSET=WEB1
700,792,1
*NGEN,NSET=WEB2
886,978,1
*NFILL,NSET=WEB4
WEB1,WEB2,2,93
*NGEN,NSET=WEB3
1165,1257,1
*NFILL,NSET=WEB5
WEB2,WEB3,3,93
**
**BC'S
```

```
**
*NSET,NSET=PINNED
793
*NSET,NSET=ROLLER
885
**
**ELEMENT DEFINITIONS
**
*ELEMENT,TYPE=S4R
1,1,2,95,94
*ELGEN,ELSET=FLANGE1
1,92,1,1,3,93,92
*ELEMENT,TYPE=S4R
277,280,281,374,373
*ELGEN,ELSET=FLANGE2
277,92,1,1,3,93,92

**
*ELEMENT,TYPE=S4R
553,280,281,701,700
*ELGEN,ELSET=WEB1
553,92,1,1
**
*ELEMENT,TYPE=S4R
645,700,701,794,793
*ELGEN,ELSET=WEB2
645,92,1,1,2,93,92
**
*ELEMENT,TYPE=S4R
829,886,887,980,979
*ELGEN,ELSET=WEB3
829,92,1,1,3,93,92
**
*ELSET,ELSET=WEB
WEB1,WEB2,WEB3
**
*ELEMENT, TYPE=B31,ELSET=RIGIDTOPFLANGE
1106,93,186
1107,186,279
1108,279,372
1109,372,465
1110,465,558
1111,558,651
*BEAM SECTION, SECTION=RECT,ELSET=RIGIDTOPFLANGE, MATERIALS=RIGID
5.,5.
0,-1,0
*ELEMENT, TYPE=B31,ELSET=RIGIDBOTTOMFLANGE
1112,1,94
1113,94,187
1114,187,280
1115,280,373
1116,373,466
1117,466,559
*BEAM SECTION, SECTION=RECT,ELSET=RIGIDBOTTOMFLANGE, MATERIALS=RIGID
5.,5.
*ELEMENT, TYPE=B31,ELSET=RIGIDTOPWEB
1118,372,792
```

```
1119,792,885
1120,885,978
1121,978,1071
1122,1071,1164
1123,1164,1257
*BEAM SECTION, SECTION=RECT,ELSET=RIGIDTOPWEB, MATERIALS=RIGID
5.,5.
0,-1,0
**
*ELEMENT, TYPE=B31,ELSET=RIGIDBOTTOMWEB
1124,280,700
1125,700,793
1126,793,886
1127,886,979
1128,979,1072
1129,1072,1165
*BEAM SECTION, SECTION=RECT,ELSET=RIGIDBOTTOMWEB, MATERIALS=RIGID
5.,5.
0,-1,0
**
**MATERIAL PROPERTIES
**
*SHELL SECTION,MATERIAL=STEEL,ELSET=FLANGE1
0.303
*SHELL SECTION,MATERIAL=STEEL,ELSET=FLANGE2
0.303
*SHELL SECTION,MATERIAL=STEEL,ELSET=WEB
0.303
*MATERIAL,NAME=STEEL
*ELASTIC
29000,0.3
*MATERIAL, NAME=RIGID
*ELASTIC
290000,0.3
*IMPERFECTION,FILE=TeeIMP2, STEP=1
1,0.09142
*BOUNDARY
PINNED,1
PINNED,2
PINNED,3
PINNED,5
ROLLER,1
ROLLER,3
ROLLER,5
*STEP,NLGEOM,INC=30
*STATIC,RIKS
0.01,1.,0.0000000001
*CLOAD
978,2,-10
*CLOAD
886,2,10
*EL PRINT,FREQ=11,ELSET=FLANGE1
S
*EL PRINT,FREQ=11,ELSET=FLANGE2
S
*NODE PRINT,FREQ=11
UR3
```

```
*END STEP
```

APPENDIX C

THEORETICAL RESULTS

Appendix C includes all calculations performed to arrive at theoretical results for this study. The computations are presented in a MathCAD worksheet with cross-sections of each member included. The results provided by these computations are used to compare with the finite element analysis in order to prove or discount the validity of the Wagner Hypothesis. Appendix C1 shows the calculations related to the simply supported 12WF50 section with a uniform moment applied to each end of the beam. Appendix C2 illustrates the theoretical results associated with the cruciform-shaped column. For this member there were equations presented by Ojalvo for both the critical buckling load including the Wagner effect and the critical load calculated without the use of the Wagner effect.

Appendix C3 demonstrates the theoretical equations used for the tee-shaped column. This member was used due to the fact that experimental tests were performed on various tee-shaped columns at the Xian Institute of Metallurgy and Construction Engineering in the late 1970's. In this case, the finite element results could be compared to both the theoretical results presented in Appendix C3 as well as the finite element results found in the ABAQUS modeling. The equations used in these computations are specified by both Galambos and Ojalvo.

APPENDIX C1

Doubly Symmetric I-Beam
Closed Form Solution presented in "Structural Members and Frames" page 59

** All measurements are in inches and kips

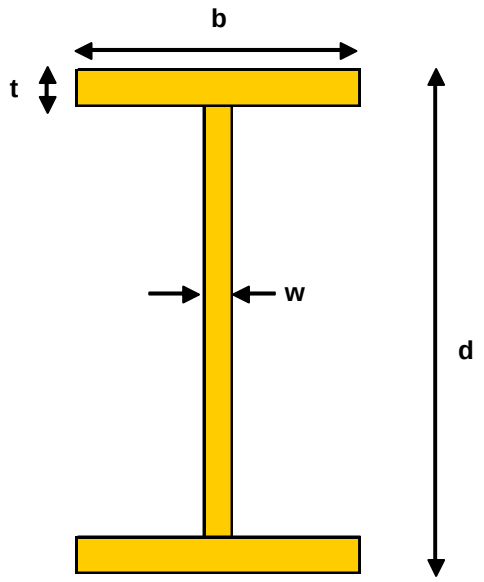

$L := 240$ $G := 11500$ $E := 30000$ $Iw := 1881$ $w := 0.371$

$Kt := 1.82$ $Iy := 56.4$ $Ix := 394.5$ $Sx := 64.7$ $Sw := 30.18$

$d := 12.19$ $b := 8.077$ $t := 0.641$ $wn := 23.32$

$$\lambda := \sqrt{\frac{G \cdot Kt}{E \cdot Iw}} \qquad \lambda^2 = 3.709 \times 10^{-4} \qquad \lambda \cdot L = 4.622$$

Critical Moment:

$n := 1$

$$Mo := \frac{\pi \cdot n}{L} \cdot \sqrt{E \cdot Iy \cdot G \cdot Kt \cdot \left(1 + \frac{n^2 \cdot \pi^2 \cdot E \cdot Iw}{G \cdot Kt \cdot L^2}\right)}$$ (Eqn. 3.32 on page 91)

$Mo = 2.978 \times 10^3$ kip·in

$\frac{Mo}{12} = 248.206$ kip·ft

Summary:

Galambos	Mcr = 248.2 kips
ABAQUS	Mcr = (6000 kips * 0.5025) = 251.25 kips

APPENDIX C2

Cruciform Cross-section with Flanges
Closed Form Solution presented in "Thin-Walled Open-Profile Bars" pages 145 and 147

** All measurements are in inches and kips

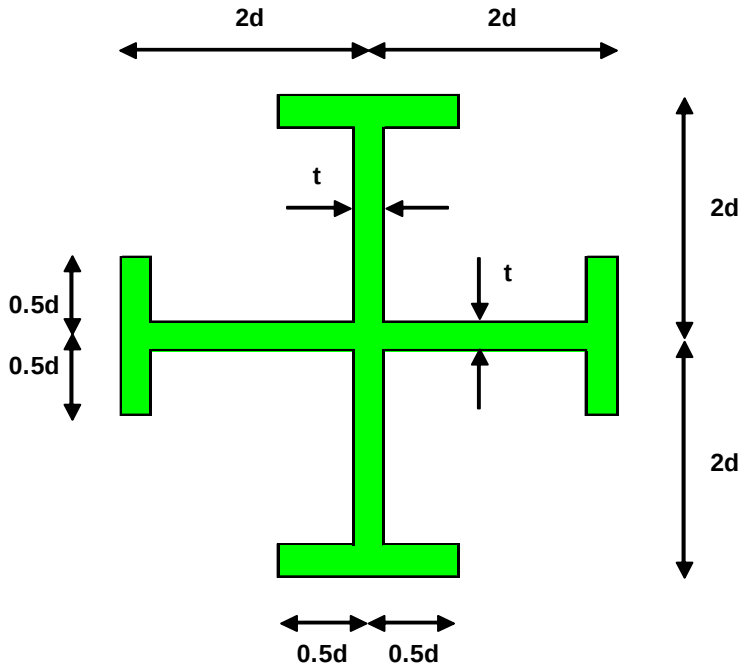

$d := 6 \qquad t := 0.25 \qquad L := 240 \qquad E := 29000 \qquad \nu := 0.3$

$$G := \frac{E}{2\cdot(1+\nu)}$$

Critical Moment (including Wagner's Hypothesis):

$$P_\theta = \frac{A}{I_0}(GJ + EI_\omega \frac{\pi^2}{L^2}) = \frac{16}{9}G\frac{t^3}{d} + \frac{16}{27}E\frac{\pi^2}{L^2}td^3$$ (Eqn. 16 on page 145)

$$P := \left(\frac{16}{9}\cdot G\cdot\frac{t^3}{d}\right) + \frac{16}{27}\cdot E\cdot\frac{\pi^2}{L^2}\cdot t\cdot d^3$$

$P = 210.648$ kips

Critical Moment (excluding Wagner's Hypothesis):

$$P_\theta = \frac{4}{a^2}(GJ + EI_\omega + EI_y\{2d^2\}\frac{\pi^2}{L^2}) = \frac{9}{4}G\frac{t^3}{d} + \frac{3}{4}\frac{\pi^2}{L^2}Etd^3$$ (Eqn. 19 on page 147)

$$P := \left(\frac{9}{4}\cdot G\cdot\frac{t^3}{d}\right) + \frac{3}{4}\cdot\frac{\pi^2}{L^2}\cdot E\cdot t\cdot d^3$$

P = 266.602 kips

Summary:

Including Wagner	Pcr = 210.65 kips
Without Using Wagner	Pcr = 266.60 kips
ABAQUS	Pcr = 206.75 kips

APPENDIX C3

Calculation of the critical buckling load of Chen's experimental specimen PD3-1 (Corrected eccentricity):

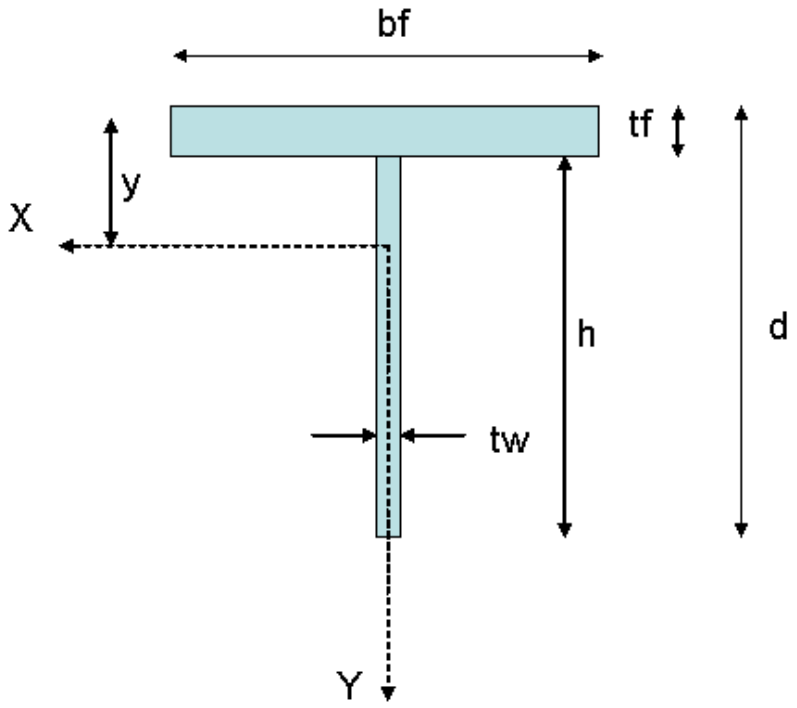

$d := 5.067$ $tf := 0.303$ $tw := 0.303$ $h := d - tf$ $bf := 4$

$Af := bf \cdot tf$ $Aw := h \cdot tw$ $A := Af + Aw$ $D := d - \frac{tf}{2}$

$y := \frac{1}{A} \cdot \left[\frac{Af \cdot tf}{2} + Aw \cdot \left(tf + \frac{h}{2} \right) \right]$ $y = 1.529$ $ybar := \left(y - \frac{tf}{2} \right) \cdot -1$ $ybar = -1.377$

$Ix := \frac{bf \cdot tf^3 + h^3 \cdot tw}{12} + Af \cdot \left(y - \frac{tf}{2} \right)^2 + Aw \cdot \left(tf + \frac{h}{2} - y \right)^2$ $Ix = 6.968$

$Iy := \frac{bf^3 \cdot tf + h \cdot tw^3}{12}$ $Iy = 1.627$ $ro := \sqrt{ybar^2 + \frac{Ix + Iy}{A}}$

$H := 1 - \left(\frac{ybar}{ro} \right)^2$ $J := \frac{bf \cdot tf^3 + D \cdot tw^3}{3}$

$$\beta x := \frac{1}{Ix}\cdot\left[\frac{tw}{4}\cdot\left[(D-y)^4-(y-tf)^4\right]-bf\cdot tf\cdot\left(y-\frac{tf}{2}\right)\cdot\left[\frac{bf^2}{12}+\left(y-\frac{tf}{2}\right)^2\right]\right]-2\cdot ybar$$

Considering TVG's solution on p.249 of "Structural Members and Frames":

Assume that: E=29000ksi, G=0.385E, Mo=-1.15P, and Iw=0

$E := 29000 \qquad G := 0.385\cdot E \qquad L := 91.5$

$$Py := \frac{\pi^2\cdot E\cdot Iy}{L^2} \qquad Pz := \frac{G\cdot J}{ro^2}$$

Buckling Condition:

$P := 10$

$$root\left[(Py-P)\cdot\left(ro^2\cdot Pz-1.15\cdot P\cdot\beta x-P\cdot ro^2\right)-(P\cdot ybar-1.15\cdot P)^2,P\right]=38.817$$

Pcritical = 38.8kips

Apply AISC LRFD Appendix E Equation (A-E3-7):

$$rx := \sqrt{\frac{Ix}{A}} \qquad ry := \sqrt{\frac{Iy}{A}} \qquad Fex := \frac{\pi^2\cdot E}{\left(\frac{L}{rx}\right)^2} \qquad Fey := \frac{\pi^2\cdot E}{\left(\frac{L}{ry}\right)^2}$$

$$Fez := \frac{G\cdot J}{A\cdot ro^2} \qquad F := 30$$

$$root\left[(F-Fex)\cdot(F-Fey)\cdot(F-Fez)-F^2\cdot(F-Fex)\cdot\left(\frac{ybar}{ro}\right)^2,F\right]=18.407$$

$18.407\cdot A = 48.88$

Pcritical = 49kips

Ojalvo p. 113 eqn (3-33b) approach to computing Pcr:

$e := 2.52$ The sign for this is consistent with regard to Ojalvo's notation (see p.111 & T3.1)

$$\rho := \frac{G \cdot J}{e \cdot ybar} \qquad Py := \frac{\pi^2 \cdot E \cdot Iy}{L^2}$$

$P := 20$

$$root\left[P^2 \cdot \left(1 - \frac{e}{ybar}\right) - P \cdot (Py + \rho) + Py \cdot \rho, P\right] = 44.131$$

Thus according to Ojalvo's theory, Pcr = 44kips

Summary:

Chen's Experiment	Pcr = 37 kips
Galambos	Pcr = 39 kips
Ojalvo	Pcr = 44 kips
ABAQUS	Pcr = 38 kips

APPENDIX D

PRINCIPAL STRESS CALCULATIONS

Appendix D includes Excel spreadsheets used to numerically verify graphical representations of inclinations of principal stresses for each column model. Appendix D1 includes the calculations performed for the cruciform-shaped column. The normal and transverse stresses were imported into the worksheet from an ABAQUS data file. These stresses were then used to calculate the inclination of the principal plane for each element along a strip from the flange piece. The stresses extracted from the data file were computed during increment 16 of the analysis which corresponds to the location of the critical buckling load where the load proportionality factor is equal to 2.07, and the critical load is equal to 207 kips. In addition to the stresses, the rotation of each element was also extracted for comparison with the inclination of the principal plane.

Appendix D2 consists of Excel spreadsheets used to calculate principal stress inclinations for the tee-shaped column. Much like the cruciform model, the normal and shear stresses for the tee are extracted from the data file produced during the finite element analysis and they are then imported into Excel. The inclination of the principal plane is then computed using these values for a strip of elements along the web plate of the tee. The stresses taken from the data file were computed during increment 11 of the analysis, which corresponds to approximately one-third of the critical buckling load. Along with the stresses, the rotation of each element was used to compare with the inclination of the principal plane along the length of the column.

APPENDIX D1

Flange 1 of Cruciform Column (Increment 16)

Table 1: Inclination of Principal Plane (Cruciform)

Node	UR3		Element	S11	S22	S12	θ	X	X/L
965	0.011343		961	1.691	0.8719	0.1118	-0.1332448	0	0
966	0.011343		962	1.252	-1.681	0.7754	-0.2431879	1	0.0041667
967	0.011617		963	-1.581	-6.525	1.369	-0.252879	2	0.0083333
968	0.011771		964	2.28	-6.378	-0.3057	0.03524987	3	0.0125
969	0.011743		965	-0.1013	-5.942	-0.020382	0.00348959	4	0.0166667
970	0.011833		966	0.7916	-6.85	-0.9435	0.12104727	5	0.0208333
971	0.011828		967	-0.0020969	-6.942	-1.015	0.14228617	6	0.025
972	0.011859		968	0.396	-7.399	-1.265	0.15692012	7	0.0291667
973	0.011863		969	0.02462	-7.695	-1.354	0.16869121	8	0.0333333
974	0.01188		970	0.314	-7.982	-1.476	0.17093139	9	0.0375
975	0.011882		971	0.064465	-8.277	-1.555	0.17843614	10	0.0416667
976	0.011893		972	0.2761	-8.525	-1.652	0.17956399	11	0.0458333
977	0.011891		973	0.085374	-8.795	-1.736	0.18635083	12	0.05
978	0.011896		974	0.2343	-9.028	-1.814	0.18666339	13	0.0541667
979	0.01189		975	0.086475	-9.275	-1.899	0.19270752	14	0.0583333
980	0.011888		976	0.1876	-9.495	-1.96	0.19234018	15	0.0625
981	0.011879		977	0.075715	-9.722	-2.037	0.19703101	16	0.0666667
982	0.011871		978	0.1416	-9.927	-2.085	0.1963262	17	0.0708333
983	0.011857		979	0.059593	-10.13	-2.149	0.19957979	18	0.075
984	0.011844		980	0.1005	-10.33	-2.185	0.19837334	19	0.0791667
985	0.011826		981	0.042234	-10.52	-2.235	0.20017503	20	0.0833333
986	0.011808		982	0.066377	-10.69	-2.263	0.19914273	21	0.0875
987	0.011785		983	0.02592	-10.87	-2.3	0.19973829	22	0.0916667
988	0.011761		984	0.039296	-11.03	-2.32	0.19846432	23	0.0958333
989	0.011734		985	0.01164	-11.2	-2.346	0.19817341	24	0.1
990	0.011705		986	0.018388	-11.35	-2.359	0.19668954	25	0.1041667
991	0.011673		987	-0.0004121	-11.51	-2.377	0.19585145	26	0.1083333
992	0.011638		988	0.0024024	-11.65	-2.385	0.1942736	27	0.1125
993	0.011602		989	-0.010444	-11.8	-2.395	0.19295928	28	0.1166667
994	0.011563		990	-0.0098799	-11.94	-2.399	0.19119013	29	0.1208333
995	0.011521		991	-0.018803	-12.07	-2.404	0.1898067	30	0.125
996	0.011477		992	-0.019472	-12.21	-2.404	0.18783672	31	0.1291667
997	0.01143		993	-0.025836	-12.34	-2.404	0.186121	32	0.1333333
998	0.011381		994	-0.02714	-12.47	-2.401	0.18415672	33	0.1375
999	0.01133		995	-0.031837	-12.6	-2.398	0.18227181	34	0.1416667
1000	0.011276		996	-0.033428	-12.73	-2.392	0.18017155	35	0.1458333
1001	0.01122		997	-0.037028	-12.85	-2.385	0.17819149	36	0.15
1002	0.011162		998	-0.038711	-12.97	-2.377	0.17614924	37	0.1541667
1003	0.011101		999	-0.041573	-13.1	-2.368	0.17396201	38	0.1583333
1004	0.011038		1000	-0.043241	-13.22	-2.358	0.17184891	39	0.1625
1005	0.010972		1001	-0.045593	-13.34	-2.346	0.1696415	40	0.1666667
1006	0.010904		1002	-0.04719	-13.46	-2.334	0.16745736	41	0.1708333
1007	0.010834		1003	-0.049175	-13.58	-2.321	0.16524324	42	0.175
1008	0.010761		1004	-0.050675	-13.7	-2.306	0.16292394	43	0.1791667
1009	0.010687		1005	-0.052389	-13.81	-2.292	0.1608141	44	0.1833333
1010	0.010609		1006	-0.053784	-13.93	-2.276	0.15849101	45	0.1875
1011	0.01053		1007	-0.055289	-14.04	-2.259	0.15624133	46	0.1916667
1012	0.010449		1008	-0.056578	-14.16	-2.242	0.15391524	47	0.1958333
1013	0.010365		1009	-0.057918	-14.27	-2.224	0.15165793	48	0.2
1014	0.010279		1010	-0.059109	-14.39	-2.206	0.14932899	49	0.2041667
1015	0.01019		1011	-0.060315	-14.5	-2.187	0.14706457	50	0.2083333
1016	0.0101		1012	-0.061415	-14.61	-2.167	0.1447638	51	0.2125
1017	0.010007		1013	-0.062511	-14.73	-2.147	0.14239902	52	0.2166667
1018	0.0099128		1014	-0.063529	-14.84	-2.126	0.14009256	53	0.2208333

1019	0.0098159		1015	-0.064534	-14.95	-2.104	0.13775156	54	0.225
1020	0.0097169		1016	-0.065479	-15.06	-2.082	0.13543799	55	0.2291667
1021	0.0096159		1017	-0.066405	-15.17	-2.06	0.13315184	56	0.2333333
1022	0.0095127		1018	-0.067285	-15.28	-2.037	0.13083116	57	0.2375
1023	0.0094076		1019	-0.068144	-15.38	-2.014	0.12861801	58	0.2416667
1024	0.0093003		1020	-0.068966	-15.49	-1.99	0.12628864	59	0.2458333
1025	0.0091911		1021	-0.069767	-15.6	-1.965	0.12392585	60	0.25
1026	0.0090799		1022	-0.070537	-15.7	-1.94	0.12166504	61	0.2541667
1027	0.0089667		1023	-0.071286	-15.8	-1.915	0.11942761	62	0.2583333
1028	0.0088515		1024	-0.072009	-15.91	-1.89	0.11714193	63	0.2625
1029	0.0087345		1025	-0.072712	-16.01	-1.864	0.11489262	64	0.2666667
1030	0.0086155		1026	-0.073392	-16.11	-1.837	0.11260711	65	0.2708333
1031	0.0084946		1027	-0.074054	-16.21	-1.81	0.1103449	66	0.275
1032	0.0083719		1028	-0.074694	-16.31	-1.783	0.10810572	67	0.2791667
1033	0.0082474		1029	-0.075318	-16.41	-1.755	0.10583083	68	0.2833333
1034	0.0081211		1030	-0.075922	-16.5	-1.727	0.10364023	69	0.2875
1035	0.0079929		1031	-0.07651	-16.6	-1.699	0.10140953	70	0.2916667
1036	0.0078631		1032	-0.077081	-16.69	-1.67	0.09920169	71	0.2958333
1037	0.0077315		1033	-0.077635	-16.79	-1.641	0.09695693	72	0.3
1038	0.0075982		1034	-0.078174	-16.88	-1.612	0.09478979	73	0.3041667
1039	0.0074632		1035	-0.078697	-16.97	-1.582	0.09258477	74	0.3083333
1040	0.0073265		1036	-0.079205	-17.06	-1.552	0.09039932	75	0.3125
1041	0.0071883		1037	-0.079699	-17.15	-1.522	0.08823327	76	0.3166667
1042	0.0070485		1038	-0.080178	-17.23	-1.491	0.08607906	77	0.3208333
1043	0.0069071		1039	-0.080643	-17.32	-1.46	0.08389369	78	0.325
1044	0.0067641		1040	-0.081094	-17.4	-1.429	0.081774	79	0.3291667
1045	0.0066197		1041	-0.081532	-17.48	-1.398	0.07967071	80	0.3333333
1046	0.0064738		1042	-0.081956	-17.56	-1.366	0.07752785	81	0.3375
1047	0.0063264		1043	-0.082368	-17.64	-1.334	0.07540152	82	0.3416667
1048	0.0061777		1044	-0.082766	-17.72	-1.301	0.07323613	83	0.3458333
1049	0.0060276		1045	-0.083151	-17.8	-1.269	0.07114271	84	0.35
1050	0.0058761		1046	-0.083524	-17.87	-1.236	0.06904869	85	0.3541667
1051	0.0057233		1047	-0.083885	-17.94	-1.203	0.06696853	86	0.3583333
1052	0.0055692		1048	-0.084233	-18.01	-1.169	0.06484733	87	0.3625
1053	0.0054139		1049	-0.084569	-18.08	-1.136	0.06279489	88	0.3666667
1054	0.0052574		1050	-0.084893	-18.15	-1.102	0.06070159	89	0.3708333
1055	0.0050996		1051	-0.085206	-18.21	-1.068	0.05865427	90	0.375
1056	0.0049408		1052	-0.085507	-18.28	-1.034	0.05658754	91	0.3791667
1057	0.0047808		1053	-0.085796	-18.34	-0.9993	0.05452637	92	0.3833333
1058	0.0046198		1054	-0.086074	-18.4	-0.9647	0.05248217	93	0.3875
1059	0.0044577		1055	-0.08634	-18.45	-0.9298	0.05046059	94	0.3916667
1060	0.0042946		1056	-0.086596	-18.51	-0.8948	0.04841676	95	0.3958333
1061	0.0041305		1057	-0.08684	-18.56	-0.8597	0.0464041	96	0.4
1062	0.0039655		1058	-0.087073	-18.61	-0.8243	0.04438465	97	0.4041667
1063	0.0037996		1059	-0.087296	-18.66	-0.7888	0.04236923	98	0.4083333
1064	0.0036329		1060	-0.087508	-18.71	-0.7531	0.04035251	99	0.4125
1065	0.0034653		1061	-0.087709	-18.75	-0.7173	0.03836035	100	0.4166667
1066	0.0032969		1062	-0.087899	-18.8	-0.6814	0.03635076	101	0.4208333
1067	0.0031278		1063	-0.088079	-18.84	-0.6453	0.03435829	102	0.425
1068	0.002958		1064	-0.088248	-18.88	-0.6091	0.03236787	103	0.4291667
1069	0.0027875		1065	-0.088408	-18.91	-0.5728	0.03039563	104	0.4333333
1070	0.0026163		1066	-0.088556	-18.95	-0.5363	0.02840307	105	0.4375
1071	0.0024446		1067	-0.088695	-18.98	-0.4998	0.02643197	106	0.4416667
1072	0.0022723		1068	-0.088823	-19.01	-0.4632	0.02446097	107	0.4458333
1073	0.0020995		1069	-0.088942	-19.04	-0.4264	0.02248489	108	0.45
1074	0.0019263		1070	-0.08905	-19.06	-0.3896	0.02052513	109	0.4541667
1075	0.0017526		1071	-0.089148	-19.09	-0.3528	0.01855906	110	0.4583333
1076	0.0015784		1072	-0.089237	-19.11	-0.3158	0.01659681	111	0.4625
1077	0.001404		1073	-0.089315	-19.12	-0.2788	0.01464583	112	0.4666667
1078	0.0012292		1074	-0.089384	-19.14	-0.2417	0.01268453	113	0.4708333
1079	0.0010541		1075	-0.089442	-19.15	-0.2046	0.01073256	114	0.475
1080	0.0008788		1076	-0.089491	-19.17	-0.1675	0.00877769	115	0.4791667
1081	0.0007033		1077	-0.08953	-19.18	-0.1303	0.00682497	116	0.4833333
1082	0.0005276		1078	-0.08956	-19.18	-0.093083	0.00487574	117	0.4875
1083	0.0003518		1079	-0.089579	-19.19	-0.055857	0.00292435	118	0.4916667

1084	0.0001759		1080	-0.089589	-19.19	-0.01862	0.00097485	119	0.4958333
1085	5.242E-14		1081	-0.089589	-19.19	0.01862	-0.0009748	120	0.5
1086	-0.0001759		1082	-0.089579	-19.19	0.055857	-0.0029244	121	0.5041667
1087	-0.0003518		1083	-0.08956	-19.18	0.093083	-0.0048757	122	0.5083333
1088	-0.0005276		1084	-0.08953	-19.18	0.1303	-0.006825	123	0.5125
1089	-0.0007033		1085	-0.089491	-19.17	0.1675	-0.0087777	124	0.5166667
1090	-0.0008788		1086	-0.089442	-19.15	0.2046	-0.0107326	125	0.5208333
1091	-0.0010541		1087	-0.089384	-19.14	0.2417	-0.0126845	126	0.525
1092	-0.0012292		1088	-0.089315	-19.12	0.2788	-0.0146458	127	0.5291667
1093	-0.001404		1089	-0.089237	-19.11	0.3158	-0.0165968	128	0.5333333
1094	-0.0015784		1090	-0.089148	-19.09	0.3528	-0.0185591	129	0.5375
1095	-0.0017526		1091	-0.08905	-19.06	0.3896	-0.0205251	130	0.5416667
1096	-0.0019263		1092	-0.088942	-19.04	0.4264	-0.0224849	131	0.5458333
1097	-0.0020995		1093	-0.088823	-19.01	0.4632	-0.024461	132	0.55
1098	-0.0022723		1094	-0.088695	-18.98	0.4998	-0.026432	133	0.5541667
1099	-0.0024446		1095	-0.088556	-18.95	0.5363	-0.0284031	134	0.5583333
1100	-0.0026163		1096	-0.088408	-18.91	0.5728	-0.0303956	135	0.5625
1101	-0.0027875		1097	-0.088248	-18.88	0.6091	-0.0323679	136	0.5666667
1102	-0.002958		1098	-0.088079	-18.84	0.6453	-0.0343583	137	0.5708333
1103	-0.0031278		1099	-0.087899	-18.8	0.6814	-0.0363508	138	0.575
1104	-0.0032969		1100	-0.087709	-18.75	0.7173	-0.0383604	139	0.5791667
1105	-0.0034653		1101	-0.087508	-18.71	0.7531	-0.0403525	140	0.5833333
1106	-0.0036329		1102	-0.087296	-18.66	0.7888	-0.0423692	141	0.5875
1107	-0.0037996		1103	-0.087073	-18.61	0.8243	-0.0443847	142	0.5916667
1108	-0.0039655		1104	-0.08684	-18.56	0.8597	-0.0464041	143	0.5958333
1109	-0.0041305		1105	-0.086596	-18.51	0.8948	-0.0484168	144	0.6
1110	-0.0042946		1106	-0.08634	-18.45	0.9298	-0.0504606	145	0.6041667
1111	-0.0044577		1107	-0.086074	-18.4	0.9647	-0.0524822	146	0.6083333
1112	-0.0046198		1108	-0.085796	-18.34	0.9993	-0.0545264	147	0.6125
1113	-0.0047808		1109	-0.085507	-18.28	1.034	-0.0565875	148	0.6166667
1114	-0.0049408		1110	-0.085206	-18.21	1.068	-0.0586543	149	0.6208333
1115	-0.0050996		1111	-0.084893	-18.15	1.102	-0.0607016	150	0.625
1116	-0.0052574		1112	-0.084569	-18.08	1.136	-0.0627949	151	0.6291667
1117	-0.0054139		1113	-0.084233	-18.01	1.169	-0.0648473	152	0.6333333
1118	-0.0055692		1114	-0.083885	-17.94	1.203	-0.0669685	153	0.6375
1119	-0.0057233		1115	-0.083524	-17.87	1.236	-0.0690487	154	0.6416667
1120	-0.0058761		1116	-0.083151	-17.8	1.269	-0.0711427	155	0.6458333
1121	-0.0060276		1117	-0.082766	-17.72	1.301	-0.0732361	156	0.65
1122	-0.0061777		1118	-0.082368	-17.64	1.334	-0.0754015	157	0.6541667
1123	-0.0063264		1119	-0.081956	-17.56	1.366	-0.0775278	158	0.6583333
1124	-0.0064738		1120	-0.081532	-17.48	1.398	-0.0796707	159	0.6625
1125	-0.0066197		1121	-0.081094	-17.4	1.429	-0.081774	160	0.6666667
1126	-0.0067641		1122	-0.080643	-17.32	1.46	-0.0838937	161	0.6708333
1127	-0.0069071		1123	-0.080178	-17.23	1.491	-0.0860791	162	0.675
1128	-0.0070485		1124	-0.079699	-17.15	1.522	-0.0882333	163	0.6791667
1129	-0.0071883		1125	-0.079205	-17.06	1.552	-0.0903993	164	0.6833333
1130	-0.0073265		1126	-0.078697	-16.97	1.582	-0.0925848	165	0.6875
1131	-0.0074632		1127	-0.078174	-16.88	1.612	-0.0947898	166	0.6916667
1132	-0.0075982		1128	-0.077635	-16.79	1.641	-0.0969569	167	0.6958333
1133	-0.0077315		1129	-0.077081	-16.69	1.67	-0.0992017	168	0.7
1134	-0.0078631		1130	-0.07651	-16.6	1.699	-0.1014095	169	0.7041667
1135	-0.0079929		1131	-0.075922	-16.5	1.727	-0.1036402	170	0.7083333
1136	-0.0081211		1132	-0.075318	-16.41	1.755	-0.1058308	171	0.7125
1137	-0.0082474		1133	-0.074694	-16.31	1.783	-0.1081057	172	0.7166667
1138	-0.0083719		1134	-0.074054	-16.21	1.81	-0.1103449	173	0.7208333
1139	-0.0084946		1135	-0.073392	-16.11	1.837	-0.1126071	174	0.725
1140	-0.0086155		1136	-0.072712	-16.01	1.864	-0.1148926	175	0.7291667
1141	-0.0087345		1137	-0.072009	-15.91	1.89	-0.1171419	176	0.7333333
1142	-0.0088515		1138	-0.071286	-15.8	1.915	-0.1194276	177	0.7375
1143	-0.0089667		1139	-0.070537	-15.7	1.94	-0.121665	178	0.7416667
1144	-0.0090799		1140	-0.069767	-15.6	1.965	-0.1239258	179	0.7458333
1145	-0.0091911		1141	-0.068966	-15.49	1.99	-0.1262886	180	0.75
1146	-0.0093003		1142	-0.068144	-15.38	2.014	-0.128618	181	0.7541667
1147	-0.0094076		1143	-0.067285	-15.28	2.037	-0.1308312	182	0.7583333
1148	-0.0095127		1144	-0.066405	-15.17	2.06	-0.1331518	183	0.7625

1149	-0.0096159		1145	-0.065479	-15.06	2.082	-0.135438	184	0.7666667
1150	-0.0097169		1146	-0.064534	-14.95	2.104	-0.1377516	185	0.7708333
1151	-0.0098159		1147	-0.063529	-14.84	2.126	-0.1400926	186	0.775
1152	-0.0099128		1148	-0.062511	-14.73	2.147	-0.142399	187	0.7791667
1153	-0.010007		1149	-0.061415	-14.61	2.167	-0.1447638	188	0.7833333
1154	-0.0101		1150	-0.060315	-14.5	2.187	-0.1470646	189	0.7875
1155	-0.01019		1151	-0.059109	-14.39	2.206	-0.149329	190	0.7916667
1156	-0.010279		1152	-0.057918	-14.27	2.224	-0.1516579	191	0.7958333
1157	-0.010365		1153	-0.056578	-14.16	2.242	-0.1539152	192	0.8
1158	-0.010449		1154	-0.055289	-14.04	2.259	-0.1562413	193	0.8041667
1159	-0.01053		1155	-0.053784	-13.93	2.276	-0.158491	194	0.8083333
1160	-0.010609		1156	-0.052389	-13.81	2.292	-0.1608141	195	0.8125
1161	-0.010687		1157	-0.050675	-13.7	2.306	-0.1629239	196	0.8166667
1162	-0.010761		1158	-0.049175	-13.58	2.321	-0.1652432	197	0.8208333
1163	-0.010834		1159	-0.04719	-13.46	2.334	-0.1674574	198	0.825
1164	-0.010904		1160	-0.045593	-13.34	2.346	-0.1696415	199	0.8291667
1165	-0.010972		1161	-0.043241	-13.22	2.358	-0.1718489	200	0.8333333
1166	-0.011038		1162	-0.041573	-13.1	2.368	-0.173962	201	0.8375
1167	-0.011101		1163	-0.038711	-12.97	2.377	-0.1761492	202	0.8416667
1168	-0.011162		1164	-0.037028	-12.85	2.385	-0.1781915	203	0.8458333
1169	-0.01122		1165	-0.033428	-12.73	2.392	-0.1801716	204	0.85
1170	-0.011276		1166	-0.031837	-12.6	2.398	-0.1822718	205	0.8541667
1171	-0.01133		1167	-0.02714	-12.47	2.401	-0.1841567	206	0.8583333
1172	-0.011381		1168	-0.025836	-12.34	2.404	-0.186121	207	0.8625
1173	-0.01143		1169	-0.019472	-12.21	2.404	-0.1878367	208	0.8666667
1174	-0.011477		1170	-0.018803	-12.07	2.404	-0.1898067	209	0.8708333
1175	-0.011521		1171	-0.0098799	-11.94	2.399	-0.1911901	210	0.875
1176	-0.011563		1172	-0.010444	-11.8	2.395	-0.1929593	211	0.8791667
1177	-0.011602		1173	0.0024024	-11.65	2.385	-0.1942736	212	0.8833333
1178	-0.011638		1174	-0.0004121	-11.51	2.377	-0.1958514	213	0.8875
1179	-0.011673		1175	0.018388	-11.35	2.359	-0.1966895	214	0.8916667
1180	-0.011705		1176	0.01164	-11.2	2.346	-0.1981734	215	0.8958333
1181	-0.011734		1177	0.039296	-11.03	2.32	-0.1984643	216	0.9
1182	-0.011761		1178	0.02592	-10.87	2.3	-0.1997383	217	0.9041667
1183	-0.011785		1179	0.066377	-10.69	2.263	-0.1991427	218	0.9083333
1184	-0.011808		1180	0.042234	-10.52	2.235	-0.200175	219	0.9125
1185	-0.011826		1181	0.1005	-10.33	2.185	-0.1983733	220	0.9166667
1186	-0.011844		1182	0.059593	-10.13	2.149	-0.1995798	221	0.9208333
1187	-0.011857		1183	0.1416	-9.927	2.085	-0.1963262	222	0.925
1188	-0.011871		1184	0.075715	-9.722	2.037	-0.197031	223	0.9291667
1189	-0.011879		1185	0.1876	-9.495	1.96	-0.1923402	224	0.9333333
1190	-0.011888		1186	0.086475	-9.275	1.899	-0.1927075	225	0.9375
1191	-0.01189		1187	0.2343	-9.028	1.814	-0.1866634	226	0.9416667
1192	-0.011896		1188	0.085374	-8.795	1.736	-0.1863508	227	0.9458333
1193	-0.011891		1189	0.2761	-8.525	1.652	-0.179564	228	0.95
1194	-0.011893		1190	0.064465	-8.277	1.555	-0.1784361	229	0.9541667
1195	-0.011882		1191	0.314	-7.982	1.476	-0.1709314	230	0.9583333
1196	-0.01188		1192	0.02462	-7.695	1.354	-0.1686912	231	0.9625
1197	-0.011863		1193	0.396	-7.399	1.265	-0.1569201	232	0.9666667
1198	-0.011859		1194	-0.0020969	-6.942	1.015	-0.1422862	233	0.9708333
1199	-0.011828		1195	0.7916	-6.85	0.9435	-0.1210473	234	0.975
1200	-0.011833		1196	-0.1013	-5.942	0.020382	-0.0034896	235	0.9791667
1201	-0.011743		1197	2.28	-6.378	0.3057	-0.0352499	236	0.9833333
1202	-0.011771		1198	-1.581	-6.525	-1.369	0.25287899	237	0.9875
1203	-0.011617		1199	1.252	-1.681	-0.7754	0.24318794	238	0.9916667
1204	-0.011343		1200	1.691	0.8719	-0.1118	0.13324482	239	0.9958333
1205	-0.011343							240	1

APPENDIX D2

Flange Plate of Tee Column (Increment 11)

Table 2: Inclination of Principal Plane (Tee)

Node	UR3	Element	S11	S22	S12	X/L	θ
559	-0.000597	461	-0.08194	-1.215	-0.21800	0.000	-0.184
560	-0.000612	462	0.06172	-1.493	-0.15520	0.011	-0.099
561	-0.000595	463	-0.00896	-1.711	-0.26130	0.022	-0.149
562	-0.000595	464	-0.00306	-1.668	-0.27190	0.033	-0.158
563	-0.000592	465	-0.00083	-1.592	-0.25730	0.044	-0.156
564	-0.000590	466	0.01092	-1.556	-0.26120	0.055	-0.161
565	-0.000587	467	0.00351	-1.524	-0.27050	0.066	-0.170
566	-0.000583	468	0.00734	-1.499	-0.27540	0.077	-0.175
567	-0.000578	469	0.00265	-1.472	-0.28340	0.088	-0.183
568	-0.000573	470	0.00283	-1.442	-0.28540	0.099	-0.188
569	-0.000568	471	0.00101	-1.411	-0.28780	0.110	-0.194
570	-0.000561	472	0.00075	-1.378	-0.28730	0.121	-0.197
571	-0.000554	473	-0.00026	-1.345	-0.28660	0.132	-0.201
572	-0.000546	474	-0.00024	-1.312	-0.28460	0.143	-0.205
573	-0.000538	475	-0.00118	-1.278	-0.28230	0.154	-0.208
574	-0.000529	476	-0.00087	-1.245	-0.27940	0.165	-0.211
575	-0.000520	477	-0.00184	-1.213	-0.27600	0.176	-0.214
576	-0.000510	478	-0.00142	-1.181	-0.27230	0.187	-0.216
577	-0.000499	479	-0.00235	-1.149	-0.26810	0.198	-0.219
578	-0.000488	480	-0.00194	-1.118	-0.26370	0.209	-0.221
579	-0.000476	481	-0.00279	-1.088	-0.25900	0.220	-0.223
580	-0.000464	482	-0.00246	-1.058	-0.25390	0.231	-0.224
581	-0.000451	483	-0.00320	-1.029	-0.24850	0.242	-0.226
582	-0.000437	484	-0.00298	-1.001	-0.24280	0.253	-0.226
583	-0.000423	485	-0.00360	-0.974	-0.23690	0.264	-0.227
584	-0.000409	486	-0.00349	-0.947	-0.23060	0.275	-0.227
585	-0.000394	487	-0.00401	-0.921	-0.22410	0.286	-0.227
586	-0.000378	488	-0.00399	-0.896	-0.21720	0.297	-0.227
587	-0.000362	489	-0.00443	-0.872	-0.21010	0.308	-0.226
588	-0.000346	490	-0.00447	-0.849	-0.20260	0.319	-0.224
589	-0.000329	491	-0.00485	-0.827	-0.19490	0.330	-0.221
590	-0.000312	492	-0.00494	-0.805	-0.18690	0.341	-0.218
591	-0.000294	493	-0.00526	-0.785	-0.17860	0.352	-0.215
592	-0.000276	494	-0.00539	-0.766	-0.17000	0.363	-0.210
593	-0.000258	495	-0.00567	-0.748	-0.16120	0.374	-0.205
594	-0.000239	496	-0.00582	-0.731	-0.15210	0.385	-0.199
595	-0.000220	497	-0.00607	-0.715	-0.14270	0.396	-0.191
596	-0.000201	498	-0.00622	-0.700	-0.13310	0.407	-0.183
597	-0.000181	499	-0.00645	-0.686	-0.12320	0.418	-0.174
598	-0.000161	500	-0.00661	-0.674	-0.11310	0.429	-0.163
599	-0.000141	501	-0.00681	-0.663	-0.10270	0.440	-0.152
600	-0.000121	502	-0.00696	-0.653	-0.09206	0.451	-0.139
601	-0.000100	503	-0.00714	-0.644	-0.08122	0.462	-0.125
602	-0.000079	504	-0.00729	-0.636	-0.07016	0.473	-0.110
603	-0.000059	505	-0.00745	-0.630	-0.05889	0.484	-0.093
604	-0.000038	506	-0.00758	-0.625	-0.04742	0.495	-0.076
605	-0.000016	507	-0.00772	-0.622	-0.03576	0.505	-0.058
606	0.000005	508	-0.00784	-0.620	-0.02391	0.516	-0.039
607	0.000026	509	-0.00794	-0.619	-0.01190	0.527	-0.019
608	0.000047	510	-0.00806	-0.619	0.00028	0.538	0.000
609	0.000068	511	-0.00813	-0.621	0.01260	0.549	0.021
610	0.000090	512	-0.00823	-0.625	0.02506	0.560	0.041
611	0.000111	513	-0.00827	-0.629	0.03764	0.571	0.060
612	0.000132	514	-0.00835	-0.635	0.05033	0.582	0.080
613	0.000153	515	-0.00836	-0.643	0.06311	0.593	0.098

614	0.000174	516	-0.00843	-0.652	0.07597	0.604	0.116
615	0.000195	517	-0.00840	-0.662	0.08890	0.615	0.133
616	0.000215	518	-0.00846	-0.674	0.10190	0.626	0.149
617	0.000235	519	-0.00837	-0.687	0.11490	0.637	0.163
618	0.000256	520	-0.00843	-0.702	0.12790	0.648	0.177
619	0.000275	521	-0.00829	-0.718	0.14090	0.659	0.189
620	0.000295	522	-0.00836	-0.736	0.15390	0.670	0.200
621	0.000314	523	-0.00813	-0.755	0.16690	0.681	0.210
622	0.000333	524	-0.00822	-0.775	0.17980	0.692	0.219
623	0.000351	525	-0.00791	-0.797	0.19270	0.703	0.227
624	0.000370	526	-0.00804	-0.820	0.20540	0.714	0.234
625	0.000387	527	-0.00761	-0.844	0.21800	0.725	0.240
626	0.000405	528	-0.00780	-0.870	0.23050	0.736	0.245
627	0.000421	529	-0.00724	-0.897	0.24280	0.747	0.250
628	0.000438	530	-0.00750	-0.926	0.25500	0.758	0.253
629	0.000453	531	-0.00679	-0.956	0.26690	0.769	0.256
630	0.000468	532	-0.00711	-0.987	0.27860	0.780	0.259
631	0.000483	533	-0.00625	-1.019	0.29000	0.791	0.260
632	0.000497	534	-0.00659	-1.052	0.30100	0.802	0.261
633	0.000511	535	-0.00557	-1.086	0.31170	0.813	0.262
634	0.000523	536	-0.00583	-1.122	0.32180	0.824	0.262
635	0.000536	537	-0.00470	-1.158	0.33130	0.835	0.261
636	0.000547	538	-0.00470	-1.195	0.34010	0.846	0.260
637	0.000558	539	-0.00347	-1.233	0.34790	0.857	0.257
638	0.000568	540	-0.00298	-1.270	0.35480	0.868	0.255
639	0.000577	541	-0.00152	-1.308	0.35970	0.879	0.252
640	0.000585	542	-0.00045	-1.345	0.36340	0.890	0.248
641	0.000593	543	0.00195	-1.381	0.36330	0.901	0.242
642	0.000600	544	0.00295	-1.415	0.36220	0.912	0.236
643	0.000607	545	0.00819	-1.447	0.35390	0.923	0.226
644	0.000612	546	0.00590	-1.475	0.34700	0.934	0.219
645	0.000617	547	0.01339	-1.511	0.33460	0.945	0.207
646	0.000621	548	0.00348	-1.551	0.32600	0.956	0.199
647	0.000623	549	-0.00006	-1.631	0.33550	0.967	0.195
648	0.000626	550	-0.00287	-1.674	0.31750	0.978	0.182
649	0.000627	551	0.06473	-1.446	0.20220	0.989	0.131
650	0.000644	552	-0.06446	-1.115	0.23800	1.000	0.213
651	0.000628					1.011	

BIBLIOGRAPHY

1. ABAQUS, (2003) *ABAQUS Standard User's Manual*, Version 6.4, Volumes 1 to 3, Hibbit, Karlsson & Sorensen, Inc., Pawtucket, Rhode Island, USA.

2. ABAQUS, (2003) *ABAQUS Theory Manual*, Version 6.4, Hibbit, Karlsson & Sorensen, Inc., Pawtucket, Rhode Island, USA.

3. Bleich, F., (1952) *Buckling Strength of Metal Structures*, McGraw-Hill, New York, USA.

4. Chen, S.F., (1980) "Lateral-Torsional Buckling of T-Section Steel Beam-Columns", *Structural Stability Research Council Meeting translated from Journal of Xian Institute of Metallurgy and Construction Engineering*, No. 3, 1978, Xian, Shaanxi, China.

5. Earls, C.J., Shah, B.J., (2002) "High Performance Steel Bridge Girder Compactness", *Journal of Constructional Steel Research*, Elsevier Science Ltd., Great Britain, Vol. 58, pp. 859-880.

6. Galambos, T.V., (1998) *Guide to Stability Design Criteria for Metal Structures*, Fifth Edition, John Wiley & Sons, Inc., New York, New York, USA.

7. Galambos, T.V., (1968) *Structural Members and Frames*, Prentice-Hall, Englewood Cliffs, New Jersey, USA.

8. Goodier, J.N., (1950) "Elastic Torsion in the Presence of Initial Axial Stress", *American Society of Mechanical Engineers Journal of Applied Mechanics*, USA.

9. Michell, A.G.M., (1899) "Elastic Stability of Long Beams Under Transverse Forces", *Phil. Mag.*, Vol. 48.

10. Ojalvo, M., (1982) "Discussion of "Lateral-Torsional Buckling of Tapered I-beams", *Journal of the Structural Division, ASCE*, Vol. 108, No.2, USA.

11. Ojalvo, M., (1987) "Discussion of "Buckling of Mono-symmetric I-beams Under Moment Gradient", *Journal of the Engineering Mechanics Division, ASCE*, Vol. 109, No.3, USA.

12. Ojalvo, M., (1990) *Thin-Walled Bars with Open Profiles*, The Olive Press, Columbus, Ohio, USA.

13. Prandtl, L., (1899) "Kipperscheinungen", *Thesis*, Munich.

14. Timoshenko, S.P., (1905) *Lateral Buckling of* Beams, Bulletin Polytechnical Institute, Vol. 4(5), Saint Petersburg.

15. Vlasov, V.Z., (1961) *Thin-Walled Elastic Beams*, 2d ed. rev. and augm. Translated from Russian [by Y. Schectman], Jerusalem, Published for the National Science Foundation, Washington, D.C., by the Israel Program for Scientific Translations.

16. Wagner, H., (1929) "Verdrehung Und Knickung Von Offenen Profilen", *25th Anniversary Publication, Technische Hochscule*, Danzig, Translated in NACA Tech. Mem. 807, 1936.